Report Title: Ceramic Proppant Design for In-situ Microbially Enhanced Methane Recovery

Type of Report: Final Scientific/Technical Report

Reporting Period Start Date: October 1, 2014

Reporting Period End Date: September 30, 2017

Principal Authors:

Assistant Professor Taylor D. Sparks

Department of Materials Science and Engineering

122 S. Central Campus Dr. Rm 304

Salt Lake City, UT 84112

sparks@eng.utah.edu

(801) 581-8632

Associate Professor John McLennan

Department of Chemical Engineering

50 S. Central Campus Dr. Rm 3290

Salt Lake City, UT 84112

jmclennan@egi.utah.edu

(801) 587-7925

Date Report was Issued December 29, 2017

DOE Award Number: DE-FE0024088

Name and Address of Submitting Organization:

University of Utah

201 Presidents Circle

Salt Lake City, UT 84112

Disclaimer

TABLE OF CONTENTS

Abstract

This project designed a new type of multi-functional lightweight proppant. The proppant is utilized as the conventional lightweight proppant but also transports microorganisms to coalbed reservoirs. The proppant is coated with a polymer which protects the methanogenic microorganisms and serves as a time-release delivery for methane generation. To produce the multifunctional proppant, we assigned five tasks: 1) culturing methanogenic microbes from natural carbon sources; 2) identifying optimized growth and methanogenesis conditions for the microbial consortia; 3) synthesizing the lightweight ceramic proppant; 4) encapsulating the consortia and proppant; and 5) demonstrating lab scale simulated performance by monitoring in-situ methane generation and hydraulic conductivity.

Task 1) To evaluate the feasibility of ex-situ cultivation, natural microbial populations were collected from various hydrocarbon-rich environments and locations characterized by natural methanogenesis. Different rank coals, complex hydrocarbon sources, hydrocarbon seeps, and natural biogenic environments were incorporated in the sampling. Three levels of screening allowed selection of microbial populations, favorable nutrient amendments, sources of the microbial community, and quantification of methane produced from various coal types. Incubation periods of up to 24 weeks were evaluated at 23ºC. Headspace concentrations of CH_4 and CO_2 were analyzed by gas chromatography. After a two-week incubation period of the most promising microbes, generated headspace gas concentrations reached 873,400 ppm for methane and 176,370 ppm for carbon dioxide.

Task 2) A central composite design (CCD) was used to explore a broad range of operational conditions, examine the effects of the important environmental factors, such as temperature, pH and salt concentration, and query a feasible region of operation to maximize methane production from coal. Coal biogasification was optimal for this consortium at an initial pH value of 5.5, at 30 °C, and at a NaCl concentration 3.7 mg/cm^3 (i.e., 145,165 ppm).

Task 3) To create the lightweight ceramic proppant, the kaolinite and iron oxide (Fe_2O_3) mixture were sintered under reducing atmosphere varying partial pressures of oxygen from 1.7×10^{-13} atm to 1.8×10^{-11} atm. The Fe_2O_3 reduces to FeO and reacts with kaolinite decomposed to mullite to form Fe_2SiO_4, $FeSiO_3$, and $FeAl_2O_4$. As a result the proppant develops large pores (~100 µm), giving it a low bulk density (1.43 g/cm^3), and high porosity (45.2 vol%) at P_{O_2} of 1.8×10^{-11} atm. The proppant sintered at P_{O_2} of 1.7×10^{-13} atm is characterized by smaller pores (26 µm), higher density (1.72 g/cm^3) and lower porosity (37.5 vol%). Crush resistance testing at 9,000 psi yields 6.8 wt% fine particles increasing to 17.7 wt% in porous samples. Acid solubility varies from 5.5 wt% loss increasing to 12.9 wt% in porous samples.

Task 4 and 5) The microbial consortia obtained from the optimized condition and lightweight proppant were encapsulated by calcium-alginate polymer. The encapsulation system, including microbes and a proppant, was stored at 20°C and 36°C. The sample stored at 36°C generated 7.1×10^3 ppm of methane at 670 h, whereas the sample incubated at 20°C generated 1.1×10^3 ppm of methane. Benchtop lab-scale bioreactors were constructed and showed with real-time measurements that, as the microbes produced methane, the pH decreased, and hydrogen and carbon dioxide gases were consumed. A calcium ion-selective sensor revealed the release mechanism of the microbes from encapsulation. The calcium ions interconnecting the alginate monomers were disassociated by counter cations such as protons and potassium ions. The counter cations bound to the carboxyl group on the alginate monomer, which thus lost its ionic interactions with the calcium ions, resulting in decomposition of the hydrogel structure. Furthermore, the conductivity was increased to ~700 mD-ft from ~530 mD-ft once the encapsulated sample was applied to the coal pack. The particle size of coal was reduced when the encapsulated sample was added to the coal. The reduced coal size implied that the microbes would consume the hydrocarbon in coal.

1. Executive summary

Introduction

Unconventional fossil fuel reservoirs - including coalbed methane play - represent an important and often unexploited component of energy production and utilization. These reservoirs can have unique economic challenges because they require specialized, costly recovery techniques. For example, in many instances, coalbed methane reservoirs are too deep to safely, economically and environmentally extract the fossil fuels. Conventional oilfield extraction methods are limited in deep, unmineable coal seams by low permeability and relatively rapid depletion of the adsorbed methane. Coalbed methane wells are abandoned when production is no longer economical even though the vast majority of the resource remains underground (as coal, rather than the comparatively small amount of adsorbed gas that has been produced).

Microbially enhanced methane recovery is an approach to stimulate and accelerate biogenic conversion of fossil fuels to methane by inoculating reservoirs with methanogenic bacteria and nutrients. Production is enhanced by the additional methane production, and by the microbes breaking down waxes and condensates that reduce reservoir permeability. Low-permeability coalbed methane reservoirs are usually exploited by hydraulic fracturing – injection of viscosified fluids with solid propping agents for maintaining fracture aperture after injection has stopped. This proposal describes an approach for developing improved ceramic proppant materials laden with methanogenic microbes to promote microbially enhanced methane recovery. Hydraulic fracturing of coal seams is historically challenging but light-weight, porous proppant materials will have greatly improved fluid transport while also providing a means for delivering methanogenic bacterial consortia and nutrients to the reservoir.

Objective

The goal was to construct a lightweight ceramic proppant particle as a delivery vehicle for microbial consortia (See Figure 1). The delivery vehicle not only performs the role of conventional proppant, but also produces methane by methanogenesis of coal and aids in consuming coal fines which normally reduce proppant pack conductivity over time.

Significant Finding

Coal biogasification was optimal for this consortium at an initial pH value of 5.5, at 30 °C, and at a NaCl concentration 3.7 mg/cm^3 (i.e., 145,165 ppm). For producing lightweight ceramic proppant, under reducing atmosphere at high temperature, the Fe_2O_3 reduces to FeO and reacts with kaolinite decomposed to mullite to form Fe_2SiO_4, $FeSiO_3$, and $FeAl_2O_4$. As a result, the proppant develops large pores. The encapsulated microbe with proppant stored at 36°C generated 7.1×10^3 ppm of methane at 670 h, whereas the sample incubated at 20°C generated 1.1×10^3 ppm of methane. Benchtop lab-scale bioreactors were constructed and showed with real-time measurements that, as the microbes produced methane, the pH decreased, and hydrogen and carbon dioxide gases were consumed. The release of microbes from encapsulated proppant was correlated to enhanced conductivity compared to the proppant without microbes. The conductivity reached ~700 mD-ft at 36^{o}C storage and ~660 mD-ft at 20^{o}C storage. The enhanced conductivity was due to a reduction in particle size as the released microbes consumed the coal particles. The estimated methane production rate was 49 ppm/gram coal/day which was more than twice greater than other laboratory studies.

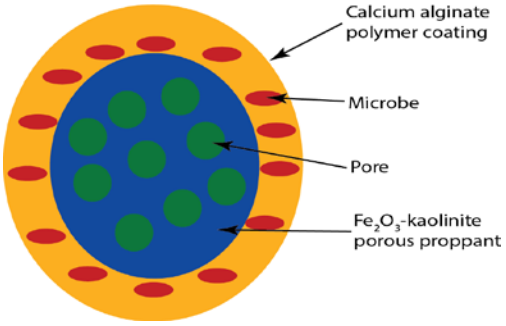

Figure 1. The design of multifunctional lightweight proppant.

2. Report details

2.1. Experimental method

2.1.1. Development of methanogenic microbial consortia from coals

Coals were collected from various provenances in the United States. Proximate and ultimate analyses of these coals are shown Table 1.[1] The coal rank was established by analysis and references.[2-4] The coal rank increases with the amount of fixed carbon, but decreases with the amount of volatile matter and moisture. The nutrient media provided nutrient compounds (e.g., nitrogen, phosphorous) to stimulate microbial growth and methane production.[5] Nutrient media included acetate, phosphate, urea, and a balanced nutrient solution of tryptic soy broth. The specific nutrient media compositions are Table 2.[1] No pH buffer was used, and all of the nutrient media were close to a neutral pH. Additionally, it is noted that acetate can mainly favor the enrichment of acetoclastic methanogens, and/or microorganisms able to use acetate as part of their metabolic functions and likely provide some H_2/CO_2 to hydrogenotrophic methanogens.

Table 1. Proximate analysis, rank, and location of coal samples, and ultimate analysis.[1]

Provenance	Moisture (wt.%)	Ash (wt.%)	Volatile (wt.%)	Fixed carbon (wt.%)	Heating value (Btu/lb)	Coal ranks	Locations
Miller Black Thunder	10.21	6.56	48.23	45.21	11,077	Sub-bituminous	Powder River Basin, WY
NARM Cook	11.31	6.02	47.32	46.66	10,821	Sub-bituminous	North Antelope Mine, WY
North River	1.58	13.26	35.13	51.61	12,811	Bituminous	Alabama, AL
Praxair Illinois	3.36	10.04	39.11	50.85	12,195	High volatile bituminous	Illinois, IL
Red Hills	11.70	24.02	43.74	32.24	8,776	Lignite	AcKerman, MI
Utah Skyline	2.98	8.85	52.79	38.36	12,816	Bituminous	Utah Skyline Mine, UT
Arkansas Lignite	11.10	9.36	58.18	32.46	11,294	Lignite	Arkansas, AR
Waste Coal	1.56	5.04	47.21	47.75	14,690	Bituminous	Deer Creek Mine, UT
Soil	1.69	51.12	28.52	20.36	6,222	N/A	Deer Creek Mine, UT
East Texas	5.01	25.86	49.37	24.77	8,790	Lignite	East Texas, TX

Provenance	Hydrogen (wt.%)	Carbon (wt.%)	Nitrogen (wt.%)	Sulfur (wt.%)	Oxygen (wt.%)
Miller Black Thunder	4.32	67.24	0.99	0.36	20.53
NARM Cook	4.35	67.71	0.98	0.28	20.66
North River	4.75	70.45	1.71	2.08	7.74
Praxair Illinois	4.54	67.15	1.34	3.59	13.34
Red Hills	3.72	51.56	1.09	0.85	18.76
Utah Skyline	5.11	71.12	1.50	0.56	12.87
Arkansas Lignite	5.39	63.34	0.88	1.20	19.83
Waste Coal	5.60	74.63	1.46	0.44	12.84
Soil	5.46	36.53	0.73	0.52	5.64
East Texas	3.86	51.80	1.03	0.98	16.47

Table 2. The nutrient composition and concentrations of chemicals.[1]

Nutrient compositions	Chemicals and concentrations	Nutrient compositions	Chemicals and concentrations
Sodium acetate -ACE	3.5 g/L	yeast-urea-phosphate medium -YUP	Yeast extract (1.25 g/L) Urea (0.15 g/L) Potassium phosphate monobasic (0.5 g/L)
Tryptic soy broth -TSB	15 g/L	lactate medium -LAC	Yeast extract (1 g/L) Sodium lactate (6.67 mL/L) Sodium acetate (1.23 g/L) Ammonium chloride (0.5 g/L) Potassium phosphate (1 g/L) Magnesium sulfate (0.2 g/L) Calcium chloride (0.1 g/L) Sodium sulfate (0.5 g/L)
Acetate-yeast-phosphate medium -AYP	Sodium acetate (2.5 g/L) Yeast extract (0.75 g/L) Potassium phosphate monobasic (0.5 g/L)		

All samples were kept at 23ºC to emulate the temperature of the natural habitat where microbial populations

were collected. Sterile, 50-mL centrifuge tubes were used as the bioreactors in all phases of the screening program. These were set aside without agitation over the prescribed reaction periods. Two-hundred microliters (200 ml) of produced gas were directly extracted under sterile conditions using a gas-tight syringe through a small hole in the caps that were completely covered with silicone gel. Silicone was periodically reapplied to the end caps to prevent leakage. Methane production was monitored in the headspace of the bioreactors using gas chromatography. Carbon dioxide was also measured because the carbon dioxide itself can be a valuable byproduct in-situ, and preferential CO_2 adsorption may enhance methane recovery from treated coal. Unless specified, control samples were created by adding sterile normal saline solution (8.5 g/L NaCl) to the respective coal samples and sediments. Gases measured from these controls were hypothesized to be residual gas desorption and/or generation by indigenous microbes.[3] It is conceived that microorganisms need salts to function. Salts provide essential elements (e.g., sodium, potassium) for the formation of new cells.

Screening protocol Phase I. The objective of this first screening phase was to select samples that could produce significant amounts of methane and carbon dioxide. Also, samples that showed unusual qualitative features, such as darkened solution from apparent breakdown of coal after enrichment, were selected for additional evaluation. Five gram aliquots of coal or sediment samples were placed separately into bioreactors. Thirty mL of nutrient medium were added. An initial set of five nutrient amendments was considered. Subsequently, some nutrient media would be selected based on the gas production for the next phase of screening. Duplicate samples were prepared for each coal and sediment aliquot with each nutrient medium. The amounts of sample and nutrient medium were chosen so that about one third of the total volume corresponded to headspace. Samples were incubated for up to 8 weeks. Measurements of headspace gas were taken after 2 weeks and 8 weeks.

Screening protocol Phase II. The objectives of this phase of screening were to keep selected microbial consortia actively stimulated by introducing nutrients for a second time and to refine and select microbial samples that would produce significant amounts of methane and carbon dioxide. Three bioreactors were used, and these contained acetate - ACE, tryptic soy broth - TSB, and lactate - LAC media, respectively. These nutrient media were chosen considering the positive stimulation observed in the preliminary phase of screening, and were used to continue the enrichment of microbes and gas production in this phase. Each bioreactor contained 10 mL of the selected sample, in two 5 mL aliquots, and 20 mL of fresh nutrient solution. These samples were set aside for 14 days. After that time the liquid media were turbid and bubble generation was observed, suggesting possible microbial growth.

Screening protocol Phase III. The objective of this final phase was to continue the enrichment of the microbial consortia with fresh nutrient media. To finally select promising methanogenic populations, the cultivated consortia could adapt to selected coal samples of different rank. Microbial samples were mixed with four coal types and three nutrient media (acetate -ACE, tryptic soy broth -TSB, and lactate -LAC). These nutrient media corresponded to the same type used in the previous phase of screening and were chosen to continue promoting the growth and metabolic activities of the microbial populations. The four coal types were sub-bituminous Miller Black Thunder MBT, bituminous Deer Creek Mine Waste Coal - DCWC, high volatile bituminous Praxair Illinois #6 -PI, and Arkansas Lignite - LIG. These coal samples were chosen to obtain microbial consortia able to use different rank coals and to select the most favorable coal substrates. Five grams of the selected coal types and 20 mL of nutrient media were combined, resulting in twelve bioreactors plus controls for each coal type with added nutrients. Twelve bioreactors were used for samples from the previous screening phase. They are denoted according to the nutrient medium added. For instance, 20 mL of acetate ACE medium and 5mL of sample RH TSB ACE were added into each of four bioreactors containing the four selected coal types. Alternatively, four bioreactors containing the coal types were mixed with 20 mL of tryptic soy broth - TSB and inoculated with 5mL of RH TSB TSB sample. The remaining four bioreactors that were mixed with 20 mL of fresh lactate LAC medium included 5 mL from the RH TSB LAC sample. Incubation periods were monitored for up to 24 weeks. Gas measurements were performed after 2 weeks and 24 weeks of incubation. As mentioned above, three screening phases were carried out to select the most favorable microbial sources, nutrient amendments, microbial consortia, and to identify prolific (in terms of methanogenesis) coal substrates. After each phase of screening, consortia were down-selected for the next phase. A flow diagram that summarizes the screening protocols is shown in Figure 2.

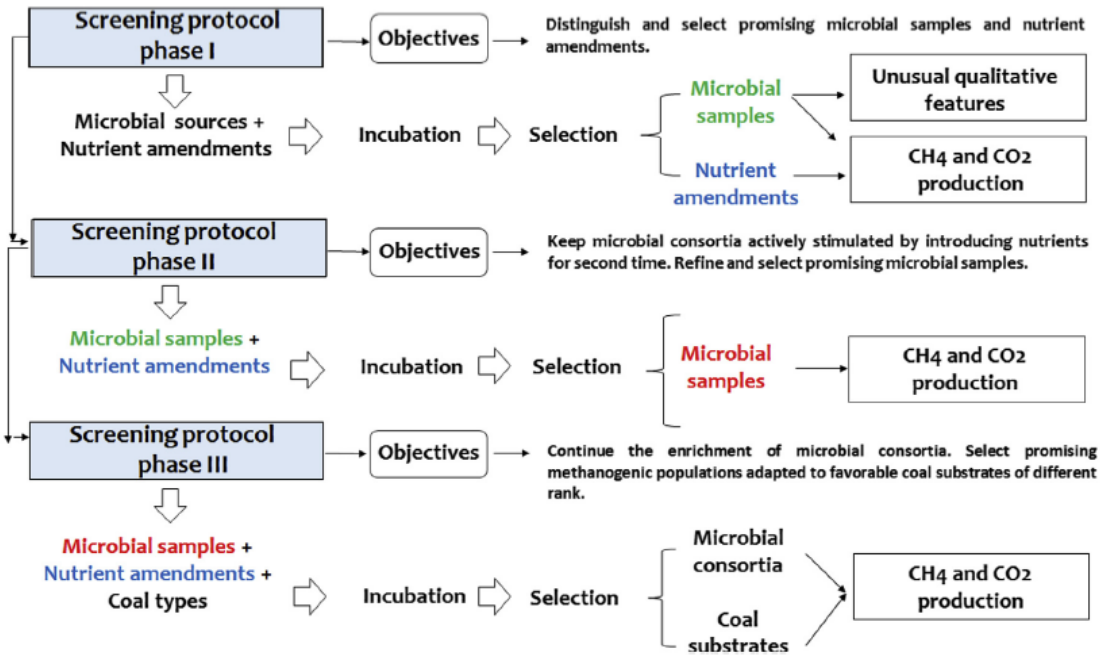

Figure 2. Diagram of screening protocol. The green, blue, and red colors highlight each item used in each stage of the screening protocols.

Methane and carbon dioxide gas measurement. The headspace methane and carbon dioxide concentrations in each bioreactor were determined with a Hewlett Packard HP6890 GC system (Palo Alto, CA) with a GS-GasPro PLOT column containing a bonded silica-based stationary phase. A flame ionization detector (FID) and thermal conductivity detector (TCD) were connected in series to analyze organic compounds and inorganic gases. Helium was used as the gas carrier. The temperature program used for this study began with 35°C for 4 min to allow for carbon dioxide and methane elution and was then increased by 25 °C/min to 260 °C. Scotty Analyzed Gases were used as standards to build calibration curves for methane and carbon dioxide. GC Chem- Station (Agilent Technologies) computer software was used.

Statistical Analysis. Microbial consortia development trends were examined using the statistical software package, STATGRAPHICS Centurion VII. The variance analysis ANOVA of a single factor was used to evaluate the 288 samples that came from Phase III screening. The statistical Kruskal-Wallis test was used to evaluate populations that did not have a normal distribution. This tests the hypothesis that medians of all levels are equal within their corresponding factor. Results or measured values of all levels were combined and ordered from the lowest to the highest, assigning a rank. Subsequently, an average rank was computed for each level, and a p-value was used to evaluate the hypothesis. High and low significances for the methane and carbon dioxide production at two and twenty-four weeks were identified by comparing the average rank, median or mean values

2.1.2. Optimization biogenic methane production from coal

Coal sources. Lignitic Red Hills coal (RH) was used as source of microbial populations during the development of microbial consortium; subbituminous Miller Black Thunder (MBT) coal was used as a substrate in this study. These different rank coal samples were provided by the Industrial Combustion & Gasification Research Facility at the University of Utah, and they were initially used to develop methanogenic microbial consortia able to convert select coal samples into methane under initial atmospheric exposure. The lignitic and subbituminous coal samples were retrieved from AcKerman, MI and Powder River Basin, WY in the U.S, respectively. The experimental program used 6 g aliquots of pulverized Miller Black Thunder (MBT) coal (−140 mesh). These were placed in 50 mL-sterile conical tubes. The conical tubes were used as bioreactors.[1] Arguably, the particle size of the coal can have a significant effect on the biogenic methane production, and the results presented herein may represent a possible and desired scenario. The coal samples

were exposed to air during storage, handling and preparation, which may have also influenced their biodegradability and bioavailability.

Inoculum preparation. The methanogenic consortium used in this work was developed using a three-phase screening program.[1] Briefly, microbial samples were initially collected from various hydrocarbon-rich environments and locations characterized by natural methanogenesis. Among the sources of microbial populations, different rank coals (i.e., lignite, subbituminous, bituminous retrieved from different coal mines), complex hydrocarbon sources (i.e., oil shale, waxy crude), hydrocarbon seeps, and natural biogenic environments were incorporated in the sampling. Three screening phases were implemented to select microbial samples that produced large amounts of methane under initial atmospheric exposure. Enrichment with favorable nutrient amendments as well as a final adaptation step to selected coal sources was carried out. This demonstrated that methane generating microbial communities from available sources (e.g., coal and lake sediments) can be sequentially enriched and adapted through a matrix of screening/high grading steps. Microbial consortia can be developed that could have commercial viability. Since groundwater associated with coal was excluded from the above screening program, it is unlikely that all the known methanogenic pathways (i.e., acetoclastic methanogenesis, hydrogenotrophic methanogenesis, and/or methylotrophic methanogenesis) in coal can be present. As part of the described study, a promising microbial consortium was chosen to carried out this subsequent investigation. This selection was made on the basis of the high methane production during the performed screening protocols.[1] Microbial populations within the chosen consortium comprised indigenous microbial populations from Red Hills lignite (RH) coal enriched with tryptic soy broth (TSB) and subsequently adapted to subbituminous Miller Black Thunder (MBT) coal for approximately twenty-four weeks. The described experimental program was used to label this consortium as RTTM. These adapted microbes were separated from the enriched culture and were maintained in 15 g/L tryptic soy broth at 30°C for 25 days. Aseptic microbiological techniques were used for all procedures reported herein.[3]

Prior to inoculation of the bioreactors, the microbial consortium was washed with a sterile saline solution - 8.5 mg/cm$_3$ NaCl - to remove any remaining nutrient media. An initial cell concentration of 2.0×10^7cfu/mL was determined by colony counting on TSA plates. Aerobic, aerotolerant and "culturable" organisms were particularly counted.[5] An aliquot of this culture was used for DNA extraction. DNA was extracted and purified using a PowerSoil DNA Isolation Kit (MoBio, Carlsbad, CA) in accordance with the manufacturer's protocols. Subsequently, analysis and identification of microbial communities were performed using a 16S rRNA gene-based amplicon sequencing at the Research and Testing Laboratory (Lubbock, TX, USA). A 97% of similarity was reported for identification of microbial populations.

Media preparation for bioreactors. Four mL of inoculum, 8.4 mL of sterile tryptic soy broth (15 g/L), and 12.6 mL of sterile sodium chloride solution were added into individual 50 mL-bioreactors each containing six grams of subbituminous Miller Black Thunder (MBT) coal. An approximate free headspace of 17.5 mL was obtained. Duplicate samples were prepared and simultaneously evaluated with two control types. Type I control samples included NaCl solution plus coal material. It is hypothesized that gases measured from these controls corresponded to residual gas desorption and/or generation from indigenous microbes.[1, 3, 5] Type II control samples included the microbial consortium plus the nutrient and the NaCl solution. These controls were used to consider gas production by the microbial consortium from the added nutrients. The concentration of the sodium chloride solution was fixed according to the design of experiments (Table 3): a sodium ion selective electrode (Thomas Scientific® model 3401BN) attached to a benchtop multiparameter meter (Thermo Scientific Orion, VSTAR00 VERSA STARMT) was initially used to estimate sodium concentration in coal, nutrient amendment and inoculum. Before inoculation, pH levels of the liquid solutions (i.e., nutrient plus NaCl solutions) and the coal samples were established. Subsequently, pH levels were double checked after inoculation with a sterilized and continuously calibrated pH soil probe (PROBSOIL, Bluelab Corporation Limited- New Zealand). Solutions of hydrochloric acid 2.4 N and potassium hydroxide 5.0 N were prepared to adjust pH levels. The bioreactors were set aside in the dark without agitation during incubation. Unless otherwise specified, gas measurements were conducted every fifteen days for two and a half months in order to identify overall trends of methane production. Gas chromatography was used for this purpose. Considering that effective methanogens can have longer regeneration times and slower growth than other microorganisms involved in the biotransformation of complex organic matter, long periods of consortia incubation were

initially evaluated. After the prescribed periods of reaction, two hundred microliters (200 µL) of produced gas were directly extracted under sterile conditions using a gas-tight syringe (Hamilton 1725, Hamilton Robotics, Reno, NV) through a small hole in the cap that had been completely covered with silicone gel. Silicone was periodically reapplied to the end caps to prevent leakage. In addition to this precautionary measure, the bioreactors can be visually checked by spreading a solution of gas leak detector and checked for bubble generation (ASTM E515-05, 2005). To allow the microbial communities to evolve under initial atmospheric conditions that would be like those during their development, the bioreactor headspace was not spared with nitrogen gas and reducing agents (e.g., Na_2S, cysteine-HCL) were not used. These initial conditions were intentionally chosen. This demonstrated the consortium's ability to survive and still produce methane at low to moderate oxygen concentrations during the experimental program. This can be an important consideration for use in field scale operations (e.g., ex-situ and/or in-situ scenarios) where oxygen exposure is anticipated.

Table 3. Central composite design with results.

Run #	Factors			Y_{CH4} - Experimental				
	T (°C)	NaCl (mg/cm^3)	pH	15 days	30 days	45 days	60 days	75 days
1	39	39	7.2	0.0609	0.0582	0.0769	0.0355	0.0046
2	39	39	7.2	0.0559	0.0633	0.0664	0.0350	0.0585
3	39	39	7.2	0.0584	0.0627	0.0598	0.0344	0.0348
4	30	18	5.4	2.6442	3.1832	7.2265	21.278	0.0447
5	48	18	5.4	1.0272	10.765	5.5308	0.0521	0.0714
6	30	60	5.4	0.0520	0.0592	0.0677	0.0645	0.0664
7	48	60	5.4	0.0538	0.0626	0.0440	0.0557	0.0566
8	30	18	9.0	0.0620	0.0601	0.0309	0.0343	0.0651
9	48	18	9.0	0.0563	0.0499	0.0454	0.0421	0.0415
10	30	60	9.0	0.0531	0.0476	0.0506	0.0334	0.0033
11	48	60	9.0	0.0464	0.0522	0.0690	0.0561	0.0573
12	23	39	7.2	0.0604	0.0680	0.0743	0.0010	0.0665
13	54	39	7.2	0.0783	0.0697	0.0703	0.0612	0.0681
14	39	3.7	7.2	11.147	60.149	37.484	100	51.335
15	39	74.3	7.2	0.0554	0.0612	0.0585	0.0545	0.0600
16	39	39	4.2	0.0561	0.0562	0.0532	0.0419	0.0515
17	39	39	10.2	0.0437	0.0536	0.0559	0.0568	0.0539

Parameter selection. Based on preliminary studies of aerotolerant methanogenic consortia, the main factors that significantly affect microbial growth and methane production from coal are temperature, salt concentration and pH. Additionally, these variables are among the main regulating factors of methanogenesis. Considering the importance of these selected factors on coal biogasification, a parametric space that includes maximum methane production was experimentally defined. A broad range of operational conditions was initially chosen:

- NaCl concentrations were varied from 3.7 mg/cm^3 to 74.3 mg/cm^3.
- pH values of the culture medium ranged between 4.2 and 10.2.
- temperatures were varied from 23 °C to 54 °C.

Central composite design. To determine a region of operation and broadly explore the effects of temperature, pH and NaCl concentration, a central composite design (CCD) was used. Gas concentrations were expressed as percentage of the maximum experimental methane concentration (76,000 ppm). This percent concentration was defined as the response variable – YCH4 to facilitate computational analysis. Preliminary studies have shown non-linear response of methane production when these important environmental factors were examined. Thus, a quadratic model was adopted as an initial approach to describe the relationships between these selected factors and methane production. This non-linear mathematical model is known to be a flexible and simple model that can take multiple functional forms.

The central composite design contained a factorial set of 23 experiments with 3 center points and 6 axial points for estimation of curvature. These axial points established extrema for the low and high settings for all factors. A total of 17 experiments were defined (Table 3). The number of experimental runs at center point, and the distance of axial points (α= 1.682) were chosen according to a rotatable design. CCD has a spherical symmetry and requires 5 levels for each factor. This allows exploring a large process space with a reduced number of

experiments. The three factors describe a sphere around a factorial cube determined by the factorial set. This experimental design provides the highest quality of predictions over the entire design space. The statistics software package STATGRAPHICS Centurion VII® was used to create the experimental design, perform regression analysis of the data obtained, and to estimate the coefficients of the model equations. Additionally, MatLab® was used for complementary graphical analysis. The analysis of variance ANOVA was conducted in order to obtain interaction of the process variables with the response variable. The overall predictive capability of the model equations was expressed by the coefficient of determination – R^2.

Determination of a region of operation. A feasible region of operation for the selected factors was sought. Methane concentrations were measured over time and analyzed with STATGRAPHICS Centurion VII®. This captured the main trends of gas production and identified important effects of the factors evaluated. Empirical models were generated at selected times. MatLab® was used as a complementary tool to visualize the predictions from the regression equations using a three-dimensional graph (i.e., scatter 3 – 3D scatter plot), and to graphically estimate a feasible region of operation: model predictions were stored and organized from the smallest to the largest value. This procedure accounted for the levels of the factors and the time when gas measurements were made. The obtained region of operation included model predictions for up to sixty days of incubation – the period where the largest methane production was measured and the "best-fitted" regression equations were found.

Verification of methane production from the predicted region of operation. To verify the predicted "sweet spot" for methane production, additional experiments were conducted. Three 50 mL-bioreactors were used. The main bioreactor contained six grams of subbituminous Miller Black Thunder coal (MBT), 8.4 mL of nutrient solution (TSB), 4 mL of inoculum with an initial cell concentration of 2.5×10^6cfu/mL, and 12.6 mL of sterile NaCl solution. An approximate free headspace of 17.5 mL was obtained. The salt concentration and pH were fixed at 3.7 mg/cm^3 and 5.5, respectively. Two control samples were also used under the same environmental conditions: The Type I control sample included NaCl solution plus coal material, and the Type II control sample included microbial consortium plus nutrient and NaCl solution. These bioreactors were kept at 30 °C in the dark. They were not agitated and were monitored over time for headspace methane production.

2.1.3. Synthesis of porous ceramic proppant

Kaolinite ($Al_2Si_2O_5(OH)_4$, natural) and iron oxide(Fe_2O_3, $\geq 99\%, < 5$ μm powder) were purchased from Sigma-Aldrich (St. Louis, MO). Kaolinite and iron oxide (0 wt%,5 wt%, 10 wt%, and 15 wt%)mixtureswere mixed in acylindrical chamber (diameter 13 in × height 15 in). Samples at 10 wt% and 15 wt% of iron oxide were unsuitable for further tests due to extensive agglomeration during sintering. The total weight of each mixture was 120 grams. Deionized (DI) water (200 mL) and ball milling zirconia media were added to the chamber for milling at 60 rpm atroom temperature for 24 hours. Then, while the chamber was rotating at 60 rpm, a30-cm ruler was placed in the chamber to obtain the spherical particles. The ruler contacted the bottom of the chamber while providing a smallspace on the side through which particles could pass. The spherical particles were selected by size using 20 mesh and 40 mesh sieves.The mixture was sintered at 1523 K, 1623 K, and 1723 K for 40 minutes with constant heating and cooling rates of 10 Kper minute. A wide range of P_{O_2} was used for reducing atmospheres and the actual P_{O_2} was determined by the sintering temperature. We achieved the range by mixing hydrogen (H_2, 20%) and nitrogen (N_2, 80%) bubbled through water, held at constant293 K. The following equation was used to calculate the partial pressure of oxygen in the reducing atmosphere (P_{O_2}):[6]

$$p_{O_2}(T) = \left(\frac{p_{H_2O}(T_b)}{p_{H_2}}\right)^2 exp\left(\frac{2\Delta G^0}{RT}\right) \quad (1)$$

where $P_{H_2O}(T_b)$ is the vapor pressure of water at a given temperature (T_b). In this study, the temperature (T_b) is 273 K. P_{H_2} is the partial pressure of hydrogen, R is the gas constant, and T is the sintering temperature in the furnace.ΔG^0 is the standard Gibb's free energy of formation of water from hydrogen and oxygen reactants which has the following temperature dependence:[6]

$$H_{2(g)} + \frac{1}{2}O_{2(g)} = H_2O_{(g)} \quad (2)$$

$$\Delta G^0(J/mol) = -246{,}000 + 54.8T \quad (3)$$

2.1.4. Characterization and performance of the porous proppant

Microstructure characterization. X-ray diffraction (XRD, D2 Phaser, Bruker Co., Billerica, MA) and full-pattern Rietveld refinement using GSAS-II software [7] was used to determine quantitative phase fraction of proppant synthesized under various conditions with Cu Kα radiation operated at 30 kV, 10 mA, and 1.0 mm slit.A scanning electron microscope (SEM, Quanta 600, FEI Co., Hillsboro, OR) was used to observe the microstructure and morphology of the proppant. For cross-sectional microscopy sampleswere mounted in epoxy and polished(TegraPol-11, Struers, Cleveland, OH) using 120, 600, 1200, and cloth grits (MD Piano and MD/DP-Nap, Struers, Cleveland, OH). Measurements of pore size were repeated on three different samples for each temperature and composition studied.

Density measurement. The Archimedes method was used to measure the bulk density of the proppant.[8] American Petroleum Institute (API) recommends the proppant roundness and sphericity for high strength greater than 0.7.[9] The specific roundness and sphericity of proppant were selected for the test following the API recommendation.The sample was dried in an oven at 373 K for 24 hours and then cooled to room temperature. The dried sample mass was determined (m_1). The dried sample was then immersed in boiling water for 30 minutes until the open pores were filled with the immersion liquid. A hydrostatic balance was used for measuring the mass of the sample (m_2) suspended in water at 293 K. The sample was placed in air, and the remaining liquid on the surface was removed with a damp sponge. The mass of the sample was then measured in air (m_3). Using the density of water (ρ_w) at 293 K, the bulk density (ρ) was calculated as follows: [10]

$$\rho = \left(\frac{m_3}{m_2 - m_1}\right) \times \rho_w \quad (4)$$

Crush resistance. A customized crush cell was usedfor the crush resistance test. The cell is a cylindrical vessel made of 306 stainless steel. The dimensions of the cell were 1 inch (inner diameter) × 2 inches (outer diameter)× 7 inches (height). Normal stress was applied by an Instron load frame (5969, Norwood, MA).
Table 4 shows the calibration of customized apparatus using commercial proppant (SinterBall Bauxite 20/40, Sintex International and North America, Rosenberg, TX). The proppant size was 20/40 (passing a number 20 sieve and retained by a number 40 sieve). The same selective roundness and sphericity of proppant was tested as the density measurement. The sample proppant (4 lb/ft2 on the piston area) was loaded into the cell, and the compressive pressure was increased to 9,000 psi (2,000 psi per minute) and held for 2 minutes. After crushing, the sample was removed and sieved to a 20/40 mesh (420 μm to 841 μm) to separate fines generated during crushing.[11] The fines that passed through the 20/40 mesh were weighed to determine weight fraction of fine generation upon crushing:

$$\text{Fine wt\%} = \frac{W_f}{W_t} \times 100\% \quad (5)$$

where W_f was the weight of fine particles after the crush test and W_t was the weight of proppant recovered from the cell.

Table 4. The crush resistance results of the commercial proppant for calibrating the customized apparatus.

	Fine particles (<40 mesh) after crush test	
Applied compressive stress at 2,000 psi/min.	Published data[12]	Tested by the customized apparatus
12,500 psi	2.1 wt.%	2.2 (+/- 0.1) wt.%

Acid solubility. Acid solubility was assessed to determine the chemical stability of the prototype proppant

following the American Petroleum Institute Standard Test (API RP 56).[13] The same selective roundness and sphericity of proppant was tested as the density measurement. The proppant sample (5 g) was dried in oven at 378 K overnight. The dried sample was soaked in a mixture of hydrochloric acid (HCl, 36.5 – 38.0% AR A.C.S. Reagent Grade, Macron Fine Chemicals TM Products, Avantor Performance Materials, LLC., Center Valley, PA) and hydrofluoric acid (HF, 48.0 – 51.0% Baker Analyzed® A.C.S. Reagent, J.T.Baker® Chemicals, Avantor Performance Materials, LLC., Center Valley, PA) at 339 K for 30 minutes without stir. The volume ratio of HCl and HF was 12 to 3. The total volume was 100 mL. In the industry jargon this is known as mud acid. After 30 minutes, the proppant sample was washed with de-ionized (DI) water and dried in the oven at 378 K overnight.[11] The sample was weighed after it was dry. The solubility(s)was calculated as follows:[11, 13]

$$s = \left(1 - \frac{m_f}{m_i}\right) \times 100\% \quad (6)$$

where $m_i$is the initial weight of sample before acid solubility test, and $m_f$is the weight after the test.

2.1.5. Encapsulation process and methane production from release bacteria

Materials. Calcium lactate and sodium alginate were purchased from WillPowder (Miami Beach, FL). Kaolinite (natural), iron oxide (Fe_2O_3, purity (≥ 99%), particle size (< 5 μm)), rhodamine 6G, and tryptic soy broth (TSB) were purchased from Sigma-Aldrich (St. Louis, MO). The coal was obtained from the Powder River Basin (Arch Coal Inc., WY). The specific particle size of coal was selected to 140 mesh. Hydrogen (MQ-8) and methane (MQ-4) gas sensors were integrated into an Arduino circuit board (Redboard) all purchased from SparkFun Electronics (Niwot, CO). The carbon dioxide gas sensor (CO2-BTA) was purchased from Vernier Software and Technology (Beaverton, OR).

Ultralight Kaolinite Proppant Synthesis. Kaolinite (120 g) and iron oxide (6 g) were milled at 60 rpm for 24 hours at room temperature with deionized water (120 mL) and zirconia milling media (60 g). Then, while the chamber was rotating at 60 rpm, a 30-cm ruler was placed in the chamber to obtain the spherical particles. The ruler provided a small opening on the side of the chamber through which particles could pass which were roughly spherical in shape. The sample was sintered in a tube furnace (TF 1700, Across International, LLC, Livingston, New Jersey, USA) at 1450°C for 40 minutes. The heating and cooling rates were 10°C/min. The proppant was sintered in a reducing atmosphere at 3.60×10^{-13} atm P_{O_2}.[14] The sintered particles were then sieved (passing through a 20 and retained on a 40 mesh).

Optimization of encapsulation time and encapsulation efficiency. 100 mg of these customized, porous proppant particles were added to a calcium lactate solution (10 mL, 2 wt%, pH 7). The encapsulation was prepared by dripping the mixture of proppant and lactate solution using a 200-μL syringe into 10 mL of sodium alginate solution (0.5 wt%, pH 7) stirred continuously at 300 rpm for different periods of time ranging from 10 s to 600 s. The encapsulated particles were transferred to DI water and soaked for one minute. The chelation reaction of calcium alginate polymer and a schematic of the encapsulation process are shown in Figure 3. The particle size was measured by optical microscopy. To determine encapsulation efficiency a dye molecule, rhodamine 6G, had been included in the proppant/calcium lactate mixture at a concentration of 10 μM. After the encapsulated proppant was removed from the sodium alginate solution, the concentration of residual dye in the alginate solution was determined by using Beer-Lambert's law. The absorption spectra were obtained with an ultraviolet-visible spectrophotometer (UV-Vis, Lambda 950, PerkinElmer, Waltham, MA, USA). The efficiency of encapsulation (α) is calculated as follows:

$$\alpha = \frac{[\mathrm{R6G}]_i V_i - [\mathrm{R6G}]_f V_f}{[\mathrm{R6G}]_i V_i} \cdot 100\% \quad (7)$$

where $[\mathrm{R6G}]_i$ is the concentration of the loaded rhodamine 6G dye (10 μM) in the calcium solution, V_i is the volume of calcium lactate, $[\mathrm{R6G}]_f$ is the non-encapsulated dye concentration in the alginate solution, and V_f is the volume of alginate solution. The calibration experiment expresses the dye concentration as a function of absorbance intensity and shows typical Beer-Lambert law behavior.

Time release of rhodamine 6g from encapsulation. For the time release experiment, the concentration of rhodamine 6G in calcium lactate solution was 0.57 mM, and the polymerization time was 600 s corresponding to an encapsulation particle size of 2.8±0.1 mm in diameter. Three encapsulated particles were placed in the bottom of a 2 mL quartz cuvette. The height of the cuvette was adjusted to avoid light scattering of the incident beam. The desired solution was added to the cuvette. The added solution was DI water with pH ranging from 4 to 11 or KCl with solution ranging from 13 mM to 46 mM at a fixed pH 7.2. The rhodamine 6G, released from calcium-alginate encapsulation, was measured by UV-Vis spectroscopy at 528 nm (λ_{max}) every 60 s for 13 h. To understand the release mechanism from the encapsulation system, a calcium ion-selective electrode (CA-BTA, Vernier, Beaverton, OR) measured the free calcium ion concentration during release, corresponding to the Ca^{2+} dissociated from the encapsulation matrix. The dissociated calcium concentration was measured under two conditions: in DI water (pH 7.2) and in a KCl solution (30 mM and pH 7.2).

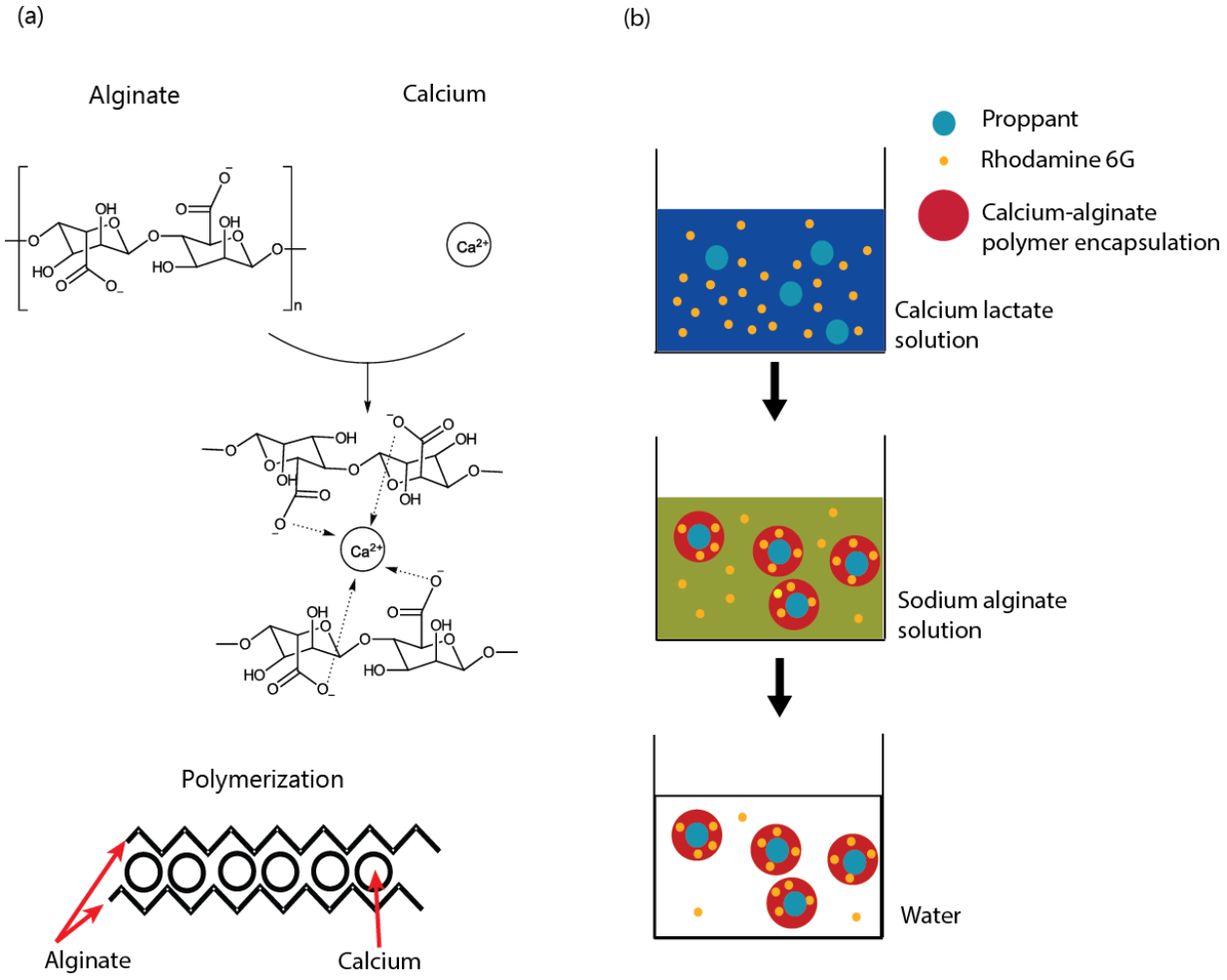

Figure 3. Schematics depicting calcium alginate polymerization (a) and the encapsulation process (b). Figure a adapted from reference.[15]

Time release of microbe from encapsulation. Microbial growth and washing processes were performed following the procedures of Fuertez, et al.[16] The washed microbial solution (10 mL) and proppant (100 mg) were added to a calcium lactate solution (10 mL) for 30 minutes. The encapsulation was prepared as in the previous section. Three particles (2.8±0.1 mm in diameter) were added to a 2 mL cuvette filled with DI water. 50 µL of the solution in the cuvette were collected approximately every 2 hours and added to a 2 mL quartz cuvette. The total volume was adjusted to 2 mL using DI water. UV-Vis measured the absorbance at 600 nm. The temperature of sample and cuvette was maintained at 20°C and 36°C using hotplates. A calibration curve was used to calculate the concentration of free (non-encapsulated) bacteria. The calibration curve of absorbance at 600 nm for cell counts. The number of microbe was determined by using the direct microscopic count method.[17]

CH_4 and CO_2 gas measurement in simulated in situ environment. The experiment was scaled up by a factor of 50 compared to the amounts given in section 2.5. One control and two samples were prepared in 50 mL conical tubes for subsequent methane and carbon dioxide measurement. Each conical tube included the autoclaved coal (5 g, 140 mesh), tryptic soy broth nutrient (TSB, 15 g/L, 8 mL, pH 7), and sodium chloride (NaCl, 2.6 g/L, 13 mL, pH 7). The sample tubes included 5 g of the encapsulated microbe-laden proppant prepared from section 2.5, while the control did not. One sample and control tubes were maintained at 20°C, and the second sample tube was maintained at 36°C. Periodically, gas chromatography (HP6890, Hewlett Packard, Palo Alto, CA) was performed to assess CH_4 and CO_2 concentrations in the tube headspace by extracting 200 µL of gas in the headspace via gastight syringe (Hamilton 1725, Hamilton Robotics, Reno, NV).

Real-time measurement in simulated in situ bioreactors. Bioreactors for samples scaled up by a factor of four relative to the previous section were prepared in 1L 4-neck flasks. The pH, hydrogen, carbon dioxide, and methane concentrations were monitored with automated sensors controlled by a LabVIEW program. Each flask was stored at the desired temperatures (20°C and 36°C) as in the previous section and the mixture was stirred at 300 rpm. Gas concentrations and pH were sampled every 30 minutes over a period of 250 hours.

2.1.6. Conductivity and coal characterization

Materials. Calcium lactate and sodium alginate were purchased from WillPowder (Miami Beach, FL). Kaolinite ($Al_2Si_2O_5(OH)_4$, natural) and iron oxide (Fe_2O_3, purity (≥ 99%), (< 5 µm)) were purchased from Sigma-Aldrich (St. Louis, MO). The 100/120 mesh coal was obtained from the Powder River Basin region (Arch Coal Inc., WY).

Synthesis of ultralight proppant. The lightweight proppant was prepared as the previous study.[14] Kaolinite and iron oxide (5 wt%) were mixed in a cylindrical chamber (diameter 13 in × height 15 in). The total weight of each mixture was 120 grams. Deionized (DI) water (200 mL) and ball milling zirconia media were added to the chamber for the milling at 60 rpm at room temperature for 24 hours. Then, while the chamber was rotating at 60 rpm, the 30-cm ruler was placed in the chamber to obtain the spherical particles. The ruler contacted the bottom of the chamber while providing little space on the side. The spherical particles were selected by size using the 20 mesh and 40 mesh sieves. The particles were sintered at 1450°C for 40 minutes with constant heating and cooling rates of 10°C per minute. The reduced atmosphere was achieved by balancing hydrogen and water. The mixed gas of hydrogen (H_2, 20%) and nitrogen (N_2, 80%) bubbled through water, held at constant 20°C.

Encapsulation of microbe and proppant. The bacteria for methane generation were cultured from the coal and grown for 30 days.[18] The bacteria were washed by the normal saline solution (NaCl, 8.9 g/L, pH 7.0) three times. The washed bacteria (20 mL, pH 7.0) were added to calcium lactate solution (2 g/L, 20 mL, pH 7.0). The proppant particles (9 g, 20/40 mesh) were immersed in the mixture for 30 minutes at room temperature to adhere the bacteria on the proppant surface. The proppant particles were transferred to sodium alginate solution (0.4 g/L, 20 mL, pH 7.0) by using a metal screen. The screen had the 300 µm hole size. The alginate solution was stirred at 300 rpm for 30 minutes at room temperature. The calcium-alginate polymer encapsulated the bacteria and proppant during the polymerization. Then, the encapsulated sample was transported to DI water at pH 7.0 and stirred at 300 rpm for 10 minutes to terminate the growth of polymer. The encapsulated sample was dried in air at room temperature overnight. The hydrogel became to solid thin film coating on the proppant surface. To verify the bacteria were released from the thin film encapsulation, the dried sample was suspended in the normal saline. The suspension was cultured in plate and stored at 10°C from 2 days to 10 days. The bacteria were released from the encapsulation showing the culture color (Figure 4).

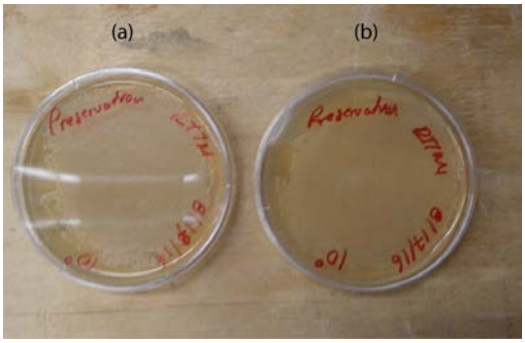

Figure 4. The color became darker as increasing the population of bacteria from (a) 2 days to (b) 10 days storage at 10°C.

Hydraulic conductivity measurement. Hydraulic conductivity was performed with a coal pack and encapsulation particles at ambient pressure. Three groups were prepared: 1) control at 20°C, 2) sample at 20°C, and 3) sample at 36°C. The control group contained the coal and water. The sample groups included the coal, water and encapsulation particles. The same coal, collected from Powder River Basin, was autoclaved at 120°C to remove bacteria. The autoclaved coal (1.2 g or 0.1 lb/ft^2), the encapsulation particles (9 g or 0.7 lb/ft^2), and DI water (pH 7.0, 2.5 mL) were added to the cylindrical chamber (5 cm height and 1.5 cm inner diameter). To prevent sweeping the coal and proppant away, 140-mesh metal screens were placed in both ends of the chamber. Each group prepared 27 chambers, stored in water bath controlling the desired temperatures at 20°C and 36°C. The conductivity was determined every 7-10 days. Three chambers were used in each measurement and averaged the results with standard deviation. The differential manometer measured the injected and flow-out water in hydraulic pressure (Figure 5). The samples were set in Figure 6. DI water was flown through the chamber for 24 hours at 0.1 cm^3/min to obtain the stable conductivity. The water was constantly pumped at 0.1 cm^3/min during measurement. The Darcy's law was employed to calculate the conductivity:[19]

$$C = kw = \mu \frac{L}{B} \frac{q}{\Delta P} \quad (8)$$

where C is conductivity (mD-ft), k is permeability (mD), w is fracture width (cm), μ is viscosity of water (Pa · s),L is conductivity cell length (cm), B is conductivity cell width (cm), q is flow rate (cm^3/min), ΔP is differential pressure drop (psi).

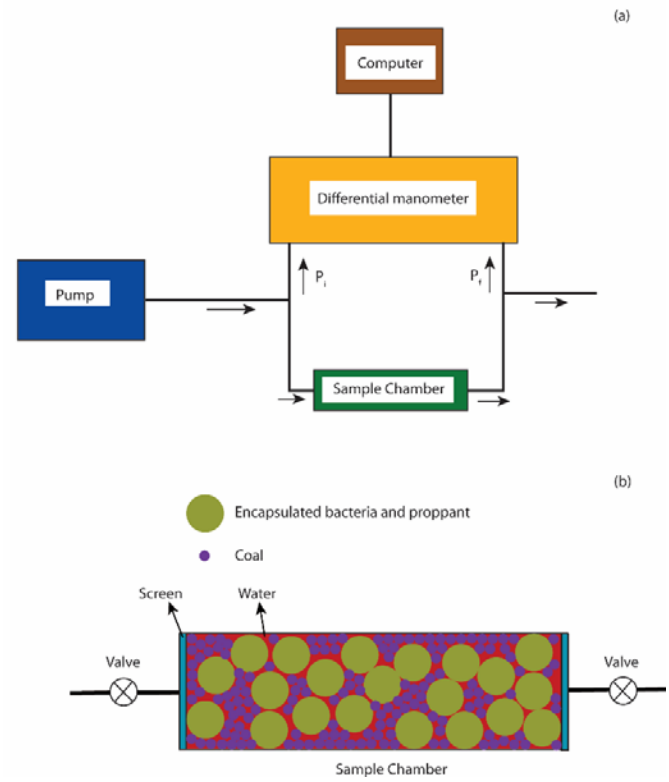

Figure 5. (a) The conductivity experimental setup and (b) assembled encapsulated sample, coal, and water in the chamber.

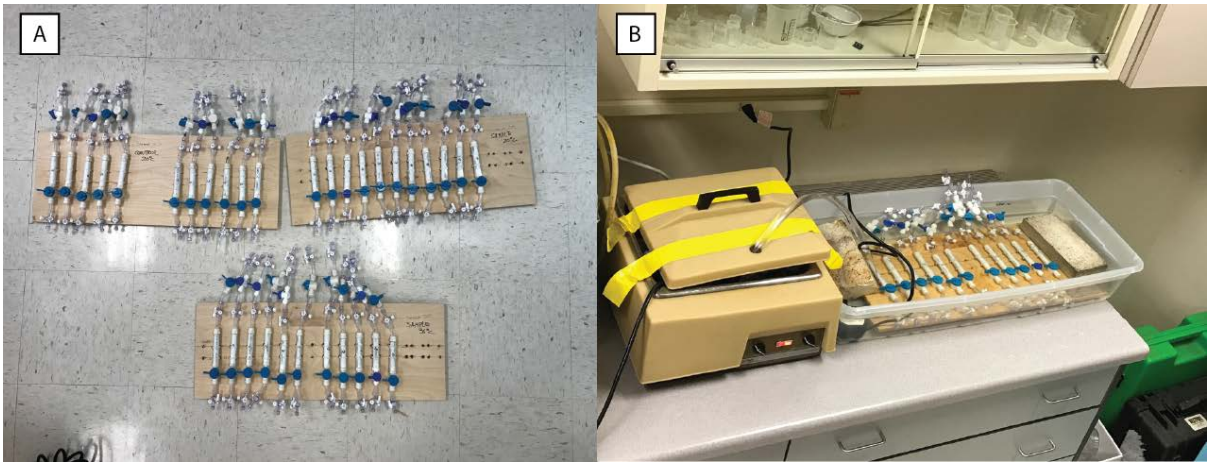

Figure 6. A) Three sets of conductivity test: the control at room temperature and the samples at room temperature and 36°C. B) The conductivity samples at 36°C in the water bath.

Characterization of coal. For characterization, the coal, used in the conductivity, was dried at 120°C for 24 hours. For Fourier transform infrared spectroscopy (FT-IR, Varian 3100, Varian, Palo Alto, CA), attenuated total reflectance (ATR,GladiATR™, Pike Technologies, Madison, WI) was employed with 100 scans and 4 cm^{-1} resolution. Thermogravimetric analysis (TGA) determined the weight change of coal after bacteria were released for 6 weeks. The coal (24 mg) was loaded to the instrument and the weight change was monitored at 5°C/min. The microstructure was observed by scanning electron microscope (SEM, TM3030Plus, Hitachi America, Ltd., Tarrytown, NY). The microporous structure of the coal samples was obtained through N_2 adsorption measurement using Gemini V (Micromeritics, Norcross, CA). The sample was degassed at 140°C for 4 h under N_2 atmosphere. The specific surface area was calculated by Brunauer-Emmett-Teller (BET),[20] and the specific pore volume and size were calculated by Barrett-Joyner-Halenda (BJH).[21]

2.1.7. Production rate of methane and nutrient/production cost

We have investigated the optimization of microbial consortia to produce methane in simulated in-situ conditions. Additionally, the proppant encapsulated with microbial consortia was tested for methane production under simulated in-situ conditions. It is a challenge to mimic all of the conditions present in actual deep subsurface reservoirs in a laboratory condition. In our studies we could carefully control variables such as salinity, pH, and temperature. However, we have not probed the influence of pressure on microbial activity in this lab scale test study. Furthermore, laboratory experiments were conducted with crushed coal having a large net surface area. Therefore, our observed reaction rates could be higher than the uncrushed or solid coal existing in reservoirs. We believe reaction rates were controlled by total surface area, indicating the amount of the generated gas was proportional to the surface area. Thus, the calculation of production rate (R) was simplified as follows:[1]

$$R = \frac{M}{W \cdot t} \quad (1)$$

where M is the measured gas concentration, W is the added coal in gram, and t is time in day. Table 3 shows the calculated production rate of methane. Furthermore, the nutrient/production cost was estimated by the material price from vendors which we purchased, and the labor time was determined by stop watch.

2.2. Results and discussions

2.2.1. *Development of methanogenic microbial consortia from coals*

Phase I screening. At 2 weeks of incubation, methane concentrations less than 4800 ppm were measured for most of the evaluated coal samples. Control samples showed much lower concentrations - up to 25 ppm. On the other hand, during this initial 14-day, CO_2 production was significant. For example, up to 400,000 ppm were measured with lactate -LAC medium and the sub-bituminous Miller Black Thunder MBT coal (Figure 7). Modest carbon dioxide concentrations up to 76,000 ppm were also measured from the control samples. The occurrence of these carbon dioxide concentrations from the different coal rank samples and nutrient media likely indicated rapid stimulation of microbial populations, despite the small volumes of methane production.

After 8 weeks of incubation, significant methane was generated in the bioreactors that included coal samples. For instance, methane concentrations up to 640,000 ppm were measured for Deer Creek Mine Waste coal with lactate media, while concentrations less than 256 ppm were determined from the control samples (Table 4). This suggests that commercially viable methane production is possible. The bioconversion of complex organic substrates into methane is thought to incorporate multiple processes. These include solubilization, hydrolysis, acidogenesis, acetogenesis, and methanogenesis. Interactions among various microbial communities take place, and the processes are characterized by different growth rates, and metabolic functions. Thus, eight weeks of incubation were used to positively stimulate microbial growth of species present in coal sources and to proceed with methanogenesis. The low rank coal samples, such as Red Hills - RH and East Texas ETL mixed with TSB and lactate eLAC (i.e., RH TSB1, ETL TSB1 and ETL LAC2) were among the highest methane producers at eight weeks. These samples probably provided significant microbial populations that were stimulated with the added nutrients. Alternatively, these coal sources were likely more susceptible to biodegradation due to their lower rank, permeability, and the fact that there were highly branched compounds accessible to active microorganisms. Carbon dioxide concentrations, on the other hand, were lower: CO_2 concentrations were less than 230,000 ppm for the coal samples after 8 weeks. When other potential methanogenic sources were evaluated such as the oil shale sample lower methane concentrations were observed. The highest methane concentration was 160 ppm while 38 ppm was measured from the control sample. This oil shale produced nearly 220,000 ppm carbon dioxide, which was significant higher than 20,000 ppm produced by the control sample. No appreciable methane production (i.e., concentrations less than 13 ppm was generally detected for the waxy crude samples and controls. The highest carbon dioxide concentration was nearly 94,000 ppm compared to 1400 ppm from control sample. Apparently, few appropriate methanogenic populations were present in those samples. In addition, bacteriostats and bactericides could be naturally present, or may have formed because of biochemical reactions inhibiting or destroying the molecular cell structure of remaining microbes. Further studies need to be conducted to evaluate the use of other hydrocarbon samples, such as those considered here (i.e., oil shale and waxy crude), as alternative sources of microbial populations suitable for coal biotransformation.

Significant methane production was measured for the environmental samples acquired from the Jordan River - JR and Utah Lake -UL sediments, even after only two weeks of incubation. These samples showed methane concentrations much larger than those for samples from the Great Salt Lake -GSL sediments (i.e., 650 ppm). This may be due to more microbial population or high activity of degrading organic matter present in sediments. Microbial populations can be positively stimulated after nutrient addition. This likely overcame the lack of essential nutrients initially present to support methanogenesis. These samples produced methane concentrations up to 208,800 ppm (e.g., UL6 ACE2). These methane concentrations were significantly higher than any control sample (71.3 ppm) and the estimated maximum methane production from added nutrients (Table 5). Carbon dioxide concentrations up to 400,000 ppm were measured for the evaluated samples (e.g., UL4 TSB2), and 6940 ppm was measured for the control samples. Methane and carbon dioxide concentrations increased when nutrient amendments were added to samples from hydrocarbon seeps adjacent to the Great Salt Lake. Lower concentrations (70 ppm) were generated from their control samples. It may be inferred that the Great Salt Lake sediments had low concentrations of easily degradable organic matter and/or relevant nutrients required to support microbial activity. In addition, it is suspected that the high salt concentration, characteristic of the Great Salt Lake's environment - with values that can exceed 250 g/L, was detrimental to methane production. The inhibitory role of salinity was confirmed in subsequent unpublished studies by the

authors and has been reported by other researchers. Figure 7 summarizes the microbial samples chosen from the Phase I screening. For illustrative purposes only, the best methane and carbon dioxide producers are shown. These samples were organized from the highest to the lowest methane concentration to show the most promising samples. It is noted that duplicate microbial samples are included in the figure. For example, UL4 TSB1 and UL4 TSB2 correspond to the environmental sample Utah Lake -UL combined with tryptic soy broth -TSB. Microbial samples include the highest methane producers after an eight-week incubation period, the highest methane producers after two weeks in an acetate medium, as well as the highest carbon dioxide producers after two and after eight weeks. Also shown are samples that were chosen subjectively based on their appearance after eight weeks (e.g., samples with visible, consistent bubble generation). These latter samples exhibited features that were presumed to be a consequence of coal breakdown and methanogenic activity. Additionally, theoretical conversion of added nutrients to methane and carbon dioxide was estimated. These results suggest that most of generated gases came from the digestion of coal and/or sediments, and just a small fraction can be attributed to the nutrient amendments added. Over seventy-five samples were selected for further refinement and subsequent evaluation.

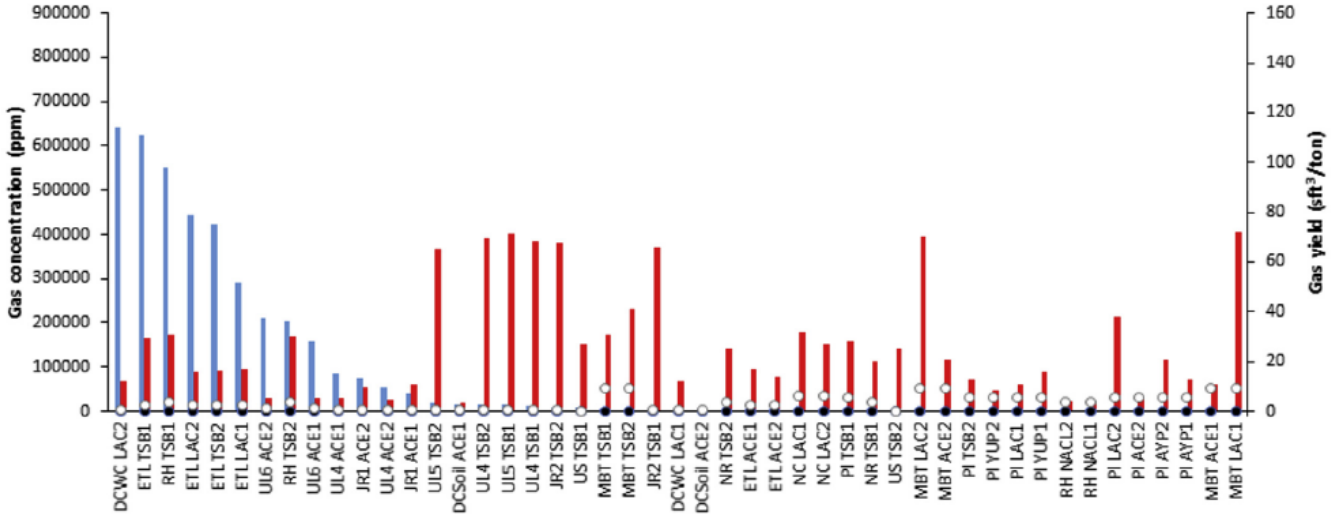

Figure 7. Methane (blue bars) and carbon dioxide (red bars) concentrations for selected samples from Phase I screening.[1] The black and white points represent methane and carbon dioxide concentrations from control samples, respectively. Microbial samples have been organized from the highest to the lowest headspace methane concentration. Hydrocarbon and environmental samples combined with selected nutrient amendments are depicted. Duplicate samples are included. (For interpretation of the references to color in this figure legend, the reader is referred to the web version of this article.)

Table 5. Results from added nutrients in Phase I screening.[1]

Nutrient amendments	TSB (ppm)	LAC (ppm)	ACE (ppm)	YUP (ppm)	AYP (ppm)
Methane	12,600	142,200	44,560	48,745	59,195
Carbon dioxide	8,420	158,720	57,297	40,390	63,163

Phase II screening. During this phase of screening, nutrient amendments were again added (i.e., acetate - ACE, lactate - LAC and tryptic soy broth - TSB). This ensured that the microbial populations remained actively stimulated. This phase can also be considered as a preliminary step for the ensuing final stage of screening. Figure 8 shows the best methane producers and their associated carbon dioxide concentrations after two weeks of incubation. Results were very promising. For example, 633,000 ppm methane were measured for sample MBT LAC ACE (Miller Black Thunder coal amended with lactate -LAC in Phase I and acetate -ACE in Phase II). In Phase II screening, the highest methane producers correlated with specific coal sources, mainly East Texas lignite - ETL and the sub-bituminous Miller Black Thunder e MBT. This might indicate that active microorganisms were continuously stimulated with new nutrients that either were depleted or were not present in Phase I screening after eight-week incubation period. Enrichment with fresh nutrients could have met the nutritional requirements of the microbial populations, affording growth and promoting methane production from remaining coal and/or sediments. Low gas concentrations from added nutrients were estimated (Table 6). This suggests that nutrient solutions effectively stimulated microbial consortia. On the other hand, some samples such as the Utah Lake - UL and Jordan River -JR sediments manifested a different behavior. For these sediments, the stimulated microbial populations continued producing significant amounts of carbon dioxide, as had been previously observed during the Phase I screening. Samples that included microbial communities

from different rank coals and environmental sources were satisfactorily stimulated. However, not all nutrient amendments were equally effective for methane production. Nitrogen and phosphorous present in lactate - LAC and tryptic soy broth – TSB media are considered essential for simulating methane generation from coal. Since different compounds were present in these nutrient amendments, it may be advantageous to identify the exact stimulants that impacted the overall performance of the microbial consortia. Once their role is identified, simplified and less expensive nutrient amendments can be used for enhancing methane yields from coal.

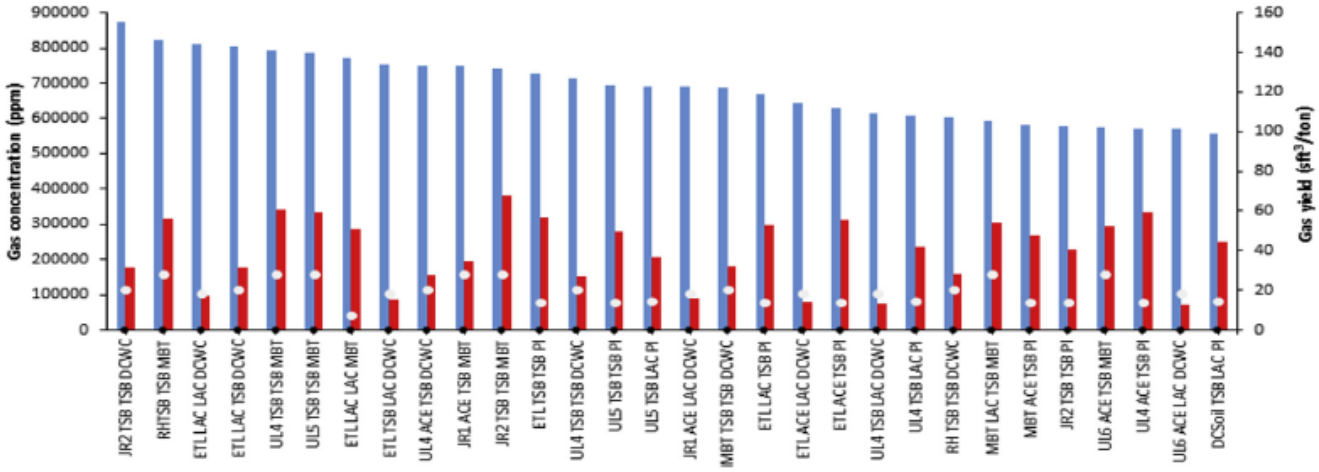

Figure 8. Methane (blue bars) and carbon dioxide (red bars) concentrations generated during the Phase III screening after two weeks of incubation.[1] The black and white points represent methane and carbon dioxide concentrations from control samples, respectively. Premium microbial samples have been organized from the highest to the lowest headspace methane concentration. Microbial consortia from hydrocarbon and environmental samples have been combined with different coal types (i.e., Miller Black Thunder MBT, Deer Creek Mine Waste Coal DCWC, Praxair Illinois #6 PI, and Arkansas Lignite LIG) and fresh nutrient amendments (i.e., tryptic soy broth TSB, lactate LAC, and acetate ACE). (For interpretation of the references to colour in this figure legend, the reader is referred to the web version of this article.)

Table 6. Results from added nutrients.[1]

Nutrient amendments	TSB (ppm)	LAC (ppm)	ACE (ppm)
Methane	8,400	105,650	30,750
Carbon dioxide	5,610	117,915	39,540

Fresh nutrient media and selected coal types were used to sequentially enrich and adapt microbial populations that had been down-selected from Phase II screening after two-week incubation period. This included four different rank coals (sub-bituminous Miller Black Thunder - MBT, bituminous Deer Creek Mine Waste Coal - DCWC, high volatile bituminous Praxair Illinois #6 - PI, and Arkansas Lignite - LIG) and the same nutrient media used in the previous phase of screening. Methane and carbon dioxide were monitored after two and twenty-four weeks of incubation. Figure 8 summarizes the premium methane producers at two weeks of incubation. In addition, results of theoretical gas production from the fresh nutrient amendments and controls related to the evaluated samples are included in Table 6 and Table 7, respectively. It is noted that the same amount and type of nutrient amendments were used in Phase II and Phase III of screening. Only a small fraction of methane and carbon dioxide can be attributed to direct result of nutrient conversion from the microbial samples amended with the selected nutrients (Table 6). The maximum methane concentration of 873,000 ppm was measured for one of the most promising samples JR2 TSB TSB DCWC. The carbon dioxide concentration for this sample was 176,370 ppm. Among the samples that included microbial populations enriched from coal sources, the lignitic Red Hills RH and East Texas ETL coals showed significant methane production. Large methane concentrations were also measured with microbial populations retrieved from the lake sediments (e.g., Jordan River -JR, Utah Lake UL in Figure 8). For each sample, an optimal microbial population, nutrient amendment and/or coal combination were obtained. Significant methane production was evident for the higher rank coals used for adaptation in this phase of screening (i.e., bituminous Deer Creek Mine Waste coal DCWC, subbituminous Miller Black Thunder coal MBT in Figure 8). For those coal samples, relatively lower methane production was observed in comparison to the lower rank coals in previous phases of screening. This observation of low methane production from the higher rank coals during the initial stages of screening, followed by higher methane concentrations in this phase of screening can be related to the

positive stimulation of methanogenic populations after subsequent enrichment, and can indicate less inhibition of ex-situ cultured microbial populations with higher rank coals rather than their lower-rank counterparts. Bituminous coal is generally characteristic of greater depths in a reservoir, and as a higher rank coal, it includes greater proportions of more recalcitrant compounds (i.e., aromatic content) that are less favorable for biogenic methane production. Thus, enrichment of methanogenic consortia and their adaptation to higher rank coals should be beneficial for enhancing methane production when such coals act as the substrate. Physicochemical analysis of the liquid phase was carried out on the coals used in this study.

Table 7. Results of controls related to samples in Figure 8.

Control samples		DCWC -TSB	DCWC -LAC	MBT -TSB	MBT -LAC	PI –TSB	PI –LAC
CH_4	ppm	8.31	5.37	5.80	8.21	13.81	17.02
	sft^3/ton	1.46×10^{-3}	9.46×10^{-4}	1.02×10^{-3}	1.44×10^{-3}	2.43×10^{-3}	2.99×10^{-3}
CO_2	ppm	114,451	103,195	157,348	43,247	78,980	83,407
	sft^3/ton	20.17	18.19	27.73	7.62	13.92	14.70

These are compiled in Table 8. Values of pH for coal samples not shown were circum-neutral (6.95-7.15). While it would be beneficial to conduct real-time pH measurements to have an exact view of bioreactors' behavior, an estimation for this environmental factor was obtained. The low pH (3.87) can be correlated with the low methane production when Arkansas lignite -LIG coal was used as substrate; concentrations less than 72,000 ppm were measured. Significant methane generated with the Praxair Illinois #6 - PI coal type, on the other hand, suggested an environment with a possible pH (4.18) condition at which some enriched methanogenic populations could effectively function (e.g., sample ETL TSB TSB PI in Figure 8). The value of pH has an important effect on bioconversion of complex organic matter. Methanogens are considered the most affected group of microorganisms within microbial consortia and their environmental requirements are usually prioritized. Changes in methane production and/or microbial populations can be attributed to shifts of the environmental conditions. Even though most methanogenic communities seem to be dominated by neutrophilic species with limited growth and methane production outside of the aforementioned optimal range (6.80-7.40) there are known methanogens that can exist in low pH environments. Values of pH lower than 4.00 are characteristic of peat bogs, where methane production has been reported. After twenty-four weeks of incubation, methane and carbon dioxide levels dropped significantly as shown in Figure 9. Results of controls related to those samples are included in Table 9. For the sample JR2 TSB TSB DCWC, for instance, a methane concentration of 4100 ppm and carbon dioxide concentration of 27,312 ppm were measured. Other samples reached methane concentrations less than 1100 ppm. This scenario of methane content increasing and subsequently decreasing has been also reported by other researchers. As a possible explanation, microbial methane oxidation (anaerobic and/or aerobic) could have occurred. Headspace gas was not completely removed nor neither replaced during sampling for gas measurements; the bioreactors operated as a closed system. It is also likely that nutrients or trace elements that are available may have depleted over time. This depletion could have led to a decrease in the microbial populations. Finally, it is speculated that only limited amounts of electron donors (i.e., acetate, or H_2) were available or were not continuously produced to support methanogenesis.

Table 8. pH of liquid phase in coals tested.

Designation	Coal samples	pH
LIG	Arkansas Lignite	3.87 ± 0.06
PI	Praxair Illinois #6	4.18 ± 0.01
NC	NARM Cook	6.68 ± 0.02
MBT	Miller Black Thunder	6.78 ± 0.01
DCWC	Deer Creek Mine Waste Coal	7.06 ± 0.02

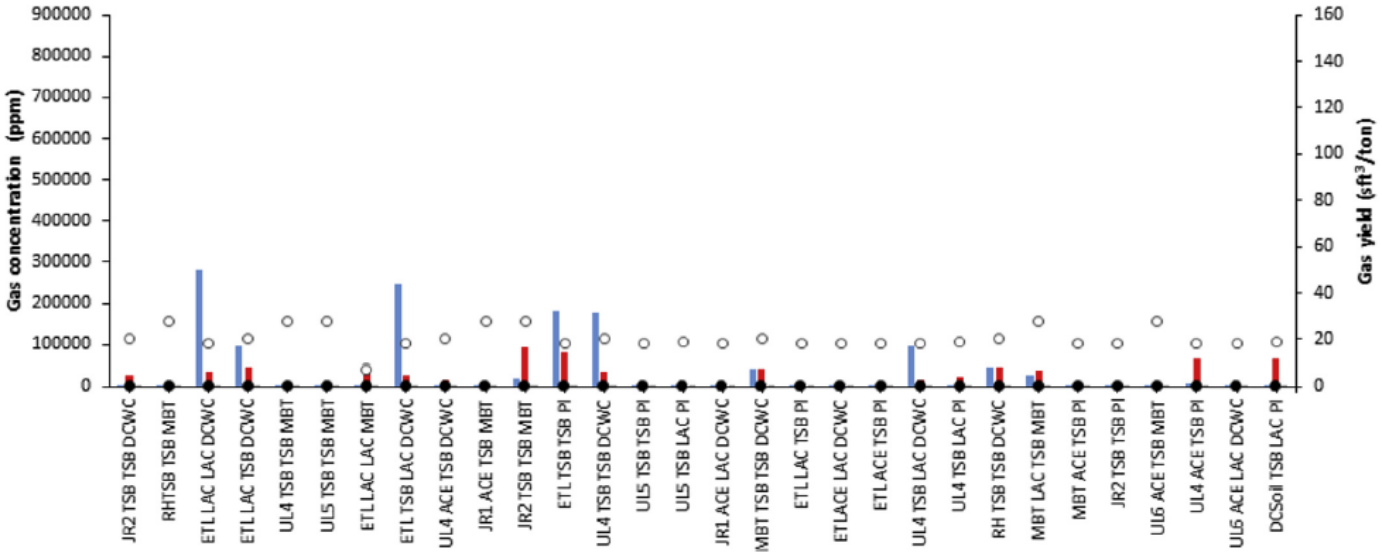

Figure 9. Methane (blue bars) and carbon dioxide (red bars) concentrations generated during the Phase III screening after twenty-four weeks of incubation. The black and white points represent methane and carbon dioxide concentrations from control samples, respectively. Microbial consortia from hydrocarbon and environmental samples combined with different coal types (i.e., Miller Black Thunder MBT, Deer Creek Mine Waste Coal eDCWC, Praxair Illinois #6 PI, and Arkansas Lignite LIG) and fresh nutrient amendments (i.e., tryptic soy broth TSB, lactate LAC, and acetate ACE) are shown after a long period of incubation. (For interpretation of the references to color in this figure legend, the reader is referred to the web version of this article.)

Table 9. Results of controls related to samples in Figure 9.

Control samples		DCWC -TSB	DCWC -LAC	MBT -TSB	MBT -LAC	PI –TSB	PI –LAC
CH_4	ppm	8.33	5.26	5.84	8.06	13.78	17.47
	sft^3/ton	1.47×10^{-3}	9.26×10^{-4}	1.03×10^{-3}	1.42×10^{-3}	2.43×10^{-3}	3.08×10^{-3}
CO_2	ppm	114,081	102,919	157,040	43,003	103,384	107,440
	sft^3/ton	20.11	18.13	27.67	7.57	18.22	18.94

Aerotolerance. An attempt was made to assess microbial consortia functionality under initial anaerobic conditions. The microbial consortium RH TSB TSB MBT under argon atmosphere showed a greater methane production (255,000 ppm) than the microbial sample under initial atmospheric exposure (100,000 ppm) at three weeks of incubation. It is shown that both microbial samples were significant methane producers (Figure 10). This suggests that the developed microbial consortia were both aerotolerant and anaerobically methanogenic, which can ease their delivering to an oxygen free environment to digest coal and produce methane. It is noted that the measured methane concentrations were less than the gas concentrations obtained after two weeks of incubation in the Phase III of the screening program (Figure 8). It is likely that low initial cell concentration, or changes of microbial communities may had been responsible for this behavior. Eventually, facultative and aerobic microorganisms present in the culture can rapidly consume oxygen, creating favorable conditions for the obligate anaerobes. Thus, a temporary air presence to the methane generating process can be handled since mentioned microorganisms are able to reduce the incoming oxygen to a low level. This feature and some intrinsic oxygen tolerance of anaerobes organisms can contribute to the coal biogasification process. A wide range of methane yields from different coal ranks and microbial communities exposed to various strictly anaerobic enrichment and cultivation conditions has been reported. However, only a limited number of evaluations have been published where initial aerobic environments were considered. Formation water was collected from a coalbed methane well in southern Illinois. Those researchers developed a microbial consortium for ex-situ bituminous coal bioconversion. Ground coal was obtained from the Illinois basin. During their experimentation, complete air exposure was avoided. Nitrogen gas was used to purge the bioreactors prior to incubation. Three different media were used: standard Tanner medium, mineral salt (MS) medium, and formation water was used as control. After sixty-five days of incubation at 28°C, selected samples were added to fresh coal and an MS medium. Some of these samples were purged with nitrogen while others were in contact with the atmosphere. After 20 days, there was no statistically significant difference in the yields of methane or carbon dioxide as functions of purging. The researchers suggested that an effective microbial consortium can be cultivated under conditions that are not strictly anaerobic. Opara and

et al. furthermore, performed a comprehensive study of methane and carbon dioxide production.[3, 5]. Those authors developed aerotolerant microbial consortia that generated significant quantities of methane and/or carbon dioxide in various down-selection screening of microbial and in consortia scale-up that included aerobic conditions. Bituminous coal and waste coal, lake sediments, wetland sediments, river sediments, digester sludge, as well as oil seep and gas well samples were used as sources for the microbial populations. An initial enrichment step with different growth media was carried out after collection. Gas production was evaluated using hydrocarbon materials (bituminous coal, waste bituminous coal, and lignite) over a thirty-day period at 23ºC. The optimal CO_2 and CH_4 producers were ultimately selected and combined into five consortia. During this experimentation, introduction of microbial populations, mainly consortia cultured from noncoal environments (i.e., not coal or waste coal), increased the rate of hydrocarbon biodegradation, with CO_2 as a product. Different behavior was observed in our study under similar environmental conditions with bituminous coal and using the same nutrient recipes. Samples that included consortia enriched and cultured from both hydrocarbon and environmental sources have shown significant methane production (Figure 8) after two weeks of incubation, suggesting their potential use to biodegrade coal and produce methane as the product.

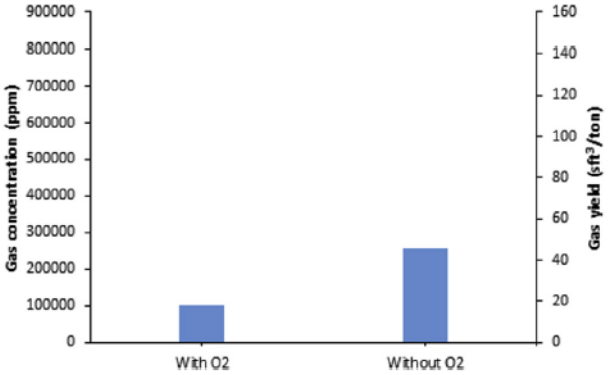

Figure 10. Methane production under initial atmospheric exposure (with oxygen) and initial anaerobic conditions (without oxygen). The functionality of the microbial consortium RH TSB TSB MBT is assessed under initial anaerobic conditions.

ANOVA of a single factor. After the three screening phases, methane and carbon dioxide concentrations at two and twenty-four weeks were separately analyzed with ANOVA single factor evaluation. Table 10 summarizes the levels that were the most or least important for methane and carbon dioxide production during the experimental program. In Table 10, a p-value lower than 0.05 means that there was a statistical difference among medians or means of each level within a defined factor with a confidence level of 95% (depending on the statistical test used). Cases where the level is not shown (p values > 0.05) indicate that there was not a significant statistical difference. In those instances, all levels had an equal or similar impact on gas production within the evaluated factor. The factors and levels used for the variance analysis ANOVA are given in Table 11.

- The following trends were observed: _ Tryptic soy broth e TSB was an important nutrient medium for enriching the microbial consortia and stimulating methane production for both of the evaluated periods of incubation. On the other hand, after two weeks of incubation, lactate LAC had a greater impact on carbon dioxide production when used as the final nutrient amendment. Yeast-urea-phosphate YUP was a suitable initial nutrient medium, causing increased carbon dioxide production after twenty-four weeks of incubation.
- Acetate ACE did not show, on average, a significant impact on gas production after two weeks nor after twenty-four weeks of incubation. This suggests that the microbes could had been inhibited or possibly required more complex nutrients than the acetate to be enriched and positively stimulated.
- NaCl - 8.5 g/L - showed a negative impact on methane production. This was expected since NaCl was used in the control samples. NaCl was included in the statistical analysis since it was associated with samples that were chosen based on their physical appearance. As mentioned earlier, nutrient amendments with specific ingredients were needed to satisfactorily stimulate microbial growth, and eventually to promote gas production.

- The coal type itself is relevant. Bituminous Deer Creek Mine Waste Coal DCWC had the greatest positive impact on methane production in both periods of incubation (i.e., two weeks and twenty-four weeks). Reduced inhibition of ex-situ cultured microbial populations could have been operative. This probably made this coal the most suitable sample for consortia adaptation and subsequent methane generation. At the other extreme, Arkansas Lignite LIG had a negative impact on methane production. As was mentioned earlier, the low pH of the liquid media associated with this coal could be correlated with the low methane concentrations, inhibiting methanogenesis to some extent.
- The initial source of the microbial community, not surprisingly, is also relevant. The Jordan River 2 JR2 sediment sample was an effective source of microbes for methane production for two weeks of incubation, but not after twenty-four weeks. This most likely indicates that active methanogenic populations were positively stimulated and initially generated significant amounts of gas. However, there were limited electron donors (i.e., acetate, or H_2) available, and/or they were not continuously produced. The East Texas Lignite ETL was an important source of microbes for methane production after twenty-four weeks in Phase III screening. The Deer Creek Mine Soil DC Soil afforded enhanced carbon dioxide production after 24 weeks of incubation.

Table 10. Main controls during microbial consortia creation.

	Factor	Statistical test	p-value	Average rank for level of highest impact	Level of highest impact	Average rank for level of lowest impact	Level of lowest impact
Methane concentration at two weeks	SM	Kruskal-Wallis	0.0	212.2	JR2	61.7	PI
	INM	Kruskal-Wallis	4.5×10^{-9}	167.4	TSB	48.1	NaCl
	CT	Kruskal-Wallis	2.7×10^{-8}	176.6	DCWC	95.8	LIG
	FNM	Kruskal-Wallis	2.6×10^{-8}	170.2	TSB	103.9	ACE
Methane concentration at twenty-four weeks	SM	Kruskal-Wallis	5.9×10^{-5}	189.8	ETL	97.7	JR2
	INM	Kruskal-Wallis	4.7×10^{-2}	156.6	TSB	95.3	NaCl
	CT	Kruskal-Wallis	1.2×10^{-2}	165.3	DCWC	119.9	LIG
	FNM	Kruskal-Wallis	3.1×10^{-5}	172.2	TSB	117.4	ACE
Carbon dioxide concentration at two weeks	SM	Kruskal-Wallis	1.7×10^{-1}	–	–	–	–
	INM	Anova	1.5×10^{-1}	–	–	–	–
	CT	Kruskal-Wallis	5.6×10^{-11}	177.9	MBT	87.0	DCWC
	FNM	Anova	0.0	–	LAC	–	ACE
Carbon dioxide concentration at twenty-four weeks	SM	Anova	2.4×10^{-3}	–	DCSoil	–	DCWC
	INM	Kruskal-Wallis	9.1×10^{-3}	202.1	YUP	133.5	LAC
	CT	Anova	1.6×10^{-1}	–	–	–	–
	FNM	Kruskal-Wallis	2.9×10^{-6}	177.7	TSB	118.3	ACE

SM = source of microbial community, INM = initial nutrient medium, CT = coal type, FNM = final nutrient medium.

Table 11. Factors and levels for variance analysis ANOVA.

Factor	Level
Sources of microbial community	Deer Creek Mine Soil -DCSoil; Deer Creek Mine Waste Coal -DCWC; Jordan River -JR Samples 1 and 2; East Texas Lignite -ETL; Miller Black Thunder -MBT; NARM Cook -NC; North River -NR; Praxair Illinois #6 -PI; Red Hills -RH; Utah Lake -UL Samples 4, 5, and 6; Utah Skyline -US.
Initial nutrient medium	Acetate -ACE; tryptic soy broth -TSB; lactate -LAC; acetate-yeast-phosphate medium -AYP; yeast-urea-phosphate medium -YUP; sodium chloride -NaCl.
Coal type	Deer Creek Mine Waste Coal -DCWC; Miller Black Thunder -MBT; Praxair Illinois #6 -PI; Arkansas Lignite -LIG
Final nutrient medium	Acetate -ACE; tryptic soy broth -TSB; lactate -LAC

2.2.2. Optimization biogenic methane production from coal

Microbial community present in the culture. The diversity assay revealed that the methanogenic microbial consortium contained 96.3% bacterial strains and 3.7% archaea. Similar percentages of total population for enriched and adapted consortia on coal can be found in the literature. The microbial consortium used for this study was separated from the initial enriched culture, and was maintained in fresh nutrient media. Thus, possible changes of microbial communities could have occurred. 19 bacterial species and one species of archaea comprised the microbial community. The most abundant bacterial species were Figure 11: Rhodococcus equi which correspond to facultative anaerobic organism able to degrade poorly water-soluble organic compounds. On the other hand, Rummeliibacillus spp., Clostridium beijerinckii, Clostridium sp., Lachnoclostridium spp., Clostridium propionicum, Desulfitobacterium hafniense, Clostridium sporosphaeroides, and Tissierella sp. included obligate and facultative anaerobes. These microbes comprised fermenters and syntrophs able to hydrolyze water-soluble macromolecular compounds, fatty acid oxidizers and acetogens. The archaea were dominated by the Methanobacteriales order: Methanobacterium sp., which

is known as a hydrogenotrophic methanogen. These identified microorganisms comprised metabolic groups commonly observed in the bioconversion of coal.

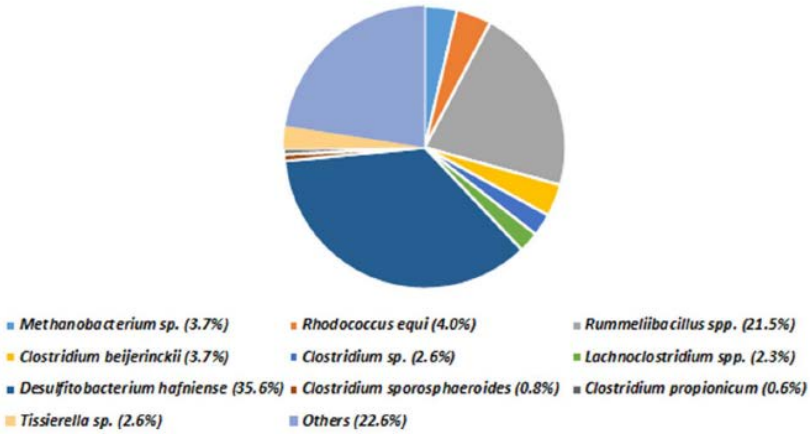

Figure 11. Diversity of microbes in the methanogenic consortium RTTM.

Experimental design and analysis of variance – ANOVA. As mentioned, experimental runs were performed in duplicate. Data points were the average of the duplicate ± standard deviation (< 25% of average). These were expressed as methane percent concentration and analyzed with STATGRAPHICS Centurion VII®. There was not significant methane production from the control samples. ANOVA results for the generated model after 60 days of incubation are represented in Table 12. Quadratic models and their coefficients of determination - R^2 are given in Table 13.

The ANOVA table partitions the variability in Y_{CH4} into separate pieces for each of the effects. It then tests the statistical significance of each effect by comparing the mean square against an estimate of the experimental error. Table 12 shows the analysis of variance after 60 days. In this table, one parameter (NaCl concentration) had a statistically significant effect with a p-value < 0.05. These results indicated that the NaCl concentration was the most significant factor controlling methane production in these experiments. The combined interaction of NaCl concentration with itself (i.e., BB in Table 12) had a statistically significant effect in comparison to the combinations of other parameters. As for the effects of temperature and pH, p-values demonstrated that pH was more significant statistically than temperature. Similar behavior was observed for incubation times other than 60 days.

Table 12. Analysis of variance for Y_{CH4} after 60 days. The column labeled "Source" refers to the source of variation. It includes the effect of each factor denoted by capital letter, and the item "Error" is related to experimental error. Df refers to degrees of freedom, and it corresponds to the number of observations in the data that are free to vary when estimating statistical parameters.

Source	Sum of squares	Df	Mean square	F-ratio	*P*-value
A:T	32.6018	1	32.6018	0.07	0.7986
B:NaCl	2623.47	1	2623.47	5.65	0.0491
C:pH	33.0938	1	33.0938	0.07	0.7971
AA	125.325	1	125.325	0.27	0.6193
AB	56.3472	1	56.3472	0.12	0.7378
AC	56.5237	1	56.5237	0.12	0.7374
BB	2318.97	1	2318.97	5.00	0.0605
BC	56.2985	1	56.2985	0.12	0.7379
CC	124.831	1	124.831	0.27	0.6200
Error	3248.83	7	464.119	–	–
Total	8676.29	16	–	–	–

The coefficient of determination - R^2 varied between 0.58 and 0.71 for methane production, depending on the incubation time (Table 13). This statistical assessment provides a measure of how well the regression approximates the real data points, or how much variability in the observed response values can be explained by the experimental factors and their selected parameter interactions. Thus, the regression models can explain a percentage up to 71 of the variability in methane production. A good "fitted" model should be characterized by a high R^2 value (> 0.5). The generated models provided satisfactory prognostic capabilities. It is seen that high salt concentration would be detrimental to methane production. In addition, factors such as particle size, coal loading and other unknown factors can also influence the biodegradation of coal and methane production. Even though additional factors can affect the response values, the key factors considered herein have mainly been evaluated by variation of single parameters using a one-variable-at-a-time technique.

Table 13. Response surface models.

Quadratic models		
t = 15 days	$Y_{CH4} = 7.01674 + 0.177371\,T - 0.490646\,NaCl + 0.427302\,pH - 0.00411721\,T^2 + 0.00106999\,T\,NaCl + 0.0123675\,T\,pH + 0.00367862\,NaCl^2 + 0.0117285\,NaCl\,pH - 0.105049\,pH^2$	$R^2 = 0.70$
t = 30 days	$Y_{CH4} = -32.1853 + 2.57839\,T - 2.0638\,NaCl + 8.7292\,pH - 0.0243579\,T^2 - 0.00500218\,T\,NaCl - 0.0585693\,T\,pH + 0.0196067\,NaCl^2 + 0.045688\,NaCl\,pH - 0.610475\,pH^2$	$R^2 = 0.67$
t = 45 days	$Y_{CH4} = 12.1331 + 0.922465\,T - 1.58028\,NaCl + 2.31875\,pH - 0.0138054\,T^2 + 0.00110846\,T\,NaCl + 0.0135204\,T\,pH + 0.0124554\,NaCl^2 + 0.0419608\,NaCl\,pH - 0.347075\,pH^2$	$R^2 = 0.71$
t = 60 days	$Y_{CH4} = 60.4177 + 1.31003\,T - 4.24967\,NaCl + 4.78854\,pH - 0.0411631\,T^2 + 0.014042\,T\,NaCl + 0.16408\,T\,pH + 0.0325223\,NaCl^2 + 0.0701797\,NaCl\,pH - 1.02705\,pH^2$	$R^2 = 0.66$
t = 75 days	$Y_{CH4} = -33.0029 + 1.92692\,T - 1.54918\,NaCl + 8.92289\,pH - 0.0247221\,T^2 + 0.000271682\,T\,NaCl + 0.000103964\,T\,pH + 0.0160072\,NaCl^2 - 0.00174963\,NaCl\,pH - 0.619646\,pH^2$	$R^2 = 0.58$

Graphical presentation of the model equations. 3D surface plots for the effect of temperature and pH on coal biogasification, the effect of salt concentration and temperature, and the effect of salt concentration and pH are shown in Figure 12a through c, respectively. Figure 12a shows that at high temperature (54°C), less methane is produced. The largest gas production is in the vicinity of 30°C. Similarly, at high values of pH (> 7.2) less methane is produced. The largest volumes of methane are generated at low pH values (< 7.2) and low temperatures (< 39°C). Fig. 2b shows that less gas is produced at elevated NaCl concentrations. A detrimental effect of salt concentration on methane production can be observed. Large amounts of methane are produced at the lowest salt concentration (3.7 mg/cm^3) and at low temperatures (< 39°C). Figure 12c again shows the prominent effect of salt concentration. The largest methane production is obtained at the lowest NaCl concentration and at low pH values (< 7.2). It is likely that salt concentrations larger than 18 mg/cm^3 created lysis pressure that broke directly the membrane of cells, ceasing cellular metabolism and affecting gas production. Salt concentrations < 18 mg/cm^3, however, might be suitable for methanogenesis. In addition, the curvature of the response surfaces above 50 mg/cm^3 of salt concentration (Figure 12b–c) is likely related to the model that is fitted and not to the true behavior of the system. Similar trends were observed for the other incubation periods. After 75 days, methane levels dropped significantly in some bioreactors (e.g., #4 and #14 in Table 2). This scenario of methane content increasing and subsequently decreasing has been reported previously, suggesting further investigation is relevant. As a possible explanation, microbial methane oxidation (anaerobic and/or aerobic) could have occurred. Headspace gas was not completely removed or replaced during sampling for gas measurements; the bioreactors operated as a closed system. It is expected that methane concentration stabilizes at some point. Coal biogasification proceeded without any external intervention to influence gas production. It is also likely that self-inhibitory byproducts may have been present (Wang et al., 2017), and/or essential nutrients or trace elements may have depleted over time. This would decrease the microbial populations and consequently affect methane production. Finally, it is speculated that insufficient electron donors (i.e., H_2, acetate, formate) were available or were not produced continuously to support methanogenesis under the conditions tested.

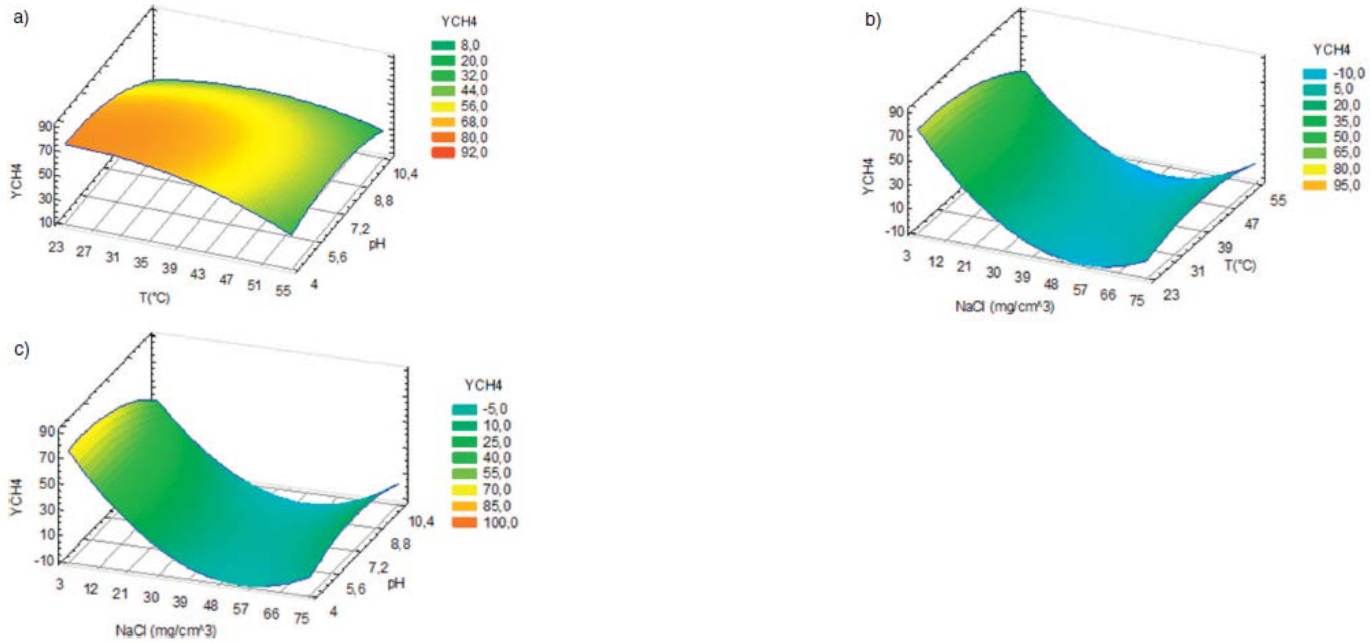

Figure 12. Response surface plots after 60 days of incubation. (a) The effect of temperature and pH on coal biogasification at [NaCl] = 3.7 mg/cm$_3$, (b) the effect of salt concentration and temperature on coal biogasification at pH =5.5, (c) the effect of salt concentration and pH on coal biogasification at T = 30 °C. Color bars depicts variation in methane production along the response surface.

Evaluation of main effects on methane production-Temperature. Methanogenic microbes can grow in a variety of temperature domains; in marine sediments at 2°C to geothermal areas above 100°C. There is a great diversity of mesophilic and thermophilic species. Most of the mesophilic methanogens grow optimally at temperatures between 30°C and 37°C while thermophiles generally grow at temperatures between 50°C and 65°C. Methanogenesis is often more affected by temperature than other biological processes. Microbial selection protocols for these experimental would have selected microbes that exhibited optimal methanogenesis at temperatures > 37°C. Different microbial screening/selection protocols can be used to select for microbial populations having optimal performance at higher temperatures and/or other conditions that are exclusive to specific. Many mesophiles prefer temperatures greater than ambient atmospheric temperature. This has been observed with the microbial community used in this study. 48°C can be considered to be the limit of tolerance since the microbial consortium was able to produce significant amounts of methane up to this temperature. This data may suggest the possible use of the consortium for enhanced biogenic methane generation at higher temperatures than 30–35°C. Elevated temperatures are often observed in coal basins at great depth. Assuming a mean surface temperature of 10°C and an average temperature gradient with depth of 1.8°C/100 m, microbial activity using the consortium developed can likely cease below 2665 m. Overall, between 23°C and 35°C, methane production is increased with temperature, and it decreases at the highest value used in the experimental program, 54°C. This trend is in agreement with performance of a mesophilic microbial community comprised by the archaea Methanosarcina mazei, which had been isolated from mine water in Jitpur, India. Using coal from this mine, incubation was characterized by an increasing trend of methane production from 25°C to 35°C followed by a decreasing trend from 35°C to 55°C. Also, for a similar microbial consortium from the Fort Union Formation in the Powder River Basin -WY, U.S, methane production from subbituminous Wyodak coal increased after increasing the incubation temperature from 22°C to 38°C. Production was impaired at 40°C. This microbial community had been obtained from formation water in the Illinois basin, in the United States. The solubility of coal substrates can be increased which in turn increases the rate and extent of substrate mass transfer from coal solids. However, if a threshold temperature is exceeded, certain microbes may be negatively affected. Above this threshold temperature, growth rate decreases and microbial activity may cease.

Evaluation of main effects on methane production-Salinity. Methanogenic populations can survive in a wide range of salinities; from freshwater to hypersaline environments. This type of salinity variation can be also found in petroleum reservoir formation waters. Freshwater methanogens generally need at least 2.3×10^{-2} mg/cm^3 of sodium for their growth and metabolic functions. Hydrogenotrophic and acetoclastic methanogens are common in subsurface settings and are generally limited to lower-salinity conditions. Methanocalculus halotolerans is the most halotolerant hydrogenotrophic methanogen reported; able to survive NaCl concentrations up to 120 mg/cm^3. This organism had been isolated from an oilfield brine. Generally, methanogens are the organisms that are most affected by increasing salt concentrations. While salt can have an inhibitory effect, the concentration at which this is evident might vary depending on the substrate type and its availability. Typically, acetoclastic methanogenesis has a relative low upper salinity limit, while methanogens that use an H_2/CO_2 pathway have a higher salinity tolerance - but never above 175 mg/cm^3. In the experimental matrix performed here, methane production degraded with salt concentrations increasing from 3.7 mg/cm^3 to 74.3 mg/cm^3. The largest methane production occurred at the lowest salt concentration of 3.7 mg/cm. Methanogenesis was dramatically affected by large salt concentrations (> 18 mg/cm^3).

Evaluation of main effects on methane production-pH. As in all biochemical processes, pH has an important effect on methane production from complex organic matter. Reduced biologic activity when conditions are far from an optimum pH range can limit gas production. Within a microbial community, methanogens are the most strongly affected by the pH. Values of pH between 6.8 and 7.4 are generally reported to be optimal for a methanogenic habitat. In this study, the experiments carried out varied pH from 4.2 to 10.2. Large methane production was obtained at a low pH value of 5.4. At pH values higher than 7.2, decreasing methane production trends were observed. Even though most methanogenic communities seem to be dominated by neutrophilic species with limited growth and methane production outside of the aforementioned optimal range (i.e., pH values 6.8–7.4), there are known methanogens that can exist in low pH environments. Acidophilic and/or acid-tolerant strains that are able to produce methane down to pH 3.0 have been cultured. Generally, hydrogenotrophic methanogens are more resistant to low pH than are acetoclastic methanogens. Alternatively,

it has been rationalized that an acidic pH may be able to encourage methane production by enhancing coal solubility; acids may enter the coal pore structure and interact with ion-exchangeable cations, resulting in limited dissolution of coal via disruption of ionic bridges. Acids may also hydrolyze ester or ether bonds within the coal matrix.

Determination of a feasible region of operation. The overall operational conditions for methane production are shown in Figure 13a. The methane percent concentration - YCH4 was computed using the regression models (Table 13) with different values of temperature, pH, and salinity (NaCl concentration). Subsequently, these predictions were organized and visualized using a 3D scatter plot. These predicted values were obtained up to a salt concentration of 28 mg/cm^3 where the best 3D- graphical representation was achieved. Figure 13b depicts the time- dependence for each point shown in Figure 13a. Thus, the visualization of the premium or the most representative operational conditions obtained at different periods of time was confirmed. In Figure 13a, bright yellow describes the region that predicted the maximum methane production from subbituminous coal - Miller Black Thunder and the microbial consortium - RTTM. This region comprised salt concentrations between 3.7 mg/cm^3 and 9.0 mg/cm^3 (Figure 13a), pH values between 4.2 and 6.8, and temperatures between 23 °C and 37 °C, as shown in the bottom view at [NaCl] 3.7 mg/cm^3 (Figure 13c).

Moderate temperature (23°C), low pH values (< 6.8), and low salt concentration (6.5 mg/cm^3 NaCl) correspond to the operational conditions imposed during microbial consortium development. As would be anticipated, there is strong dependency on the environment conditions and methane production from coal. Methanogenic activity can be influenced by culturing conditions, coal bioavailability and selectivity of the in-situ coal seam environment. Within the predicted region of operation, a maximum methane production is expected. In fact, these environmental conditions should favor the metabolism of the single archaea Methanobacterium sp. contained in the consortium of this experimental work. The genus Methanobacterium has been found in producing coalbed methane reserves in Powder River Basin - WY, U.S and Southern Qinshui Basin, China.

Some hydrogenotrophic methanogens that belong to the genus Methanobacterium have been identified in moderately acidic environments. These at least transiently have excess carbon, and low or limited supply of essential minerals (i.e., some peat bogs, paddies, polluted aquifers, groundwater, and oil reservoirs). These methanogens can grow at pH 7.0 down to values as low as 3.8, and to produce some methane down to pH 3.0. In addition, maximum rates of methane production for pH between 5.0 and 6.0, and temperatures between 25°C and 30°C have been reported for the same genus. It is known that some strains may readily adapt to extreme pH conditions. There are also alkaliphilic species (e.g., Methanobacterium alcaliphilum) that are able to grow at pH values up to 9.0. As for salinity tolerance, some members of the Methanobacterium genus have been shown to grow and produce methane at NaCl concentrations between 2.3×10^{-2} mg/cm^3 and 15.4 mg/cm^3; other species, however, seem to be very susceptible (e.g., Methanobacterium thermoautotrophicum) to large salt concentrations.

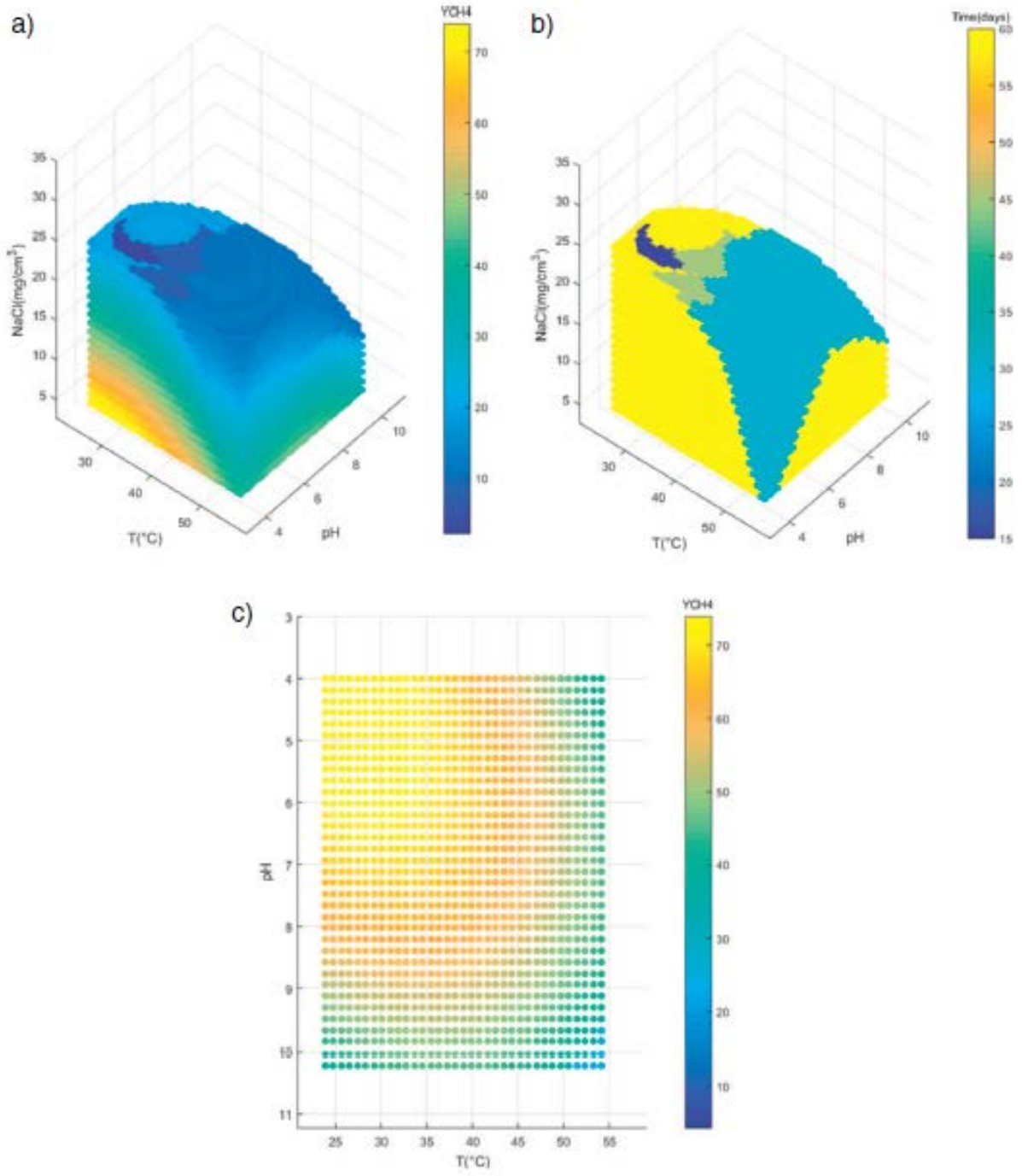

Figure 13. Overall operational conditions for methane production. (a) The effect of temperature, pH and salt concentration on coal biogasification. Color bars depicts variation in methane production along the surfaces. (b) Dependence on time of evaluated effects on coal biogasification. Color bars depicts variation in time along the surfaces. (c) The effect of pH and temperature on coal biogasification. Bottom view at [NaCl] = 3.7 mg/cm^3. Color bars depicts variation in methane production along the surface.

Validation of experiment. Validation of predicted methane production for the microbial consortium, RTTM, used 6 g of subbituminous coal, tryptic soy broth (33.6% v/v), a salinity of 3.7 mg/cm^3 (0.37% w/v) NaCl, and was carried out at a temperature of 30°C and pH 5.5. The maximum headspace methane was 145,165 ppm (25.6 sft^3/ton) after the 105th day of incubation (Fig. 4). This was considerably larger than the maximum value (76,000 ppm) measured in the earlier experimentation. For demonstration purposes, gas measurements were only conducted up to 112 days. As indicated in Figure 14, there was a remarkable increase in methane production after the 66th day. This trend was in agreement with model's predictions: the largest methane concentrations would be obtained after 60 days of incubation. However, a prolonged, restricted growth phase, is observed initially. It is likely that the low initial cell concentration of 2.5 × 10^6 cfu/mL, or changes of microbial communities, and/or a transition between nutrient utilization and coal utilization at the tested conditions may had been responsible for this behavior. These results confirmed the suitability of the microbial consortium to produce large amounts of methane within the predicted region of operation with low

concentration of nutrient amendments (33.6% v/v). Nutrient solutions should be added at low enough volumes to maintain commercial viability. Favorable operational conditions were successfully recreated to maximize methane production for the foreign microbial consortium and the subbituminous Miller Black Thunder coal. However, an on-site pilot study for enhanced methane generation from coalbed methane wells is needed to evaluate laboratory tested conditions. The literature reports a wide range of methane yields for different coal ranks and microbial communities exposed to various strictly anaerobic enrichment and cultivation conditions. However, only a limited number of evaluations have been published where initial aerobic conditions were considered. Opara et al., for instance, reported methane yields up to 21 sft^3/ton with addition of 50% (38.5% v/v total liquid) nutrient solution, using aerotolerant microbial consortia and bituminous Deer Creek Mine coal (< 75 μm particle size, −200 mesh) at 23 °C and 30 days of incubation.[3] Similar methane yields were obtained for lignite (11 sft^3/ton) and coal waste (12 sft^3/ton) materials. Results of this study fells within this range.

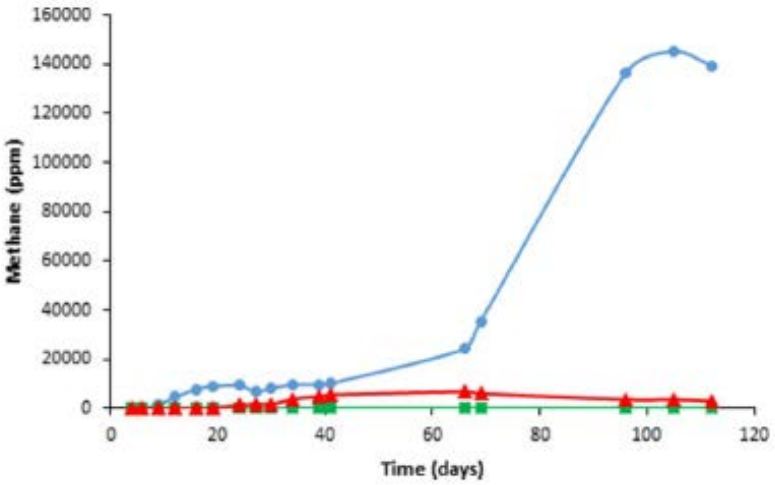

Figure 14. Verification experiment. Blue line depicts headspace methane for the microbial consortium, coal, nutrient and salt media. The green line shows methane production for the Type I control sample (the coal and salt media). The red line is for methane content for the Type II control sample (the microbial consortium, the nutrient and salt media). An additional control sample was used for this experiment (the coal, nutrient and salt media), however, not significant methane production was measured (not shown in the graph).

2.2.3. Characterization and performance of the porous proppant

Quantitative phase evaluation in porous proppant. Rietveld refinement of XRD patterns identified the crystalline phases of the kaolinite ($Al_2Si_2O_5(OH)_4$) and iron oxide (Fe_2O_3) mixtures after the combined sintering and pore forming heat treatment in reducing atmosphere. Rietveld refinement fits with weighted residuals <10% were obtained and used to calculate quantitative phase fractions of each phase accurate to ±4 wt%. Results for 5 wt% Fe_2O_3 compositions are shown in Figure 15 for several different temperatures in both air and reducing atmospheres. The sample, sintered at 1723 K in air, showed 73.4 wt% mullite ($Al_6Si_2O_{13}$), 22.8 wt% cristobalite (SiO_2), 1.1 wt% fayalite (Fe_2SiO_4), and 2.7 wt% unreacted Fe_2O_3. The large fraction of unreacted Fe_2O_3 and limited presence of hercynite ($FeAl_2O_4$)or fayalite confirms that samples fired in air are not reduced but remain relatively inert. On the other hand, samples fired in a reducing atmosphere are initially similar at 1523 K heat treatment but significantly different at 1623 K and 1723 K heat treatment. At these temperatures, where oxygen partial pressure is decreased, the fraction of Fe_2O_3 plummets to essentially 0 wt% and significant amounts of hercynite and fayalite phases were formed (up to 8.3 wt%).By 1723 K the fraction of mullite decreased from 72.2 wt% to 60.9 wt% even as cristobalite increased from 24.0 wt% to 29.6 wt%, and hercynite and fayalite increased from 0.0 wt% to 6.2 wt.%, and 1.0 wt% to 2.1 wt.%, respectively. The fraction of phases presents as a function of sintering temperature in reducing atmosphere is plotted in Figure 16.

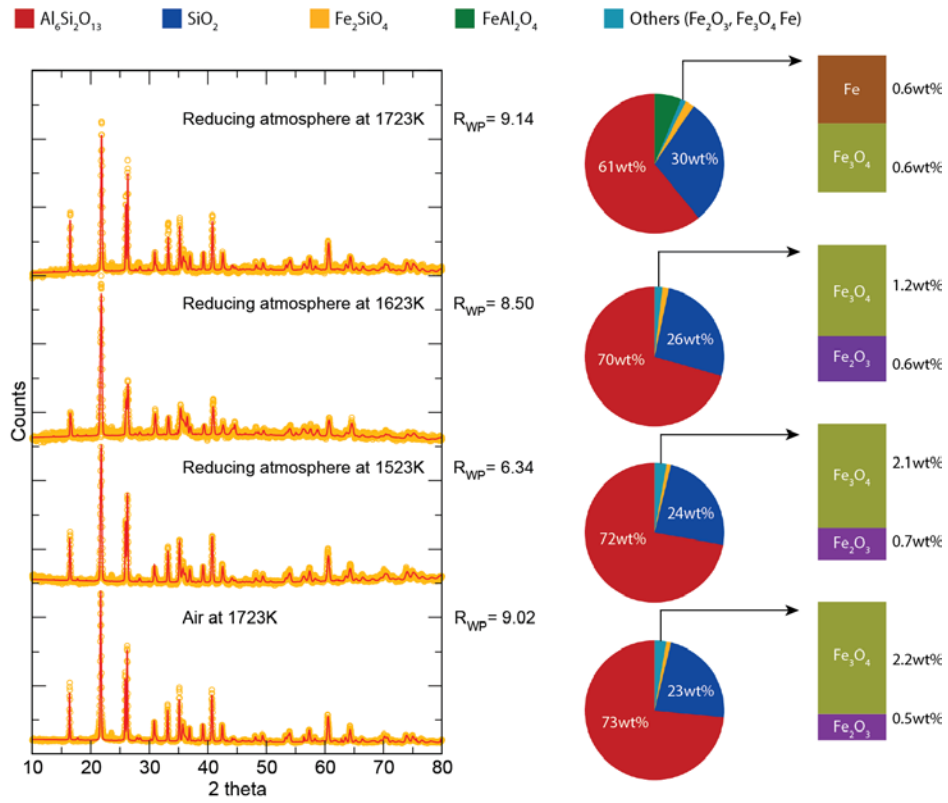

Figure 15. The X-ray diffraction (XRD) Rietveld refined results of kaolinite mixed with iron oxide (Fe_2O_3) in air at 1723 K and in reducing atmosphere at 1523 K, 1623 K, and 1723 K. Quantitative phase analysis are shown on the right. Other phases included Fe_2O_3, Fe_3O_4, and Fe. All Rwp values were below 10%.

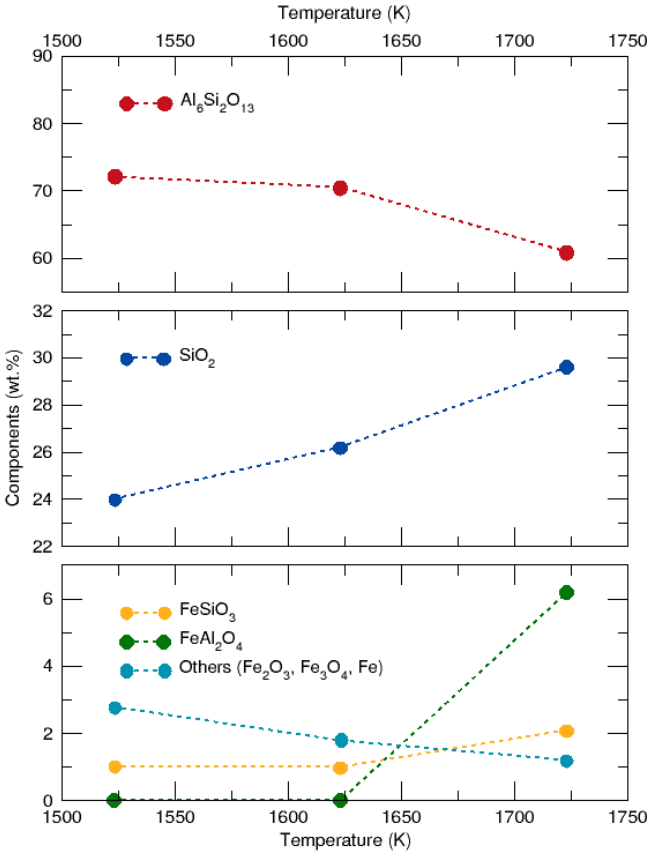

Figure 16. The calculated components from XRD refinement in weight percent for 5 wt% Fe_2O_3 samples sintered in reducing atmosphere.

Monitoring phase fraction is critically important since reduced iron reacting with aluminum to form hercynite ($FeAl_2O_4$) has been associated with pore formation due to negative molar volume change.[22] When fired in air hematite will not decompose into magnetite until ~1600 K. However, under a reducing atmosphere, hematite is reduced to magnetite, wustite, and, eventually, iron at very low temperatures.[23-25] For example, Wagner et al. performed in situ studies of hematite heated to 1073 K in flowing 10% H_2 gas and found that decomposition of hematite to magnetite, wüstite, and eventually iron metal occurred within ~1000 s.[26] Meanwhile, kaolinite undergoes a phase transformation first to metakaolinte (dehydroxylated), then to a mixture of mullite ($Al_6Si_2O_{13}$) and cristobalite (SiO_2) upon thermal treatment above 1323 K.[27-28] In this work we did not measure in situ XRD but rather, we quantified the phases present after the experiment ended. However, thermodynamic Gibbs free energy calculations for various iron oxide decomposition reactions in air and low P_{O_2} are calculated and shown in Figure 17(a). Assuming that hematite has been reduced to wüstite there are a number of plausible energetically favorable reactions for the observed formation of hercynite and fayalite:[22, 29-31]

$$7FeO + Al_6SiO_{13} \rightarrow 2Fe_2SiO_4 + 3FeAl_2O_4 \quad (7)$$
$$3FeO + Al_6SiO_{13} \rightarrow 3FeAl_2O_4 + 2SiO_2 \quad (8)$$
$$Fe_2O_3 + SiO_2 \rightarrow Fe_2SiO_4 + \frac{1}{2}O_2 \quad (9)$$

The Gibbs free energy for these expressions is plotted as a function of temperature in Figure 17(b). Given that we observe hercynite even when fayalite is absent we can assume that Equation 7 is unlikely to dominate which coincides with the fact that of the three routes it is the least negative in total change in free energy in Equations 7-9. On the other hand, the drop in mullite and rise in hercynite as well as cristobalite going from 1623 K to 1723 K suggests Equation 8 is dominant in this range.

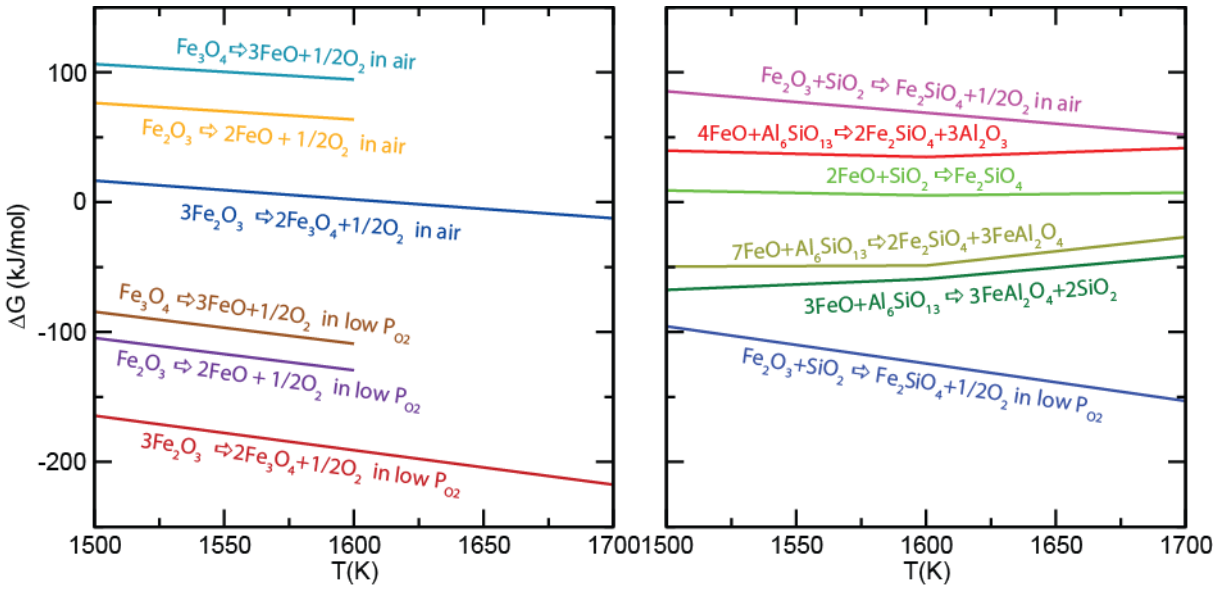

Figure 17. Gibbs free energies for various reactions involving decomposition of precursor materials to products in air and reducing atmospheres.[32]

Microstructure of pore in proppant. The SEM images taken in backscatter electron (BSE) mode show the microstructure and size of the pores formed (Figure 18). When pure kaolinite was sintered in air at 1723 K, the particles obtained were highly dense. The average pore size was 5.1µm (± 2.4 µm). Once Fe_2O_3 was added to kaolinite and sintered in air at the same temperature, the pore size was slightly increased to 13.8 µm (+/- 4.3 µm). However, Fe_2O_3 and kaolinite mixtures fired in reducing atmospheres had much larger pores with pore diameter size and standard deviation increasing with firing temperature. Samples fired at 1723 K had pores with 102.4 µm (+/- 55.5 µm) diameters whereas those samples fired at 1523 K had 25.6 µm (+/- 15.2 µm) diameters. The number of pores showed the opposite trend with fewer pores and a narrow standard deviation with increasing temperature (Figure 19). These microstructural observations are consistent with XRD results since we observe an increasing pore size and fraction with increasing formation of hercynite

and fayalite as mullite fraction decreases. Other studies showed that the pore size in kaolinite was grown by reducing hematite to magnetite and wüstite.[31, 33-35] When the sintering temperature was above 1473 K, the local pores in kaolinite started interconnecting each other.[35] Moreover, pores can be bloated by excessive gas formation in the particle during sintering.[35-39] In addition, inspection of the microstructure within the pores Figure 18 (d) and (f))shows needle-like grains whereas sintered mullite compacts normally exhibit platelet grain structures.[31] Seo and Tasukihashi have suggested that iron oxide accelerates grain growth in mullite which could explain the needle-like grains in the vicinity of pores but not elsewhere.[40]

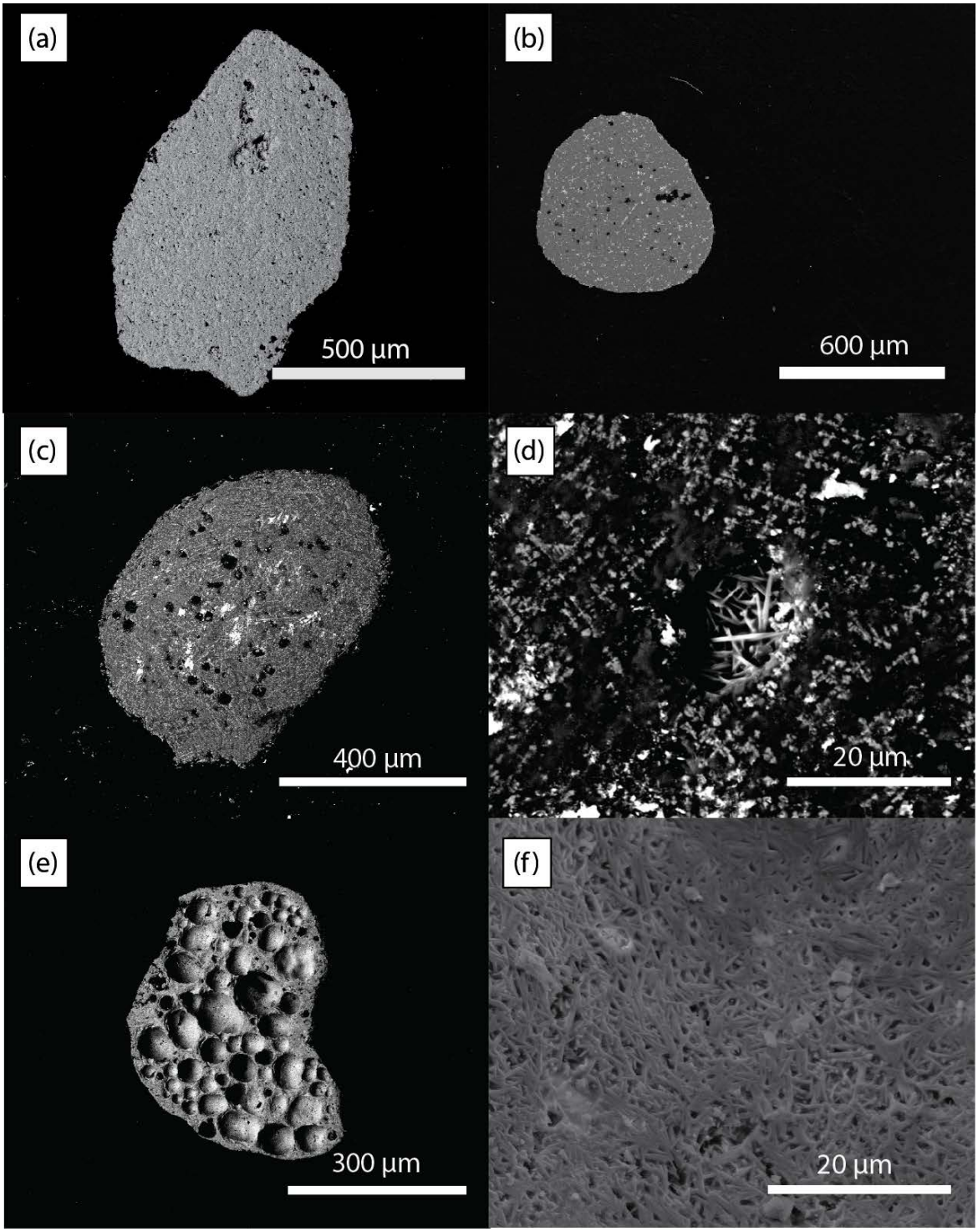

Figure 18. SEM micrographs taken in backscatter mode. (a) sintered kaolinite and (b) 5 wt% Fe_2O_3 added sintered kaolinite in air at 1723 K, and 5 wt% Fe_2O_3 sintered kaolinite fired in reducing atmosphere at [(c) and (d)] 1523 K and [(e) and (f)] 1723 K.

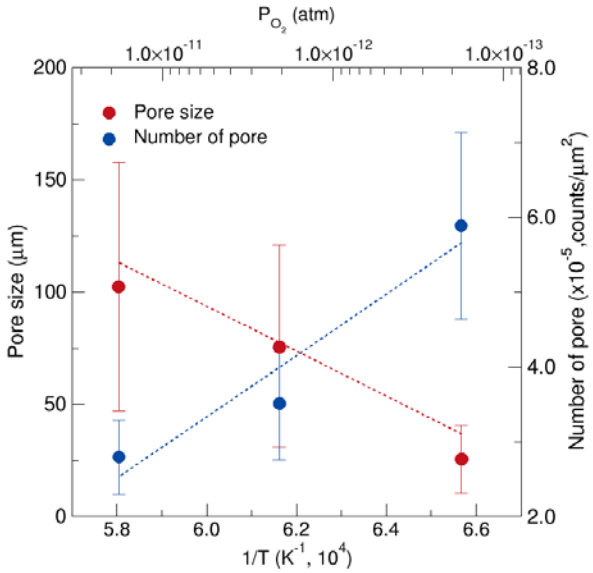

Figure 19. The pore size and the number of pores measured through SEM on 3 samples for each condition. The particles were 5 wt% Fe_2O_3 added to kaolinite and sintered at various temperatures and P_{O_2} atmospheres.

Measured density and porosity. Measured density and porosity. The bulk density of sintered kaolinitewas decreased by adding Fe_2O_3. Samples sintered in the reducing atmosphere decreased more in density than did those sintered in air (Figure 20). The sample sintered in air without Fe_2O_3 had a density of 2.5 g/cm^3 but the density decreased to 1.43 g/cm^3 when the sintering conditions had a reducing atmosphere and a temperature of 1723 K. The apparent porosity(Φ), a summation of open and close porosity, was calculated from the bulk density. The calculation is as follows:[10]

$$\Phi = \frac{\rho_t - \rho_b}{\rho_t} \cdot 100\% \quad (10)$$

where ρ_b and ρ_t were the measured bulkdensity of sample and theoretical density of the sample, re spectively.The theoretical density was calculated by using the weight fraction from the refined XRD and following pure component densities. The porosity was 7.1 vol% to 9.9 vol% in air without the additional Fe_2O_3 and this increased to 45.3 vol.% in a reducing atmosphere.

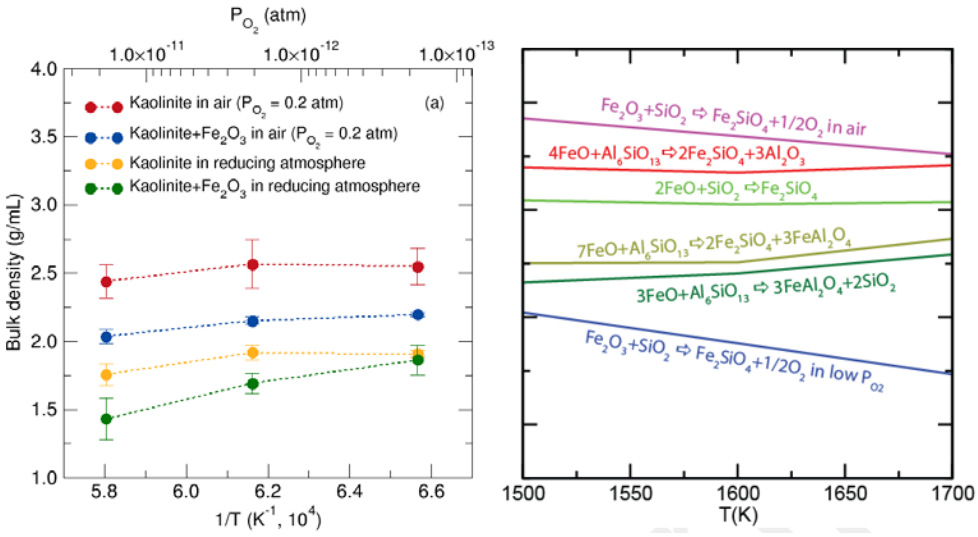

Figure 20. (a) The measured bulk density and (b) apparent porosity of kaolinite and Fe_2O_3 mixed with kaolinite, when sintered at various temperatures in air and different P_{O_2} atmospheres.

Crush resistance and acid solubility. The crush resistance test simulated an in-situ condition by physically compressing proppant particles. All of the proppant particles were initially 420 μm to 840 μm in nominal dimension (20/40 mesh). Sphericity is describable to minimize concentrations at point contacts. After prescribing the prescribed normal stress, some of the particles had been crushed with ensuring dimensions smaller than 420 μm. These fines are able to pass through a 40 mesh sieve after the testing. The kaolinite sintered in air yielded the smallest fraction of fine particles, while the samples of iron oxide mixed with kaolinite sintered in a reducing atmosphere had the largest fraction (Figure 21). In both sintering conditions, the sample yielded more fine particles once we added iron oxide to the kaolinite. The sample yielded 6.8 wt% of fine particles when the apparent porosity was 9.9 vol% and this increased to17.7 wt% with an apparent porosity of 45.3 vol%.

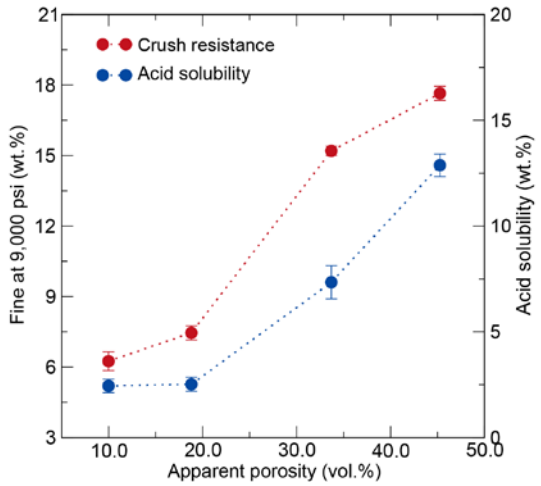

Figure 21. The crush resistance and acid solubility of the ceramic proppant as a function of apparent porosity.

Enhanced crush resistance with increasing density is a standard tradeoff in developing light-weight proppant. The pores which reduce density also weaken the material. In commercial bauxite proppant low fine yield (3 wt % to 5 wt%) at 10,000 psi is observed but the density is high (2.2 g/cm^3).[41] Luscher *et al.* found that kaolinite and aluminum oxide proppant (no iron oxide) showed the strength from 36,000 psi to 13,000 psi and the density was very high (3.1 g/cm^3 to 3.9 g/cm^3), but they measured a single proppant particle instead of pack.[42-43] It is therefore difficult to compare the results from Luscher *et al.* with others in crush resistance. On the other hand, sand has a lower density (1.7 g/cm^3) but generates a very high amount of fines (43 wt% at 10,000 psi).[41] Other attempts have been carried out to reach a compromise between strength and density. For example, aluminum oxide proppant doped by magnesium oxide showed a low density at 0.92 g/cm^{3}but yielded 29 wt% fines at 400 psi.[44] The American Petroleum Institute (API) committee suggested the maximum fines of 14% at 4,000 psi for 20/40 mesh.[45] The 5 wt% iron oxide doped kaolinite proppant in this study fired at 1723 K in a reducing atmosphere demonstrated nearly suitable yield of fines at 9,000 psi (18 wt%) while also achieving a very low density of 1.4 g/cm^3 due to the highly porous structure.

Acid solubility testing was also performed to assess the chemical resistance of proppant. The API committee suggested less than 2 wt% loss for 20/40 mesh proppant.[46] When samples prepared in this work were exposed to acids we observed 5.5 wt% loss at 9.9 vol% apparent porosity and 12.9 wt% at 45.3 vol% porosity. Increasing the surface porosity increased the overall reactive surface area with acid. Therefore, higher porosity accelerates the dissolution by acid and confirms another study which found that increased surface roughness also enhances acid solubility.[47]

Furthermore, the materials determine the acid solubility in given particle size at 20/40 mesh. Aluminum oxide based proppant doped with CaO, MgO, or BaO showed low solubility (0.73 wt% to 1.79 wt%).[13] Montmorillonite and red mud proppants yielded high solubility of 8 wt% and 16 wt%, respectively.[47-48] However, acid solubility resistance could be improved by adding other materials. For example, the red mud proppant lowered the solubility to 3.1 wt.% from 14.4 wt% by adding 17 wt% of barium carbonate ($BaCO_3$).[47] Even though this study showed the kaolinite proppant with additive iron oxide did not meet API standard in

acid solubility, the proppant did demonstrate high strength with low density suggesting it could serve well in applications where acid treatments are not necessary. It is also possible to use this material as a starting point for future studies to reduce acid solubility.

2.2.4. Encapsulation and methane production

Polymer encapsulation and dye retention efficiency. Droplets containing the proppant and calcium lactate were left in the sodium alginate solution over time to polymerize. The average size of the encapsulated particles increased asymptotically from 2.58 mm at 10 s to 2.85 mm at 300 s. The coating thickness was calculated by subtracting the initial proppant diameter from the temporarily measured encapsulated particle dimension (Figure 22). Coating thickness approached an asymptote after 120 s of polymerization. Polymerization occurs as Ca^{2+} ions diffuse from the solution-filled pores within the particle through the gel which has formed until it reaches the exterior surface where it can be chelated by the alginate polymer strands in solution to grow the encapsulating layer.[49] Encapsulating layer thickness is limited to the amount of Ca^{2+} ions present in the proppant particle.[15, 49-51] This dependence explains the observed high initial rate of growth, which slowly plateaus after the calcium ions in the initial droplet are exhausted. The amount of encapsulated dye after polymerization was calculated using Eq 1. The encapsulation efficiency decreased only slightly from 99% to 97% when the polymerization time was increased from 30 s to 600 s (Figure 23).

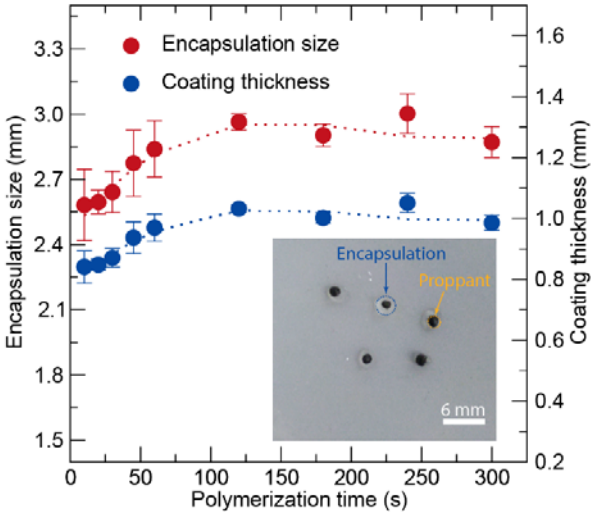

Figure 22**.** Encapsulated particle size and coating thickness as a function of polymerization time. (Inset) Optical image of the encapsulated proppant.

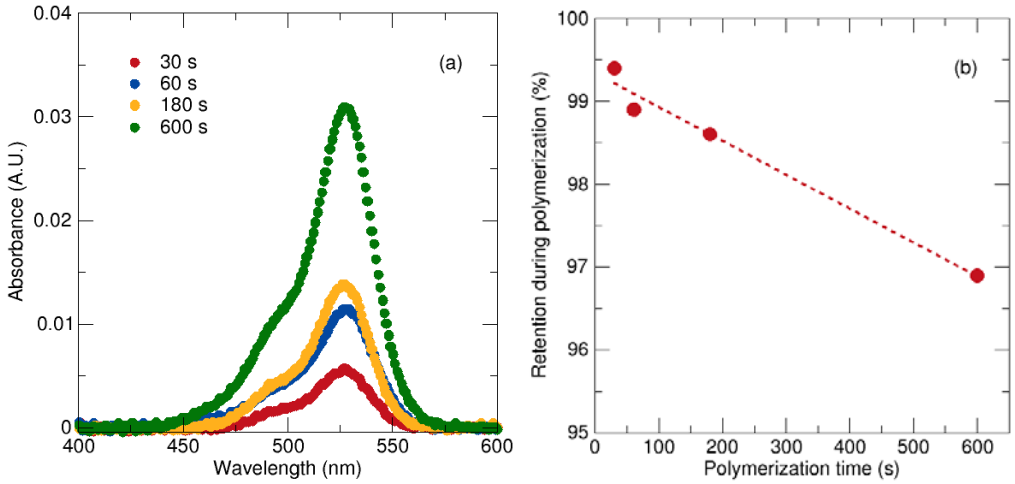

Figure 23. (a) UV-Vis spectra of residual rhodamine 6G in the alginate solution at various polymerization times, and (b) the calculated retention efficiency of the dye at various polymerization times (b).

Release of encapsulated dye and release mechanism**.** Figure 24 shows the dye released from the encapsulation coating in solutions with various proton and potassium concentrations. The encapsulation, containing proppant and dye, was exposed to pH conditions of 4.3, 7.2, and 11.2. A greater amount of dye was released from the encapsulation coating when the surrounding aqueous environment had a lower pH. The dye released from encapsulation was 5.4 µM at pH 4.3 and 4.4 µM at pH 11.2. Dye release was also measured in saline solutions containing various concentrations of KCl at pH 7.2. The KCl concentration ranged from 13 mM to 46 mM. When rhodamine 6G release was monitored in the KCl solutions, a trend similar to that for solutions with different pH levels was observed; a greater amount of dye was also released at higher concentrations of KCl. As the pH was lowered, H^+ ions protonated the carboxyl groups in the alginate gel which broke the bond with the calcium ions.[52] Alginate stability was influenced by the addition of cations such as protons and potassium ions.[53-54] The bond between calcium ions and the alginate polymer served as the backbone for the gel. Breaking these bonds resulted in the release of Ca^{2+} ions into the solution and subsequently enabled the release of dye and bacteria into the surrounding solution (Figure 25).

Solutions with low pH contained greater proton concentrations. As a result, the gel was less stable and less tightly bound, enabling faster dye release. Similarly, when potassium ions were exchanged for calcium ions, the gel was also less tightly bound, facilitating faster dye release. The release amount increased with increasing potassium ionic exchange. Kikuchi *et al*. also showed that an increase in sodium chloride concentration generated a higher release rate of encapsulated molecules from a calcium-alginate bead.[55] Ionic exchange with protons and potassium ions should result in an increase in the concentration of dissociated calcium ions at a given time until an equilibrium is reached. To verify this hypothesis, encapsulated samples were suspended in DI water at pH 7.2 and in KCl solution (30 mM) at pH 7.2 for 13 h with continuous measurement of the calcium ion concentration (Figure 26). The KCl solution showed a higher dissociated calcium concentration compared to the low pH condition. In both instances, the extent of calcium ion dissociation from the encapsulation coating increased coincidently with dye release. These results suggest that ion exchange is a viable mechanism for increased dye release.

Dye-laden encapsulated proppant particles were also exposed to ammonium persulfate, which is a commonly used oxidizing agent in some oil and gas wells to reduce viscosity of fracturing fluids. UV-Vis spectroscopy initially showed an increase in the intensity of the rhodamine 6G signal, with a steep slope (17.70 µM/h), suggesting rapid dye release. For comparison, the slope at KCl (46 mM) concentration was only 1.02 µM/h. However, after a short time (0.4 h), the rhodamine 6G signal intensity began to decrease, which suggested that the ammonium persulfate was oxidizing the dye molecules themselves.

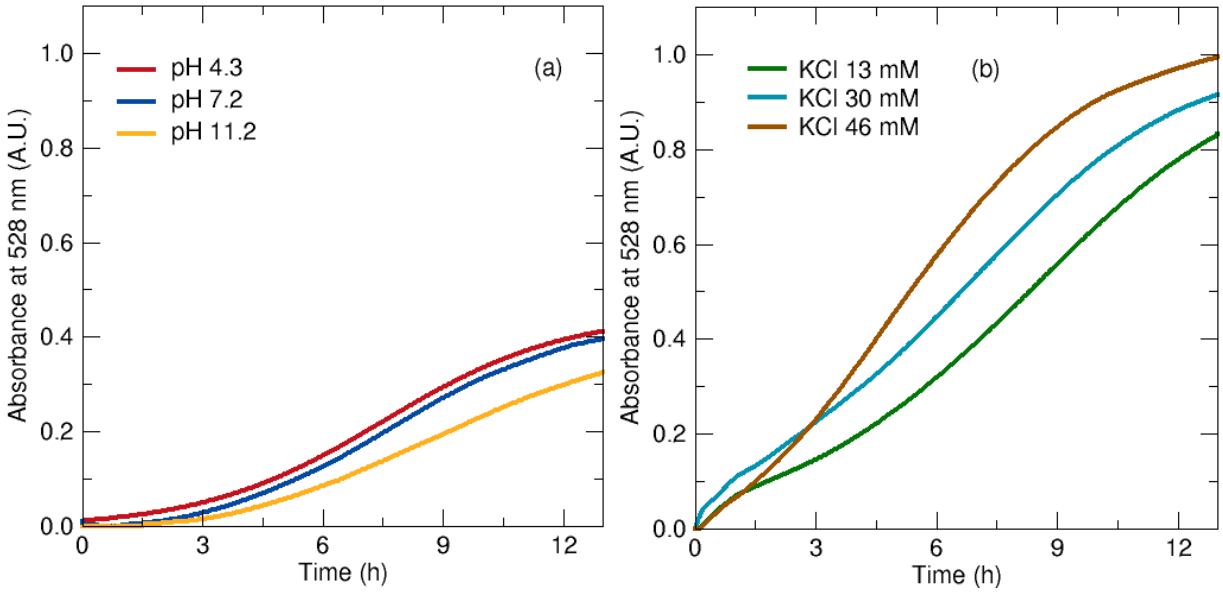

Figure 24. The time release of rhodamine 6G from the encapsulation coating was measured by ultraviolet-visible (UV-Vis) in solutions of (a) various pH, and (b) concentrations of KCl at pH 7.2.

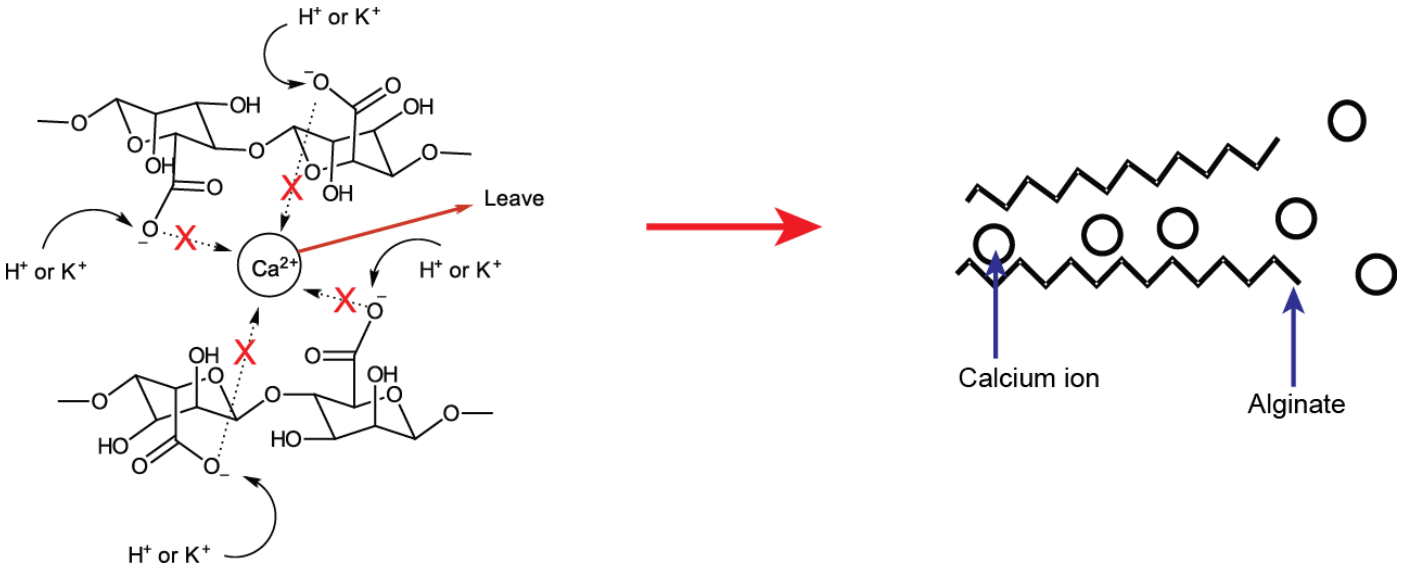

Figure 25. Schematic of competitive bonding of the polymer with various cations leading to the release of Ca^{2+} ions into the surrounding solution.

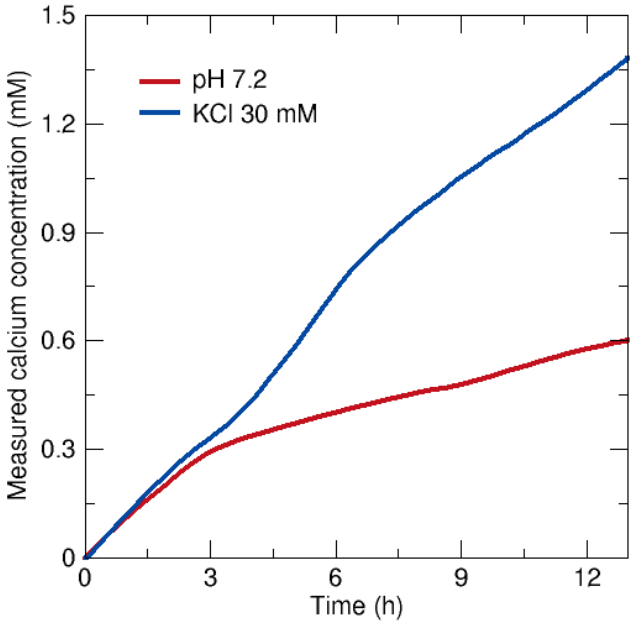

Figure 26. Free calcium ion concentration as a function of time due to dissociation of the Ca^{2+} alginate bond at pH 7.2 and 30 mM KCl also at pH 7.2.

Temperature dependent release of encapsulated microbes. In a complimentary set of experiments, methanogenic bacteria were encapsulated at room temperature at pH 7.2 in the same manner described above for rhodamine 6G encapsulation. Figure 27 shows the release of bacteria at 20°C and 36°C. Little difference is observed between the samples held at the two temperatures before 12 h but after this time a ~25% higher concentration of free bacteria was found in the sample maintained at a higher temperature. The number of released microbes increased with time and temperature. The increased microbe release is partly due to higher diffusion at higher temperatures since the gel itself swells more at elevated temperatures.[56-57] Swelling opens the structure and modifies the pore size to enhance conductivity.[56] The release of microbes is lower than the release of the smaller dye molecules suggesting that swelling did not increase pore size sufficiently to allow for a large increase in bacterial diffusion.

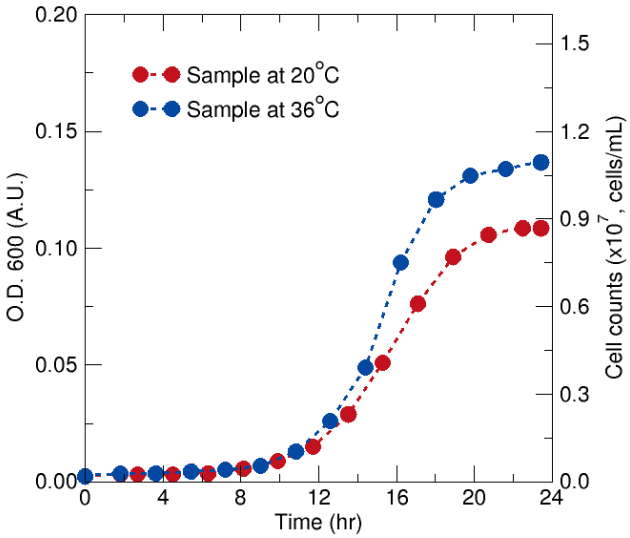

Figure 27. Released bacteria concentration measured via UV-vis spectroscopy absorption released from the encapsulation coating at 20ºC and 36ºC as a function of time.

Methane production from released microbe in simulated in situ environment. Carbon dioxide and methane gases were monitored in the headspace of the conical tubes using gas chromatography (Figure 8). All samples produced carbon dioxide within the first 72 h: control sample $(1.78 \times 10^5$ ppm) and samples at 20°C $(3.18 \times 10^5$ ppm) and 36°C $(4.13 \times 10^5$ ppm). The amount of carbon dioxide released from the encapsulated samples decreased over time, whereas the carbon dioxide concentration in the control was constant. At 680 hours, the carbon dioxide content measured for the sample at 20ºC was reduced to 2.24×10^5ppm, whereas that in the case of the 36ºC sample decreased to 1.52×10^5 ppm. The methane gas concentration was inversely related to the carbon dioxide concentration. The control sample, which did not contain microbes, showed a constant methane concentration of approximately 6 ppm over the entire time interval. The sample containing encapsulated proppant with microbial consortia showed methane production after 240 h. The sample maintained at 36°C produced a higher methane concentration(7.15×10^3 ppm) over the measurement period, whereas the sample maintained at 20°C produced 1.12×10^3 ppm of methane - at its maximum - over the measuring period.

Figure 29 shows the real-time measurements from samples in the simulated in situ environment bioreactors. After ~12 hours, in agreement with time-release delivery experimental results shown in Figure 27, the samples both exhibited the production or change in pH, hydrogen, carbon dioxide, and methane associated with microbial release from encapsulation and interaction with coal present in the bioreactors. The pH of the 36°C sample decreased more than that of the at 20°C sample. The pH of both samples increased back to neutral over time. Similar volumes of hydrogen gas were produced from the two samples. However, the 36°C sample consumed more hydrogen gas than the 20°C sample and produced more methane over the same time period. More carbon dioxide was produced at 36°C than at 20°C, and both samples consumed carbon dioxide gas. Ultimately, the sample at 36°C produced 1.5 times more methane than that at 20°C.

In the generation of biogenic methane from coal, methane gas can be produced from either acetate or the reaction of hydrogen and carbon dioxide: the reaction is $2H_2 + CO_2 \rightarrow CH_4 + O_2$.[58] The low measured pH could be caused by acetate from organic compounds derived from the coal and methanogenic microbes. During methane generation from coal, hydrogen can be produced as a byproduct.[59-61] Carbon dioxide can be generated largely from fermentation. The production rate of CO_2 depends on the coal rank.[62-63] The generated hydrogen gas is consumed by reaction with carbon dioxide to produce methane.[58]

Compared to other studies in which methane was produced at 100 to 300 ppm, more gas was generated in this experimental program.[64-65] This increased gas generation is attributed to the nutrient accelerating methane gas production by stimulating the microbes.[352,53] Furthermore, microbes at the elevated temperature produced more methane because the microbes are more active at 35ºC – 40ºC than below 35ºC or above 40ºC.[66]

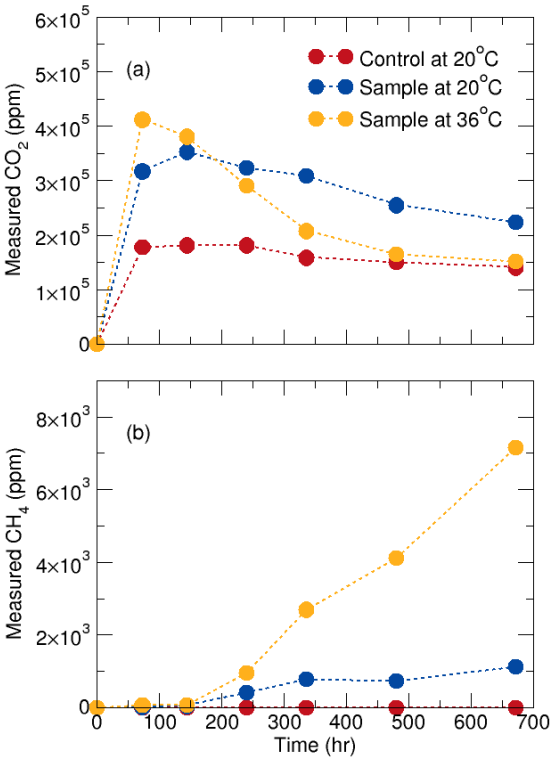

Figure 28. Gas chromatography measurements of (a) carbon dioxide gas, and (b) methane gas produced from the encapsulated microbial consortia and proppant over time.

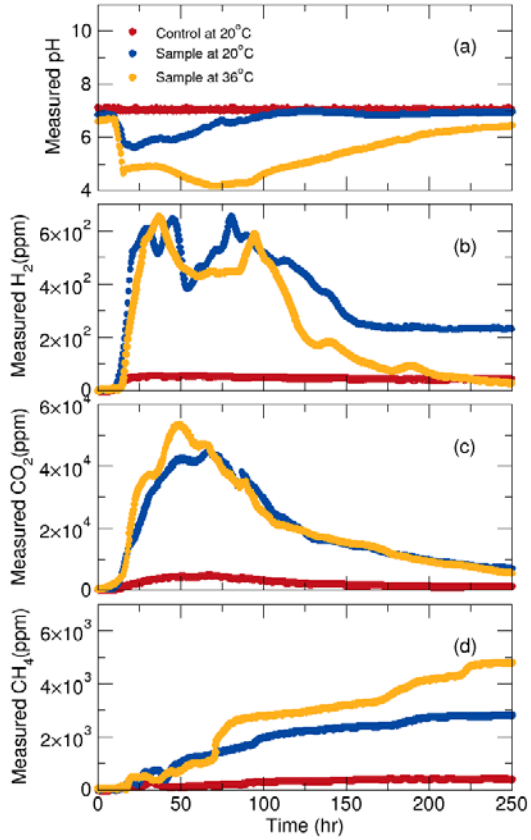

Figure 29. Real time measurements of (a) pH, (b) hydrogen gas, (c) carbon dioxide gas, and (d) methane gas produced from bioreactors containing encapsulated microbe-laden proppant and coal in a simulated in situ environment.

2.2.5. Conductivity and coal characterization

Conductivity at ambient pressure. Figure 30 shows the conductivity for control at 20°C and the samples at 20°C and 36°C. The conductivity of the samples started being increased after 20 days. The conductivity of control was constant for 57 days at ~530 mD-ft. The sample at 36°C demonstrated the greater increase of conductivity than 20°C over time. In day-54, the sample at 36°C was 680 mD-ft while 20°C condition was 650 mD-ft. The result implied that the encapsulated bacteria with proppant interacted with the coal pack.

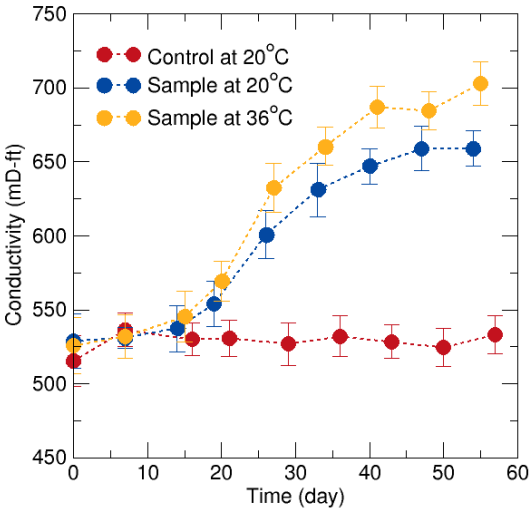

Figure 30. The conductivity measurement of the coal and samples as a function of time.

Coal surface structure analysis.
Table 14 shows that the surface structure analysis of the samples by BET and BJH. The surface area was decreased from 12.34 m^2/g at 0 week to 4.80 m^2/g at 6 weeks, whereas the pore size was increased from 4.23 nm to 16.13 nm. Figure 31 shows the coal particles which were used in the conductivity measurement at various days. The coal particle size was decreased by a half after 6-week storage with the bacteria encapsulation. The shards on the particle surface were appeared over time. The recovery of fracture conductivity results from microbial activity in a proppant pack intentionally damaged by entrainment of coal fines. The consortium degraded the coal and restored conductivity or increased conductivity. Conductivity is the product of the fracture width and the permeability of the material propping the fracture open.

The coal sample contained the encapsulated bacteria with proppant and stored at room temperature from 0 week to 6 weeks. The relative change of peak intensity can inform the interaction between the coal and bacteria. Figure 32 exhibits wavenumber peaks from 1500 cm^{-1} to 900 cm^{-1}. The spectra at 1440 cm^{-1} and 1370 cm^{-1}, assigned to aliphatic chains (CH_3, CH_2) and CH bending of CH_2/CH_3 groups, were decreased over time. The spectrum at 1370 cm^{-1} was the absorption of methyl symmetric bending vibrations in tertiary butyl groups, normally present in low rank coals.[67] The relatively decreased peak intensities supported the hypothesis that the released bacteria would consume the hydrocarbons. Furthermore, the spectra at 1165 cm^{-1}, 1100 cm^{-1}, 1030 cm^{-1}, 1010 cm^{-1}, and 910 cm^{-1} were C-O, SiO_2, Si-O-Si, and C=C. Below 1250 cm^{-1} wavenumbers generally indicated the quartz and minerals.[68-70] These spectra were relatively increased comparing with 1440 cm^{-1} and 1370 cm^{-1}. Hydrocarbon is an important material; it is the primary resource for growing microbes, and the coal mostly consisted of hydrocarbon chains. The possible chemical functional groups in coal are aliphatic CH_x, aromatic C=C ring, C-H out-of-plane, rare C=O, and aliphatic C-O-C and alcohol C-O.[71] The encapsulated microbes could also react with these functional groups in the coal.

Thermogravimetric analysis (TGA) determined weight loss upon heat treating. For example, samples that loss significant hydrocarbons due to biogasification will have less weight loss than pristine coal samples. The control was the coal, and the sample was the encapsulated microbes in the coal. The encapsulated microbes with proppant were loaded into the coal. After incubating the sample for 6 weeks at room temperature, the coal and the proppant were separated by sieves. Both control and the sample were completely dried in the

oven at 60°C overnight. The samples were placed in TGA and monitored for a change of weight from room temperature to 950°C. The atmosphere condition was 70% of nitrogen and 30% oxygen. At 950°C, the coal and the sample lost 40.2 wt.% and 45.3 wt.% (see Figure 3). The difference of weight loss indicated that the sample with microbial activity was more favorable to burn the coal (greater weight loss means greater oxidation of hydrocarbon). The mechanism and exact origin of improved combustion is not yet determined but one likely reason is that bacterial activity increases porosity in the sample leading to more facile combustion.

Table 14. Surface structure analysis of the coal samples determined by BET and BJH in mean value and standard deviation of three measurements.

Samples	Specific surface area (m^2/g)	Total pore size (nm)
Coal 6 week	12.34 ± 0.99	4.23 ± 1.50
Coal 2 weak	10.39 ± 0.42	1.08 ± 1.77
Coal 0 weak	4.80 ± 0.47	16.13 ± 2.94

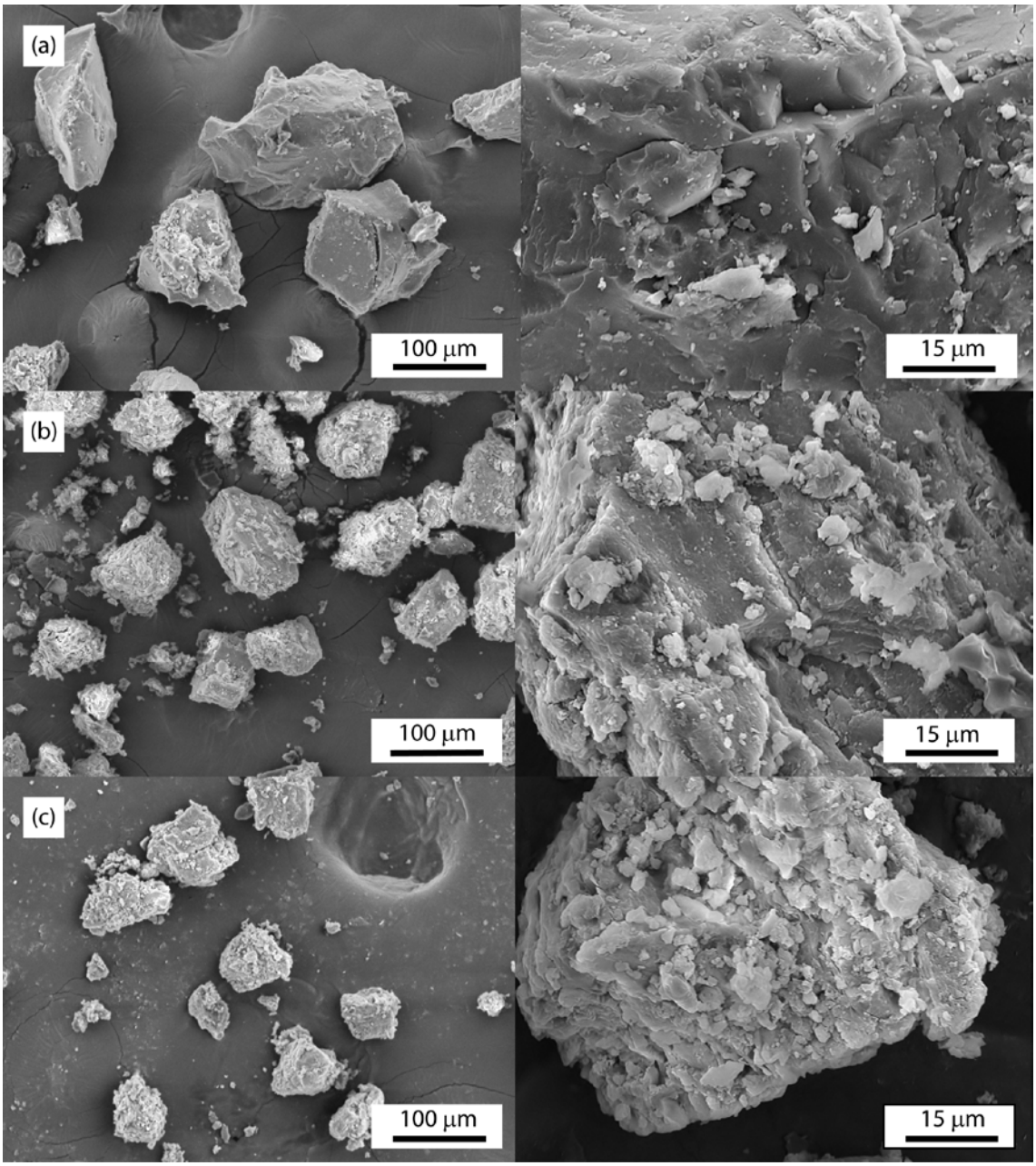

Figure 31. Scanning electron microscopy images of coal at 0 week (a), 2 weeks (b), and 6 weeks (c) incubated with the bacteria encapsulated sample at 20°C.

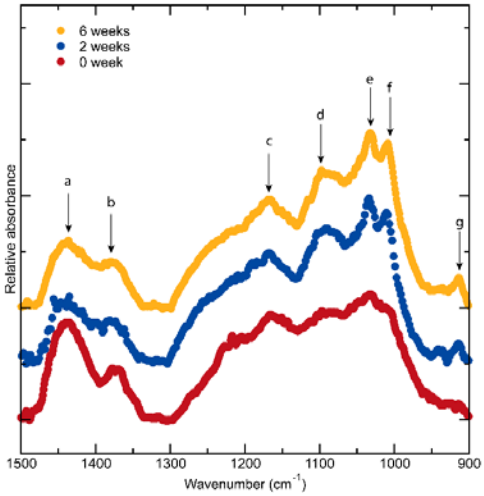

Figure 32. Fourier transform infrared spectroscopy (FTIR).

Table 15. Band assignments in FT-IR spectra of the sample.[71-73]

Labels	Wavenumber (cm^{-1})	Assignments
a	1440	Aliphatic chains (CH_3, CH_2)
b	1370	CH bending of CH_2/CH_3 groups
c	1165	C-O aliphatic ether stretching
d	1100	Quartz (SiO_2)
e	1030	S=O sulfoxide stretching Si-O-Si bending vibrations
f	1010	Si-O-Si bending vibrations
g	910	C=C alkene bending

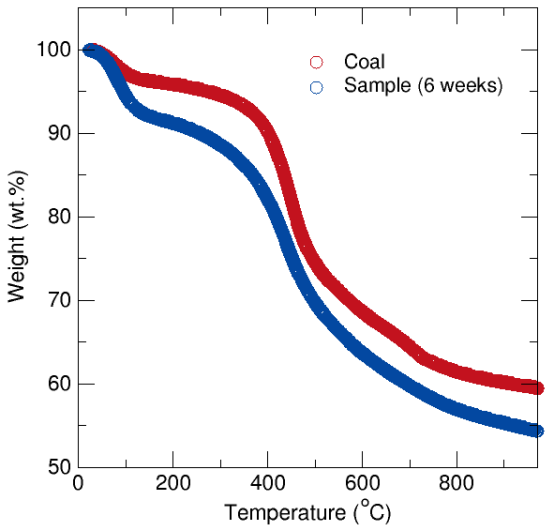

Figure 33. The result of thermogravimetric analysis. The control was the autoclaved coal, and the sample was the autoclaved coal mixed with the bacteria encapsulated proppant. The sample was incubated at room temperature for 6 weeks.

2.2.6. Production rate of methane and nutrient/production cost

Production rate of methane. Sample A and B refer to the same microbial consortia mixed with coal except that Sample B is delivered to the coal via encapsulated proppant whereas Sample A is simply mixed from solution. In the last quarterly report, we measured the conductivity as a function of temperature periodically. However, it was a challenge to simultaneously collect the gas while measuring the conductivity due to the limited access in our customized chamber. Thus, we made extra samples to measure the production of methane gas. The methane gas of Sample B was measured from the extra samples, which were stored for 80 days at 20°C and 36°C. Sample A (no proppant) generated greater methane at both 20°C and 36°C than Sample B (encapsulated in proppant). The difference is likely due to the different volumes of bacteria present in the two conditions; Sample A had more microbes present than those housed within

proppant in Sample B. Nevertheless, Sample B has a way to deliver bacteria directly to coal reservoirs and even with its reduced volume of bacteria delivery, it exhibits a rate of methane production that exceeds other studies performed at lab scale. For example, literature methane production ranges between 0.02 ppm/gram coal/day to 18.6 ppm/gram coal/day at room temperature but here we observe that Sample B can reach between 6.9 ppm/gram coal/day and 49 ppm/gram coal/day.[74-78] Sample B with slightly lower production rates may still be desirable over Sample A because a small volume of bacteria could be generated and delivered to a specific location rather than preparing enormous volumes of bacteria to permeate the entire well bore.

Table 16. The calculated production rate of methane.

Temperatures (ºC)	Sample A (ppm/gram coal/day)	Sample B (ppm/gram coal/day)
20	16.1	6.9
36	233.3	49.0

Nutrient/production cost. Table 17 shows the estimated manufacturing time and cost of raw materials and process for 1 kg production. The detailed recipe for optimized nutrients was mentioned in the previous quarterly reports. This report shows the overall estimated cost of nutrient. In this project proppant batches were around 400 g per production. The cost estimation for 1 kg of proppant was scaled by a factor of 2.5. Currently, the costliest raw material is kaolinite because the vendor, Sigma-Aldrich, was providing higher purity materials intended for laboratory studies. In the future, the cost of kaolinite can be greatly reduced by exploring other suppliers. The microbial growth in our lab studies were costly because of the extended time required to culture and grow an initial bacterial colony. However, if bacteria were to be used in methanogenic coal biogasification the cost would be far lower because the bacteria can be maintained rather than continuously re-cultured.

Table 18 shows the estimated production cost and selling price of our proppant. The cost of raw materials was approximated from the current market value. The gross margin value was set up to 30%.[79] The selling price, including the 30% gross margin, was $383.45. The calculated selling price was close to the price of Chinese proppant product (Figure 34). Even if the selling price includes the detail cost, the price of our proppant product can be the average price between China and United States markets. Furthermore, the conductivity has been increased by embedding the bacteria encapsulated proppant as shown in the last quarterly report. American market has been served by product from China due to the low product price.[80] We have demonstrated that the encapsulated proppant has an excellent competitive product in the market in product price and the high performance.

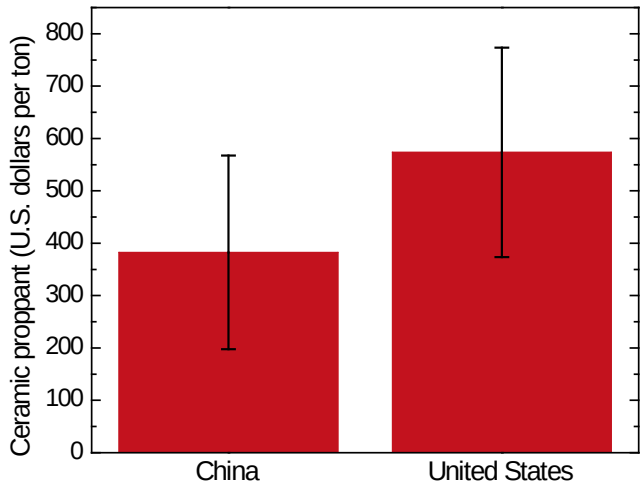

Figure 34. The ceramic proppant selling price in 2017 in China and United States.[80-82]

Table 17. The estimated manufacturing time and cost of raw materials and process based on 1 kg production.

Raw material estimation for 1 kg production				
Categories	Raw materials	Price per kg raw material	Required amount per kg product	Total price
Proppant	Kaolinite	$ 47.30	541 grams	$ 25.57
	Iron oxide	$ 60.16	28 grams	$ 1.71
Polymer	Calcium lactate	$ 29.96	8 grams	$ 0.24
	Sodium alginate	$ 51.81	2 grams	$ 0.11
Microbe	Coal (Miller Black Thunder)	$ 3.16	5 grams	$ 0.02
	Nutrient (Tryptic soy broth)	$ 85.80	9 grams	$ 0.77
	Sodium chloride	$ 55.70	2 grams	$ 0.12
Net total price				$ 28.54

Tools for processing 1 kg production			
	Price per unit	Required operation time or unit for 1 kg product	Total price
Hydrogen gas	$ 26.09 per tank size 220	28 hours operation with 20 sccm	$ 0.15
Nitrogen gas	$ 7.20 per tank size 220	28 hours operation with 80 sccm	$ 0.16
TSA plates	$ 0.90 per plate	2 plates	$ 1.80
Net total price			$ 2.11

Manufacturing hours for 1 kg product			
Manufacture	Process	Total hours	Direct labor hours
Proppant	Milling	26	2
	Sintering	7	2
Microbe	Culture and growth	336	3
Encapsulation	Encapsulation	4	4
Net total hours		373	11

Note: sccm is standard cubic centimeter per minute.

Table 18. The estimated production cost and selling price.

Estimated production capacity		1 ton
Production cost components	**Per unit**	**Totals**
Raw materials	$ 188.66 per ton	$188.66
Direct labor hours based on two labors	11 hours	$ 79.75
Total production costs		$ 268.41
Selling price (including 30% gross margin)		$ 383.45

2.3. Conclusion

We successfully achieved all of the goals of this project. Each task with its associated milestone was completed successfully. The methanogenic microbial consortia were cultured from coals. The cultured microbes were grown in the optimized conditions such as temperature, pH, and salinity. The lightweight ceramic proppant was effectively produced under reducing atmosphere, and the porous structure was characterized by XRD and SEM. The lightweight proppant performed in acid and crush resistance. Both microbes and proppant were successfully encapsulated by calcium-alginate polymer. The encapsulated microbes were released and produced methane gas in the simulated in-situ condition. The elevated temperature produced more methane than room temperature. The conductivity was increased once the microbes were released from the encapsulation system. The coal particle size was reduced by microbe consumption.

3. Products

Accepted peer-reviewed publications:

1. John Fuertez, Van Nguyen, D. Jack Adams, John D. McLennan, Kyu-Bum Han, and Taylor D. Sparks “Optimization of Biogenic Methane Production from Coal” *International Journal of Coal Geology*, 183, (2017) 14-24. DOI: https://doi.org/10.1016/j.coal.2017.09.014.
2. John Fuertez, Richard Baokye, Austin Gottschalk, Jack Adams, John McLennan, and Taylor D. Sparks “Developing Methanogenic Microbial Consortia from Diverse Coal Sources and

Environments" *Journal of Natural Gas Science & Engineering,* 46, 637-650 (2017). DOI: http://dx.doi.org/10.1016/j.jngse.2017.07.028.

Peer-reviewed publications currently under review:

1. John Fuertez, Gloria Cordoba, John McLennan, D. Jack Adams, and Taylor D. Sparks "Potential application of developed methanogenic microbial consortia for coal biogasification" *under review.*
2. Kyu-Bum Han, Alexandre Stella, John Fuertez, Alexandre Szendrei, Van Nguyen, John McLennan, and Taylor D. Sparks "Calcium alginate polymer encapsulation of proppant with time-release delivery of microbial consortia for methanogenesis" *under review*.
3. Kyu-Bum Han, Christian J. Robert, Laercio Martins de Mendonca Filho, John McLennan, and Taylor D. Sparks "Synthesis and microstructural evolution in iron oxide kaolinite based proppant as a function of reducing atmosphere, sintering conditions, and composition" *under review*.

Peer-reviewed publications in preparation:

1. Kyu-Bum Han, John McLennan, and Taylor D. Sparks "Enhanced conductivity due to methanogenic bacteria incorporation into ultralightweight proppant." *In preparation.*

Patents and Licensing Agreements:

1. "Encapsulated porous proppant" filed June 2 2017 as U.S. Application No. 15/612,659.
2. "Encapsulated porous proppant" license agreement (November 2017) between University of Utah and HiFunda LLC, Salt Lake City, UT.

Conference presentations:

1. Gasification Systems and Coal & Coal-Biomass to Liquid Workshop (Bio Gasification Panel), "Ceramic Proppant Design for In-Situ Microbially Enhanced Methane Recovery", Morgantown, WV, August 10-11, 2015.
2. Pittsburgh Coal Conference, "Ceramic Proppant Design for In-situ Microbially Enhanced Methane Recovery" Pittsburgh, PA in October 8, 2015.
3. Northeastern University, Chemical Engineering Department Seminar "Ceramic Proppant Design for In-situ Microbially Enhanced Methane Recovery", December 2, 2015.
4. Montana State University Bozeman, "Ceramic Proppant Design for In-situ Microbially Enhanced Methane Recovery" December 4, 2015.
5. Gasification Systems and Coal & Coal-Biomass to Liquid Workshop, "Synthesis of the Polymer Encapsulated Porous Proppant for Bacteria Delivery", Morgantown, WV, August 10-11, 2015.
6. nanoUtah conference, "Encapsulated Fe2O3 Doped Kaolin Proppant for Microbial Enhanced Coalbed Methane Recovery", Salt Lake City, UT in October 13, 2015.
7. Materials Science and Technology conference, "Performance of methanogen encapsulated proppant in release and conductivity", October 23, 2016, Salt Lake City, UT.
8. USTAR Confluence, "Polymer encapsulated ceramic proppant for in-situ microbial enhanced methane recovery", October 4, 2016, Salt Lake City, UT.
9. American Chemistry Society, "Microbial consortia encapsulated with ultralight kaolinite proppant for in-situ microbially enhanced methane recovery", April 2, 2017, San Francisco, CA.

Appendices

Synthesis setup for milling and sintering

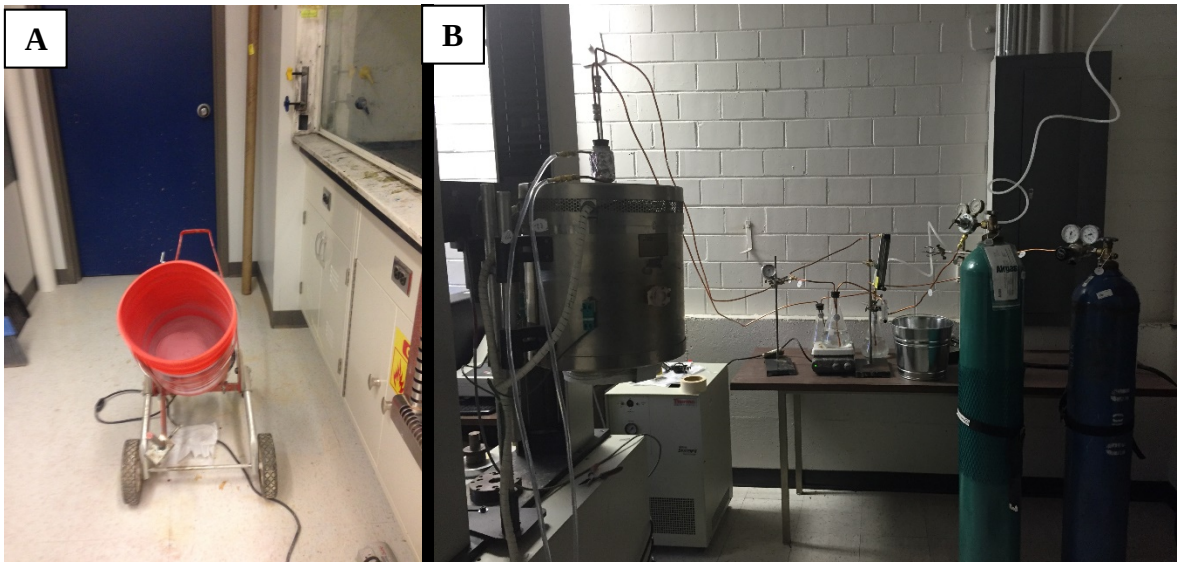

S 1. The synthesis setup. A) Milling step. The mixed powder was milled for 24 hours at room temperature. In order to make the slurry, DI water was added to the mixture during the process. B) Sintering step. The milled sample was placed in the vertical tube furnace. By purging the forming gas (5 mol.% hydrogen, balanced with nitrogen) with water and controlling the temperature of water, the partial pressure of oxygen (P_{O2}) was dropped to the desired pressure.

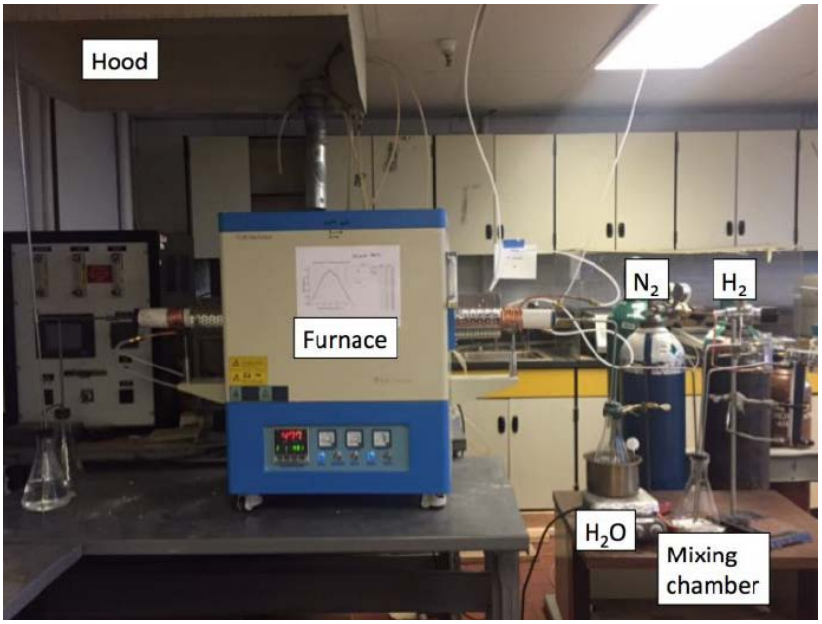

S 2. The experimental setup to create the reducing atmosphere balancing H_2/H_2O.

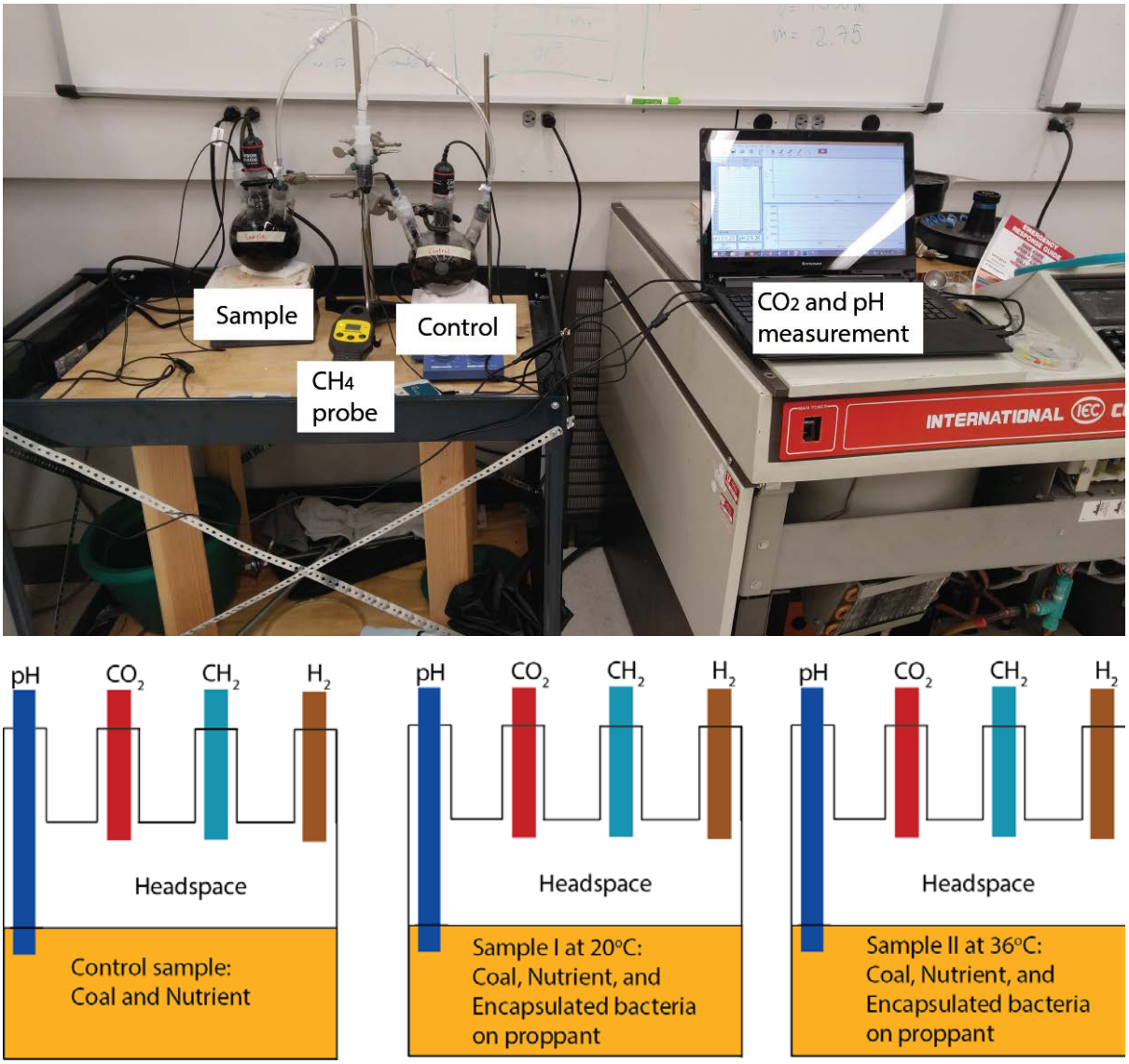

S 3. Top) The experiment setup for the real-time measurement of methane (CH_4), carbon dioxide (CO_2), and pH. The control contains water and coal (Miller Thunder Black, Powder River Basin, WY). The test sample adds the encapsulated bacteria and nutrient with proppant (3 lb per gallon of water) in the same composition as the control. Bottom) The experimental setup for real-time measurement. It will monitor the change of pH and gases (CO_2, CH_4, and H_2).

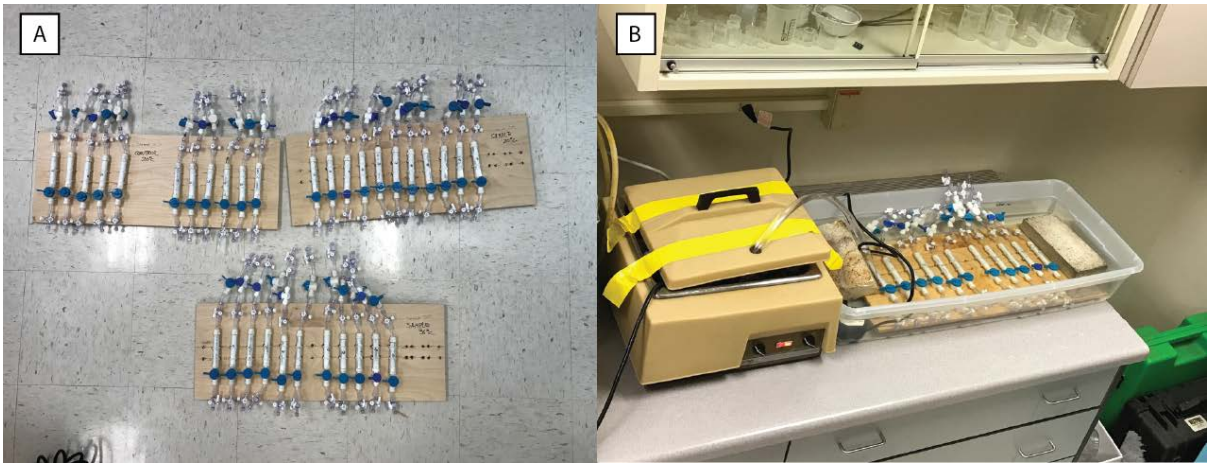

S 4. A) Three sets of conductivity test: the control at room temperature and the samples at room temperature and 36°C. B) The conductivity samples at 36°C in the water bath.

References

1. Fuertez, J.; Boakye, R.; McLennan, J.; Adams, J.; Sparks, T.; Gottschalk, A., Developing methanogenic microbial consortia from diverse coal sources and environments. *J. Nat. Gas Sci. Eng.* **2017,** *46* (Supplement C), 637-650.
2. Hecht, E.; Lighty, J.; Shad dix, C. In *Kinetics rates of oxidation and gasification reaction of coal chars reacting in oxy-combustion environments*, 8th US National Combustion Meeting, Park City, UT, May 19-22, 2013; US National Combustion Meeting: Park City, UT, 2013.
3. Opara, A.; Adams, D.; Free, M.; McLennan, J.; Hamilton, J., Microbial production of methane and carbon dioxide from lignite, bituminous coal, and coal waste materials. *Int. J. Coal Geo.* **2012,** *96-97*, 1-8.
4. Sarv, H. C., Z.; Sayre, A.; Maringo, G. In *oxygen-enriched combustion of a Powder River Basin Black Thunder coal for NOx reduction in a cyclone furnace*, The 34th Internaitional Technical Conference on Clean Coal and Fuel Systems, Florida, May 31-June 4; Florida, 2009.
5. Opara, A.; Adams, D.; Free, M.; McLennan, J.; Hamilton, J., *Microbial production of methane and carbon dioxide from lignite, bituminous coal, and waste coal materials*. Utah Division of Oil, Gas and Mining: Salt Lake City, UT, 2012.
6. Gaskell, D., *Introduction to Metallurgical Thermodynamics*. 2nd ed.; McGraw-Hill: New York, NY, 1981.
7. Toby, B. H.; Von Dreele, R. B., GSAS-II: the genesis of a modern open-source all purpose crystallography software package. *J. Appl. Crystallogr.* **2013,** *46* (2), 544-549.
8. ISO, *Petroleum and natural gas industries completion fluids and materials: Measurement of properties of proppants used in hydraulic fracturing and gravel-packing operations*. ASTM International: West Conshohocken, PA, 2006.
9. *American Petroleum Institute (API), Recommended practice for measurement of proppants used in hydraulic fracturing and gravel-packing operations*. American Petroleum Institute: Dallas, TX, 2008.
10. Sartorius, *Manual of weighing applications: part 1 density*. Sartorius: Bohemia, NY, 1999; p 22-25.
11. ISO, *Petroleum and natural gas industries-completion fluids and materials-part 2: measurement of properties of proppants used in hydraulic fracturing and gravel-packing operations*. ASTM International: Geneva, Switzerland, 2006.
12. *Sintex International & North America, Inc., Proppant technical data: SinterBall bauxite*. Sintex International & North America, Inc.: Rosenberg, TX, 2016.
13. Wu, T.; Wu, B.; Zhao, S., Acid resistance of silicon-free ceramic proppant. *Mater. Lett.* **2013,** *92* (1), 210-212.
14. Han, K.; Robert, C.; Filho, M.; McLennan, J.; Sparks, T., Synthesis and microstructural evolution in iron oxide kaolinite based proppant as a function of reducing atmosphere, sintering, conditions, and composition. *J. Am. Ceram. Soc.* **2017 In progress**.
15. Voo, W.; Ooi, C.; Islam, A.; Tey, B.; Chan, E., Calcium alginate hydrogel beads with high stiffness and extended dissolution behaviour. *Euro. Poly. J.* **2016,** *75*, 343-353.
16. Fuertez, J.; Nguyen, V.; Adams, D.; McLennan, J.; Sparks, T.; Han, K., Optimization of biogenic methane production from coal. *Int J Coal Geol* **2017**, May 5 (submitted).
17. Lim, D., *Microbiology*. Kendall Hunt Publishing: Dubuque, IW, 2003.
18. Fuertez, J.; Nguyen, V.; McLennan, J.; Adams, J.; Han, K.; Sparks, T., Optimization of biogenic methane production from coal. *International Journal of Coal Geology* **2017,** *183* (Supplement C), 14-24.
19. Cooke, C. E., Jr., Conductivity of fracture proppants in multiple layers. *J. Petro. Eng.* **1973,** *25* (9), SPE-4117-PA.
20. Brunauer, S.; Emmett, P.; Teller, E., Adsorption of gases in multi-molecular layers. *J. Am. Chem. Soc.* **1938,** *60*, 309-319.
21. Barrett, E.; Joyner, L.; Halenda, L., The determination of pore volume and area distribution in porous substances computations from nitrogen isotherms. *J. Am. Chem. Soc.* **1951,** *73* (1), 373-380.
22. Botta, P.; Bercoff, P.; Aglietti, E.; Bertorello, H.; Porto L'O Pez, J., Magnetic and structural study of mechanochemical reactions in the Al-Fe_3O_4 system. *J. Mater. Sci.* **2002,** *37* (12), 2563-2568.
23. Monazam, E.; Breault, R.; Siriwardane, R., Reduction of hematite (Fe_2O_3) to wustite (FeO) by carbon monoxide (CO) for chemical looping combustion. *Chem. Eng. J.* **2014,** *242*, 204-210.

24. Baolin, H.; Haiying, Z.; Hongzhong, L.; Qingshan, Z., Study on kinetics of iron oxide reduction by hydrogen. *Chinese J. Chem. Eng.* **2012,** *20* (1), 10-17.
25. Meyers, C.; Mason, T.; Petuskey, W.; Halloran, J.; Bowen, H., Phase equilibrium in the iron-aluminum-oxygen system. *J. Am. Ceram. Soc.* **1981,** *63*, 659-663.
26. Wanger, D.; Devisme, O.; Patisson, F.; Alblitzer, D., A laboratory study of the reduction of iron oxides by hydrogen. In *Sohn International Symposium*, Kongoli, F.; Reddy, R., Eds. TMS Meeting Services: San Diego, CA, 2006; Vol. 2, pp 111-120.
27. Chen, Y.; Wang, M.; Hon, M., Phase transformation and growth of mullite in kaolin ceramics. *J. Euro. Ceram. Soc.* **2004,** *24*, 2389-2397.
28. Worrall, W., *Clays and ceramic raw materials*. 2nd ed.; Halsted Press: New York, NY, 1986; p 151-152.
29. Zhou, Q.; Li, C.; Li, X.; Peng, Z.; Liu, G.; Qi, T., Reaction behavior of ferric oxide in system Fe_2O_3-SiO_2-Al_2O_3 during reductive sintering process. *Trans. Nonferrous Met. Soc. China* **2016,** *26* (3), 842-848.
30. Pillay, T.; D'entremont, J.; Chipman, J., Stability of hercynite at high temperatures. *J. Am. Ceram. Soc.* **1960,** *43*, 583-585.
31. Chen, C.; Lan, G.; Tuan, W., Microstructural evolution of mllite during the sintering of kaolin powder compacts. *Ceram. Int.* **2000,** *26*, 715-720.
32. Barin, I., *Thermochemical Data of Pure Substances*. 3rd ed.; Wiley-VCH: New York, NY, 1997.
33. Chen, C.; Lan, G.; Tuan, W., Preparation of mullite by the reaction sintering of kaolinite and alumina. *J. Euro. Ceram. Soc.* **2000,** *20*, 2519-2525.
34. Kobayashi, Y.; Ohira, O.; Satch, T., Compositions for strengthening porcelain bodies in alumina-feldspar-kaolin system. *Br. Ceram. Trans.* **1994,** *93* (2), 49-52.
35. Papargyris, A.; Cooke, R., Structure and mechanical properties of kaolin based ceramics. *Br. Ceram. Trans.* **1996,** *95* (3), 107-120.
36. Hoffman, D.; Roy, R.; Komarneni, S., Diphasic xerogels, a new class of materials: phases in the system Al_2O_3-SiO_2. *J. Am. Ceram. Soc.* **2006,** *67* (7), 468-471.
37. Maniatis, Y.; Tite, M., Scanning electron microscope examination of the bloating of fired clays. *Trans. J. Br. Ceram. Soc.* **1975,** *74*, 229-232.
38. Kromer, H., Mineralogical composition of bloating clays and their behavior in the hot-stage microscope. *Interceram.* **1970,** *19* (4), 259-262.
39. Kromer, H., Mineral composition and properties of two north Spanish kaolins from the region of Vivero (Galicia). *Interceram.* **1972,** *21* (4), 259-264.
40. Seo, W.; Tsukihashi, F., Thermodynamic and structural properties for the FeO–SiO_2 system by using molecular dynamics calculation. *Mater. Trans.* **2005,** *46* (6), 1240-1247.
41. Laird, J.; Beck, W. Ceramic spheroids having low density and high crush resistance. 1986.
42. Luscher, W. Role of composition and oxygen partial pressure on microstructural and crystalline phase evolution in aluminosilicate derived aggregates. Pensylvania State University, University Park, PA, 2007.
43. Liang, F.; Sayed, M.; Al-Muntasheri, G.; Chang, F.; Li, L., A comprehensive review on proppant technologies. *Petroleum* **2016,** *2* (1), 1-14.
44. Gibb, J.; Laird, J.; Lee, G.; Whitcomb, W. Particulate ceramic useful as a proppant. 1987.
45. *American Petroleum Institute, Recommended practices for testing sand used in hydraulic fracturing operations*. American Petroleum Institute: Dallas, TX, 1995.
46. Belyadi, H.; Fathi, E.; Belyadi, F., *Hydraulic fracturing in unconvetional reservoirs*. 1st ed.; Gulf Professional Publishing: Cambridge, MA, 2017.
47. Tian, X.; Wu, B.; Li, J., The exploration of making acidproof fracturing proppants using red mud. *J. Hazard. Mater.* **2008,** *160*, 589-593.
48. Gibb, J.; Laird, J.; Berntson, L. Novolac coated ceramic particulate. 1990.
49. Lee, P.; Rogers, M., Effect of calcium source and exposure-time on basic caviar spherification using sodium alginate. *J. Gastron. Food Sci.* **2012,** *1*, 96-100.
50. Montero, P.; Perez-Mateos, M., Effects of Na+, K+ and Ca2+ on gels formed from fish mince containing a carrageenan or alginate. *Food Hydrocolloids* **2002,** *16* (4), 375-386.
51. Blandino, A.; Macias, M.; Cantero, D., Formation of calcium alginate gel capsules: influence of sodium alginate and $CaCl_2$ concentration on gelation kinetics. *J. Biosci. Bioeng.* **1999,** *88* (6), 686-689.
52. Shiro, O., Interaction of thaumatin with carrageenans. I. Effects of pH. temperature and competing

cations. *Food Hydrocolloids* **1990,** *4* (2), 105-119.
53. Oyaas, J.; Storro, I.; Svedsen, H.; Levine, D., The effective diffusion coefficient and the distribution constant for small molecules in calcium-alginate gel beads. *Biotech. Bioeng.* **1995,** *47* (4), 492-500.
54. Tromp, R.; Vink, C.; Stijnman, A., *Encapsulation by Electrospinning of Live Bacteria used in the Food Industry*. Royal Society of Chemistry: Cambidge, UK, 2011.
55. Kikuchi, A.; Kawabuchi, M.; Watanabe, A.; Sugihara, M.; Sakurai, Y.; Okano, T., Effect of Ca^{2+}-alginate gel dissolution on release of dextran with different molecular weights. *J. Controlled Release* **1990,** *58*, 21-28.
56. Aravindhan, R.; Fathima, N.; Rao, J.; Nair, B., Equilibrium and thermodynamic studies on the removal of basic black dye using calcium alginate beads. *Colloids Surf., A* **2007,** *299*, 232-238.
57. Iskakov, R.; Kikuchi, A.; Okano, T., Time-programmed pulsatile release of dextran from calcium alginate gel beads coated with carboxy-*n*-propylacrylamide copolymers. *J. Controlled Release* **2002,** *80*, 57-68.
58. Jones, E.; Voytek, M.; Corum, M.; Orem, W., Stimulation of methane generation from nonproductive coal by addition of nutrients or a microbial consortium. *Appl. Environ. Microb.* **2010,** *76* (21), 7013-7021.
59. Elashahed, M.; McInerney, M., Benzoate fermentation by the anaerobic bacterium syntrophus aciditrophicus in the absence of hydrogenusing methanogens. *Appl. Environ. Microb.* **2001,** *67*, 5520-5525.
60. Fox, M.; Dickinson, F.; Rateledge, C., Long-chain alcohol and aldehyde dehydrogenase activities in Acinetobacter calcoaceticus strain HO1-N. *J. Gen. Microbiol.* **1992,** *138*, 1963-1972.
61. Hatamoto, M.; Imachi, H.; Ohashi, A.; Harada, H., Identification and cultivation of anaerobic, syntrophic long-chain fatty acid-degrading microbes from mesophilic and thermophilic methanogenic sludges. *Appl. Environ. Microb.* **2007,** *73*, 1332-1340.
62. Fallgren, P.; Jin, S.; Zeng, C.; Ren, Z.; Lu, A.; Colberg, P., Comparison of coal rank for enhanced biogenic natural gas production. *Int. J. Coal Geo.* **2013,** *115*, 92-96.
63. Jin, S. *Enhancement of biogenic coalbed methane production and back injection of coalbed methane co-produced water*; Deparment of Energy: Maryland, 2007.
64. Stephen, A.; Adebusuyi, A.; Baldygin, A.; Shuster, J.; Southam, G.; Budwill, K.; Foght, J.; Nobes, D.; Mitra, S., Bioconversion of coal: new insights from a core flooding study. *RSC* **2014,** *4*, 22779-22791.
65. Mayumi, D.; Mochimaru, H.; Tamaki, H.; Yamamoto, K.; Yoshioka, H.; Suzuki, Y.; Kamagata, Y.; Sakata, S., Methane production from coal by a single methanogen. *Science* **2016,** *354* (6309), 222-225.
66. Fey, A.; Conrad, R., Effect of temperature on carbon and electron flow and on the archaeal community in methanogenic rice field soil. *Appl. Environ. Microb.* **2000,** *66*, 4790-4797.
67. Manoj, B.; Kunjomana, A., Chemical leaching of an Indian bituminous coal and characterization of the products by vibrational spectroscopic techniques. *Int. J. Miner. Metall. Mater.* **2012,** *19*, 279-283.
68. Suraj, G.; Iyer, C. S. P.; Rugmini, S.; Lalithambika, M., The effect of micronization on kaolinites and their sorption behaviour. *Applied Clay Science* **1997,** *12* (1), 111-130.
69. Saikia, B. K.; Boruah, R. K.; Gogoi, P. K., FT-IR and XRD analysis of coal from Makum coalfield of Assam. *Journal of Earth System Science* **2007,** *116* (6), 575-579.
70. Abdel-Khalek, M. A.; El-Midany, A. A., Application of Bacillus subtilis for reducing ash and sulfur in coal. *Environmental Earth Sciences* **2013,** *70* (2), 753-760.
71. Xuguang, S., The investigation of chemical structure of coal macerals via transmitted-light FT-IR microscpectroscopy. *Spectrochimica Acta Part A* **2005,** *62*, 557-564.
72. Cooke, N.; Fuller, O.; Gaikwad, R., FTIR spectroscopic analysis of coal and coal extracts. *Fuel* **1986,** *65* (9), 1254-1260.
73. Sharma, D.; Wadhwa, G., Demineralization of coal by stepwise bioleaching: a comparative study of three Indian coals by Fourier Transform Infra Red and X-ray diffraction techniques. *World J. Microbio. Biotech.* **1997,** *13*, 29-36.
74. Scott, A., Improving coal gas recovery with microbially enhanced coalbed methane. In *Coalbed Methane: Scientific, Environmental, and Economic Evaluations*, Mastalerz, M.; Glikson, M.; Golding, S., Eds. Springer: Netherlands, 1999; pp 89-110.
75. Green, M.; Flanegan, K.; Gilcrease, P., Characterization of a methanogenic consortium enriched from a coalbed methane well in the Powder River Basin, U.S.A. *Int J Coal Geol* **2008,** *76*, 34-45.
76. De Bruin, R.; Lyman, R.; Jones, R.; Cook, L., *Coalbed methane in Wyoming*. Information Pamphlet: Laramie, WY, 2000.

77. Harding, R.; Czarnecki, S.; Isbister, J.; Barik, S., *Biogasification of low-rank coal*. ARCTECH, Inc.: Chantilly, VA, 1993.
78. *LUCA Technologies, LLC., Active biogenesis of methane in Wyoming's Powder River Basin*; LUCA Technologies, LLC.: Golden, CO, 2004.
79. Averkamp, H. How do you compute a selling price if you know the cost and the required gross margin? https://www.accountingcoach.com/blog/compute-selling-price (accessed July 30).
80. Hughes, E. Proppants market could be worth $10bn by 2017. http://www.indmin.com/Article/3251450/Proppants-market-could-be-worth-10bn-by-2017.html (accessed July 30, 2017).
81. FortressProppantsLtd In *"Ceramics versus resin coated supply dynamics*, Frac Sand Logistics Supply Chain, Houston, TX, November 20; Houston, TX, 2013.
82. O'Driscoll, M. Ceramic proppant outlook: trying to build a market on sand. https://imformed.com/ceramic-proppant-outlook-trying-to-build-a-market-on-sand/ (accessed July 30).